Sensor and Simulation Notes

Note 173

March 1973

Transient Electromagnetic Properties of Two Parallel Wires

Lennart Marin
Dikewood Corporation, Westwood Research Branch
Los Angeles, California

Abstract

An analysis is presented of the transient electromagnetic field around two parallel wires. It is shown that the field can be expressed in terms of a discrete spectrum and a continuous spectrum. The discrete part of the spectrum can be interpreted as modes. The frequency variations of the propagation and attenuation constants of some of these modes are determined for different values of the radius-to-separation ratio of the two wires. The time history of the current at different points on the wires is also calculated when each wire is excited by a slice generator with a step-voltage source. Two different modes of excitation are considered: (1) the two voltage generators have opposite polarity and (2) they have the same polarity.

Contents

I. Introduction

Certain types of EMP simulators make use of parallel-plate transmission lines as a guiding structure for the electromagnetic field. One reason for using parallel-plate simulators is based on the fact that they can support a TEM mode. For many types of cylindrical transmission lines the field distribution of the TEM mode is nearly uniform over a significant portion of their cross section. This means that the TEM mode provides a good approximation to the free-space nuclear EMP. The TEM mode propagates at all frequencies, but for frequencies such that the free-space wavelength is of the order of the cross sectional dimensions of the simulator, other modes may become important. In many cases it is desirable to launch fast rising pulses on these simulators where the rise time of the pulse is significantly shorter than the transit time across the cross section of the simulator. In doing so many higher-order modes may be generated.

In order to develop a quantitative understanding of the relative importance of the higher-order mode contribution we will, in this note, investigate a structure consisting of two parallel wires. Each wire is supposed to be fed by a delta gap generator with a step-voltage source. The field distribution of the TEM wave on this structure has been determined previously [1] by the method of conformal mapping. However, as of now, there seems to be no calculations made of the properties of the higher-order modes that can exist on this structure. One reason for investigating this particular problem is that we can find an explicit solution of a transient problem with the assumption that the radius of each wire is much smaller than the distance separating the wires. It is believed that many properties of the higher-order modes on this structure are shared by the higher-order modes that exist on other structures, for example, two parallel, perfectly conducting plates of finite width. Unfortunately, it is not possible to find an explicit solution of the two-plate problem. Although, an integral equation for the induced current density on the plates can be formulated, this equation has to be solved numerically. Another reason for investigating the two-wire problem is to gain some insight concerning the type of modes that can exist on an open waveguide consisting of two parallel conductors, before undertaking a numerical study of a more complicated structure.

A thorough investigation of the TEM mode on two parallel wires is given in [1]. An antenna consisting of two parallel wires of finite length and fed at their midpoint by a slice generator has been treated in [2]. The approach in [2] is based on an electric-field integral equation and this equation is solved for low frequencies by using the Wiener Hopf method. A frequency domain analysis of two parallel wires is given in [3]. However, there exists no analysis of the transient behavior of the field around two wires.

The analysis in this note is based on a solution of the Maxwell equations in the frequency domain which can be obtained by employing Laplace transform methods. In evaluating the inverse Laplace transform integrals we follow the approach used in references [4] through [7] when calculating the transient fields of a cylindrical antenna in free space. There is one important difference: the field of one cylindrical antenna can, in the time domain, be represented by one single integral, whereas the field around two parallel wires can be represented by an integral and an infinite sum. Using spectral notation, the integral can be called the contribution from the continuous part of the spectrum, whereas the sum is the contribution from the discrete part of the spectrum. Physically, each term in the sum can be thought of as due to a mode. These modes can be obtained from the nontrivial solutions of the source-free Maxwell equations. One mode is the TEM mode and it propagates with the speed of light. The propagation constants of the other modes are complex, i.e., each mode is attenuated as it propagates along the line. However, the field components of each higher-order mode grow exponentially in the transverse direction far away from the structure. Therefore, the use of these modes is limited to a region in the vicinity of the guiding structure. Mathematically, this fact can be expressed in the following way: the propagation constants of the higher-order modes belong to the Riemann sheet in which the radiation condition is violated. Many of these questions have been treated in the literature (see, for example, references [8] and [9]).

Laplace transform methods are used in Section II to derive an integral expression for the transverse magnetic field in the time domain. This expression is then simplified in Section II to real valued integrals suitable for numerical computations. Some analytical properties of the field are derived in Section IV and the results of the numerical computations are

presented in Section VI in graphical form for the time behavior of the induced current on two parallel wires due to two slice generators with step-function voltage sources. Two different modes of excitation are considered: (1) the line is excited antisymmetrically (push-pull), and (2) the line is excited symmetrically (push-push). It should be pointed out that in the first excitation a differential TEM mode is excited, whereas in the second excitation no TEM mode is excited. Some frequency domain properties of the field are determined in Section VII including the frequency dependence of the propagation constants of some of the modes.

The analytical methods recently developed to solve transient electromagnetic scattering problems [19,20] can, of course, be applied to the calculation of the fields around two perfectly conducting wires excited by two slice generators whose output voltage are step-functions in time. When the scattering bodies are of finite extent, poles are the only singularities in the complex frequency plane of the scattered field provided that the incident field is an entire function of the complex frequency [20]. In the two-wire problem, however, the scattering body is of infinite extent and the scattered field has branch points in the complex frequency plane. The branch points are associated with the propagation constants of the modes that can exist on these wires and they remind us of the branch points of the field scattered from a perfectly conducting body located in a parallel-plate region [21].

II. Formulation of the Problem

Consider two perfectly conducting, parallel, thin wires with radii a and separated by a distance d (see Figure 1). Throughout this note it will be assumed that a << d. We introduce two cylindrical coordinate systems (ρ_1,ϕ_1,z) and (ρ_2,ϕ_2,z) such that $\rho_1 = a$ is the surface of the "upper" wire and $\rho_2 = a$ is the surface of the "lower" wire. Each wire is fed by an infinitesimal gap at z = 0 and independent of the respective azimuthal angles ϕ_1 and ϕ_2. To solve the Maxwell equations in the region outside the wires we will make use of Laplace transforms with respect to the time t and the coordinate z. Let $f(\rho,z,t)$ denote an arbitrary field component. We then define the two sided Laplace transform

$$\tilde{f}(\rho,z,\gamma) = \int_{-\infty}^{\infty} f(\rho,z,t)\exp(-c\gamma t)dt \tag{1}$$

that has the inverse transform

$$f(\rho,z,t) = c(2\pi i)^{-1}\int_{C_\gamma} \tilde{f}(\rho,z,\gamma)\exp(c\gamma t)d\gamma \tag{2}$$

where the path of integration, C_γ, is parallel to the imaginary axis in the complex γ-plane (see Figure 2a) and $\gamma = s/c$ where s is the complex frequency, and the vacuum speed of light is denoted by c. We also define the two-sided Laplace transform

$$\hat{\tilde{f}}(\rho,\zeta,\gamma) = \int_{-\infty}^{\infty} \tilde{f}(\rho,z,\gamma)\exp(-\zeta z)dz \tag{3}$$

with the inverse transform

$$\tilde{f}(\rho,\zeta,\gamma) = (2\pi i)^{-1}\int_{C_\zeta} \hat{\tilde{f}}(\rho,\zeta,\gamma)\exp(\zeta z)d\zeta \tag{4}$$

and the path of integration, C_ζ, is parallel to the imaginary axis in the complex ζ-plane as indicated in Figure 2b.

Assuming that the current distributions on the two wires are independent of the azimuthal angles ϕ_1 and ϕ_2, respectively, we arrive at the following solutions of the Maxwell equations, valid for $\rho_1 > a$ and $\rho_2 > a$,

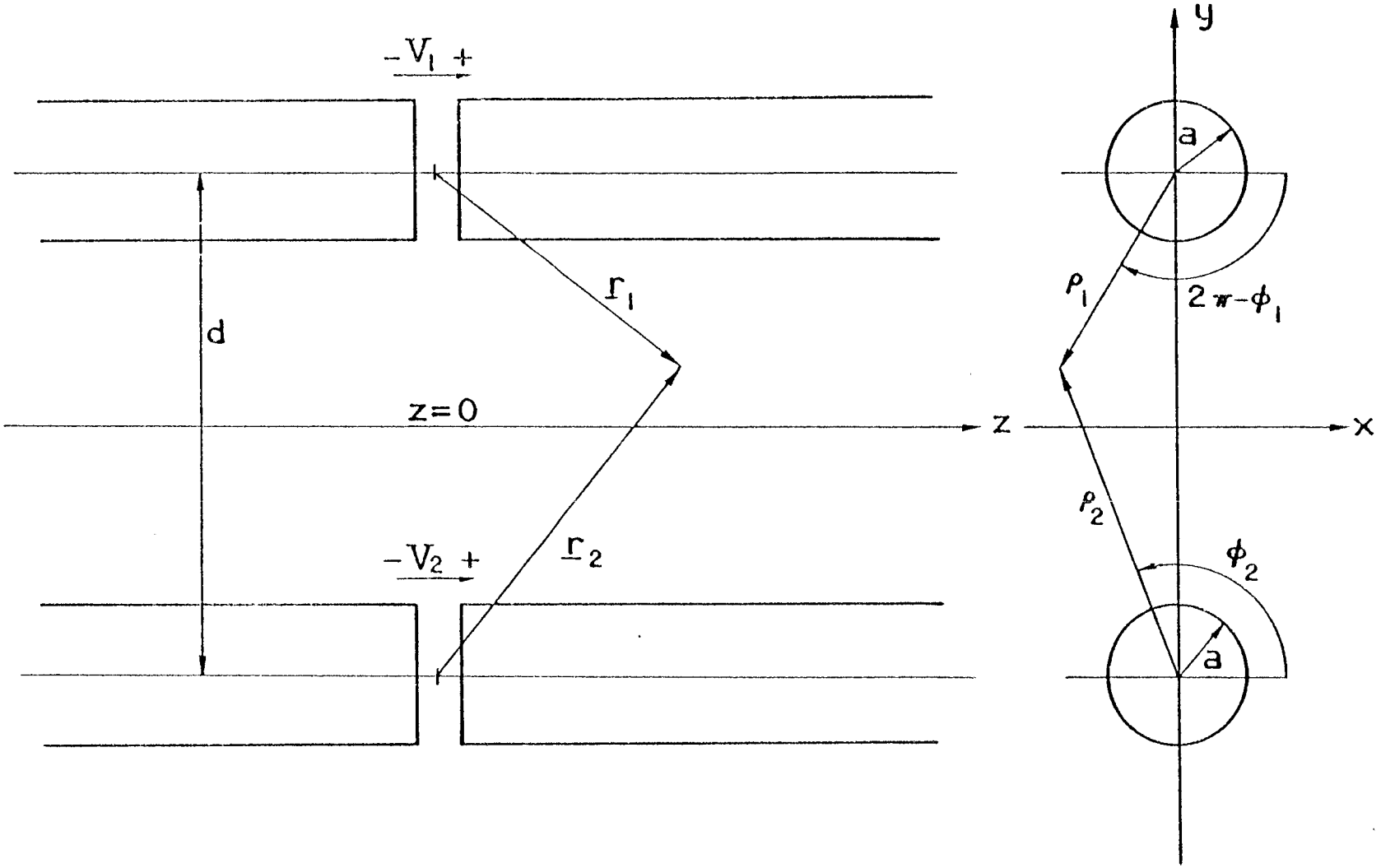

Figure 1. The geometry of the problem.

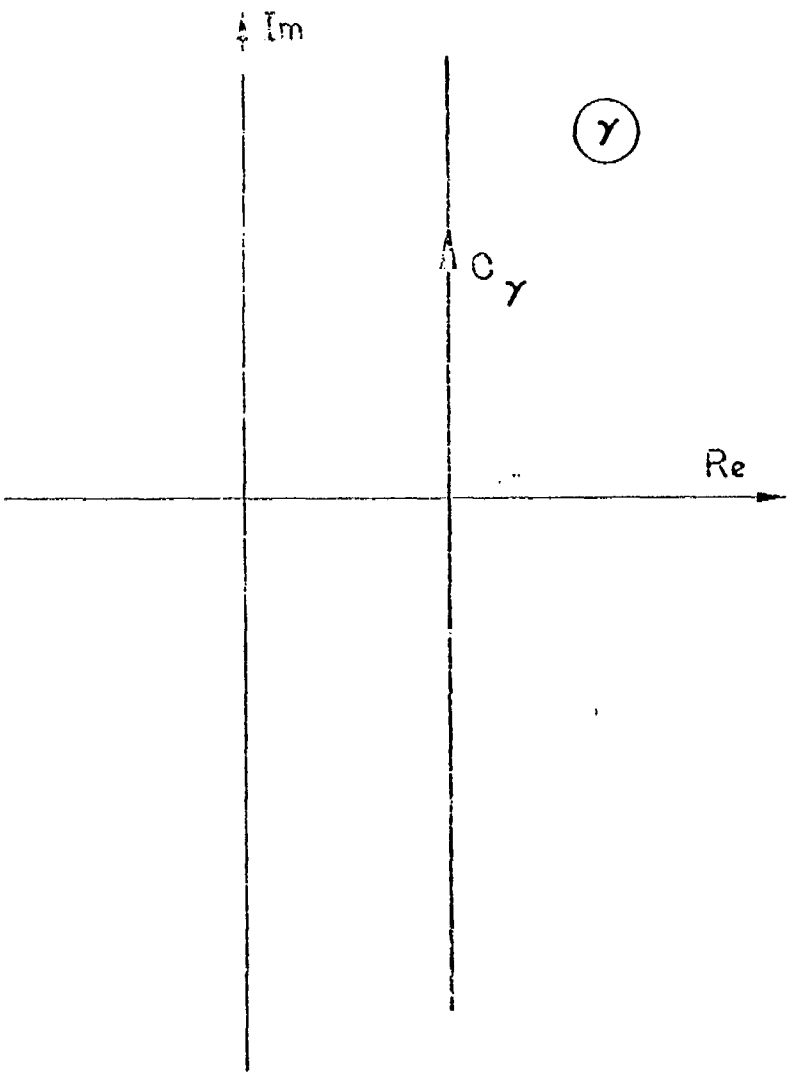

Figure 2a. The path of integration, C_γ, for the inverse Laplace transform.

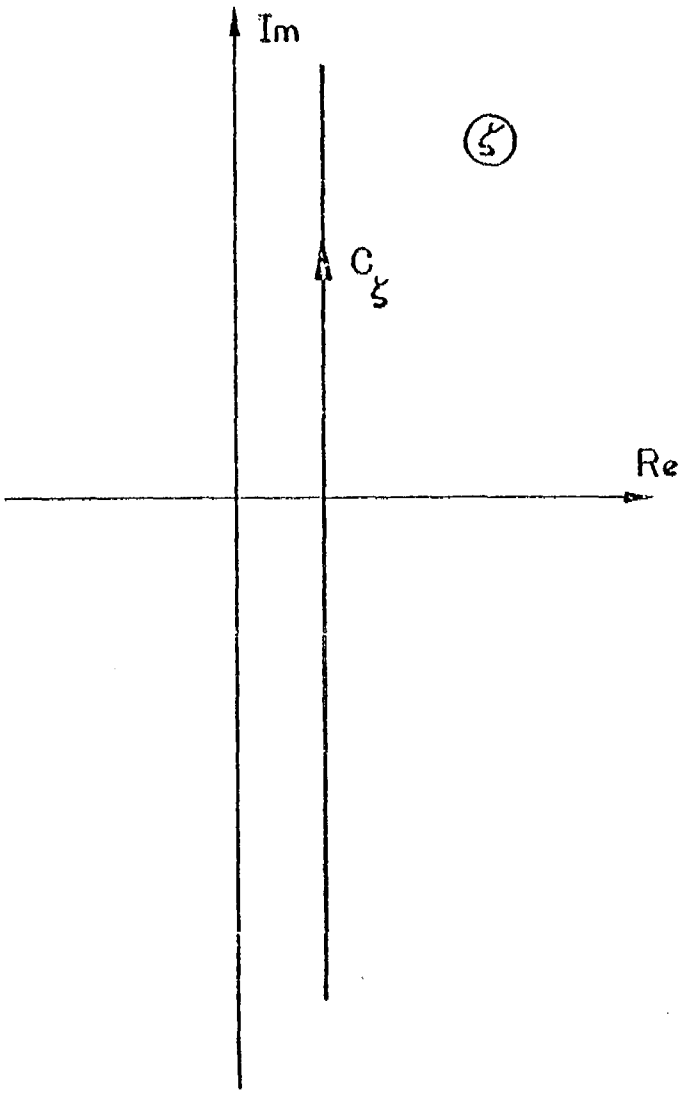

Figure 2b. The path of integration, C_ζ, for the inverse Laplace transform.

$$\hat{\tilde{E}}_z(x,y,\zeta,\gamma) = \sum_{\ell=1}^{2} K_o(p\rho_\ell)K_o^{-1}(pa)\hat{\tilde{E}}_\ell(\zeta,\gamma)$$

$$\underline{\hat{\tilde{E}}}_{tr}(x,y,\zeta,\gamma) = \sum_{\ell=1}^{2} \{\zeta p^{-1}K_1(p\rho_\ell)K_o^{-1}(pa)\hat{\tilde{E}}_\ell(\zeta,\gamma)[\hat{x}\cos\phi_\ell + \hat{y}\sin\phi_\ell]\} \qquad (5)$$

$$\underline{\hat{\tilde{H}}}(x,y,\zeta,\gamma) = \sum_{\ell=1}^{2} \{\gamma p^{-1}Z_o^{-1}K_1(p\rho_\ell)K_o^{-1}(pa)\hat{\tilde{E}}_\ell(\zeta,\gamma)[\hat{x}\sin\phi_\ell - \hat{y}\cos\phi_\ell]\}$$

where $p = (\gamma^2 - \zeta^2)^{1/2}$ and the subscript tr denotes the transverse components with respect to z. Moreover, $I_o(x)$, $K_o(x)$ and $K_1(x)$ are the modified Bessel functions, Z_o is the wave impedance of free space and $\hat{\tilde{E}}_\ell(\zeta,\gamma)$, $\ell = 1, 2$, is the transform of the z-component of the electric field on one wire, due to the current on the same wire. With each wire being driven by a slice generator located at z = 0 and having the out put voltage $V_\ell(t)$, $\ell = 1,2$, we arrive at the following equation from the boundary conditions at $\rho_\ell = a$,

$$[K_o(pa)\hat{\tilde{E}}_1(\zeta,\gamma) + K_o(pd)\hat{\tilde{E}}_2(\zeta,\gamma)]/K_o(pa) = -\tilde{V}_1(\gamma)$$

$$[K_o(pd)\hat{\tilde{E}}_1(\zeta,\gamma) + K_o(pa)\hat{\tilde{E}}_2(\zeta,\gamma)]/K_o(pa) = -\tilde{V}_2(\gamma). \qquad (6)$$

In deriving (6) we have assumed that the current distribution on each wire is independent of the azimuthal angle and that $d >> a$. This equation is obtained by keeping one term in a Fourier series expansions of the current and the tangential electric field on the surface of each wire. Equation (6) yields

$$\hat{\tilde{E}}_\ell(\zeta,\gamma) = -K_o(pa)A_+(p)\tilde{V}_+(\gamma) + (-1)^\ell K_o(pa)A_-(p)\tilde{V}_-(\gamma), \quad \ell = 1,2 \qquad (7)$$

where

$$A_\pm(p) = [K_o(pa) \pm K_o(pd)]^{-1} \qquad (8)$$

and

$$\tilde{V}_\pm(\gamma) = [\tilde{V}_1(\gamma) \pm \tilde{V}_2(\gamma)]/2. \qquad (9)$$

From (5) and (7) we derive the following representation for the magnetic field

$$\underline{\hat{\hat{H}}}(x,y,\zeta,\gamma) = \sum_{\ell=1}^{2} \hat{\hat{H}}_\ell(\rho_\ell,\zeta,\gamma)\hat{\phi}_\ell \tag{10}$$

where

$$Z_o\hat{\hat{H}}_\ell(\rho,\zeta,\gamma) = \gamma p^{-1}K_1(p\rho)[A_+(p)\tilde{V}_+(\gamma) - (-1)^\ell A_-(p)\tilde{V}_-(\gamma)]. \tag{11}$$

The transform, $\hat{\hat{I}}_\ell(\zeta,\gamma)$, of the total current, $I_\ell(z,t)$, on each wire is given by

$$Z_o\hat{\hat{I}}_\ell(\zeta,\gamma) = 2\pi a\gamma p^{-1}K_1(pa)[A_+(p)\tilde{V}_+(\gamma) - (-1)^\ell A_-(p)\tilde{V}_-(\gamma)]. \tag{12}$$

We now go on to treat the case where $V_1(t)$ and $V_2(t)$ are both step-functions in time and turned on simultaneously, i.e.,

$$\tilde{V}_\ell(\gamma) = V_\ell(c\gamma)^{-1}, \qquad \ell = 1,2 \tag{13}$$

so that

$$\tilde{V}_\pm(\gamma) = V_\pm(c\gamma)^{-1}, \qquad V_\pm = (V_1 \pm V_2)/2. \tag{14}$$

In this case we have

$$\rho_\ell Z_o\hat{\hat{H}}_\ell(\rho_\ell,\zeta,\gamma) = V_+G_+(p,\rho_\ell) - (-1)^\ell V_-G_-(p,\rho_\ell) \tag{15}$$

where

$$G_\pm(p,\rho) = \rho p^{-1}K_1(p\rho)A_\pm(p). \tag{16}$$

Equations (2), (4), (13), (15) and (16) enable us to derive the following time-domain representation of the magnetic field

$$\underline{H}(x,y,z,t) = \sum_{\ell=1}^{2} H_\ell(\rho_\ell,z,t)\hat{\phi}_\ell \tag{17}$$

where

$$\rho Z_o H_\ell(\rho,z,t) = V_+F_+(\rho,z,t) - (-1)^\ell V_-F_-(\rho,z,t) \tag{18}$$

and

$$F_\pm(\rho,z,t) = c(2\pi i)^{-1}\int_{C_\gamma}\left[(2\pi i)^{-1}\int_{C_\zeta} G_\pm(p,\rho)\exp(\zeta z)d\zeta\right]\exp(c\gamma t)d\gamma. \tag{19}$$

From equations (17) and (19) it follows that all properties of the magnetic field can be determined from the integral representation (19) of $F_\pm(\rho,z,t)$. In the same way the total current, $I_\ell(z,t)$, on each wire is given by (c.f. (12))

$$Z_o I_\ell(z,t) = 2\pi V_+F_+(a,z,t) - (-1)^\ell 2\pi V_-F_-(a,z,t). \tag{20}$$

In the next section we will evaluate the integrals defined by (19).

III. The Magnetic Field Due to Step Voltages

In this section we will evaluate the integrals given by (19), i.e.,

$$F_{\pm}(\rho,z,t) = c(2\pi i)^{-1}\int_{C_\gamma}\left[(2\pi i)^{-1}\int_{C_\zeta} G_{\pm}(p,\rho)\exp(\zeta z)d\zeta\right]\exp(c\gamma t)d\gamma. \quad (19')$$

The path of integration, C_γ, is to the right of all singularities in the complex γ-plane of the inner integral. Moreover, from the radiation condition it follows that the proper branch of $p = (\gamma^2 - \zeta^2)^{1/2}$ is defined such that $\mathrm{Re}\{p\} \geq 0$ in that branch, and it is depicted in Figure 3. Since we can always choose C_γ to the right of the imaginary axis in the complex γ-plane it follows immediately that $p = \gamma$ at the origin of the proper branch of the ζ-plane. The path of integration, C_ζ, is parallel to the imaginary axis and such that $-\mathrm{Re}\{\gamma\} < \mathrm{Re}\{\zeta\} < \mathrm{Re}\{\gamma\}$ when ζ belongs to C_ζ and γ belongs to C_γ. To ensure convergence of the integral for all values of z we choose to let C_ζ coincide with the imaginary axis (see Figure 3). It is clear from (19) that $F(\rho,z,t) = F(\rho,-z,t)$ so there is no loss of generality to only consider the case $z > 0$. In the following we will limit our investigations to $z > 0$.

Next, we introduce the transformation

$$p = (\gamma^2 - \zeta^2)^{1/2}, \qquad \zeta = (\gamma^2 - p^2)^{1/2}.$$

The branch of the square root defining ζ as a function of p is chosen so that $\mathrm{Re}\{\zeta\} \leq 0$ in that branch, and it is shown in Figure 4. Making use of the technique introduced in [5] we can transform the inner integral in (19) to get

$$F_{\pm}(\rho,z,t) = c(2\pi i)^{-1}\int_{C_\gamma}\left[(2\pi i)^{-1}\int_{C_p}(\gamma^2 - p^2)^{1/2}H_{\pm}(p,\rho)\exp[-z(\gamma^2 - p^2)^{1/2}]dp\right]d\gamma \quad (21)$$

where

$$H_{\pm}(p,\rho) = pG_{\pm}(p,\rho) = \rho K_1(p\rho)A_{\pm}(p). \quad (22)$$

The path of integration, C_p, is around the branch cut in the p-plane. This branch cut is given by the part of the hyperbola $\mathrm{Re}\{p\}\mathrm{Im}\{p\} = \mathrm{Re}\{\gamma\}\mathrm{Im}\{\gamma\}$ for which $\mathrm{Re}\{p\} \geq \mathrm{Re}\{\gamma\}$ (c.f. Figure 4).

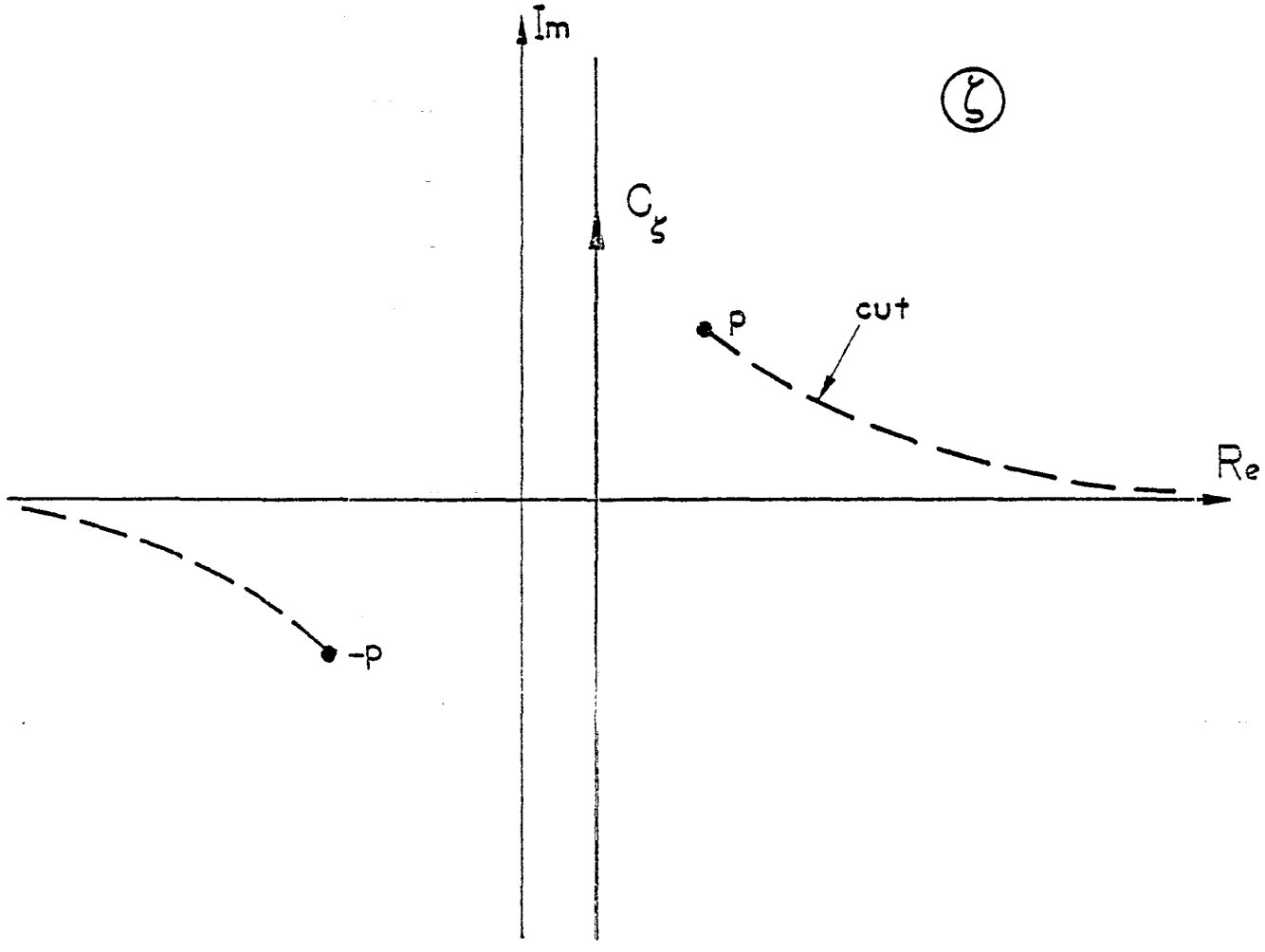

Figure 3. The proper branch of $p = \sqrt{\gamma^2 - \zeta^2}$ where $p = \gamma$ at $\zeta = 0$.

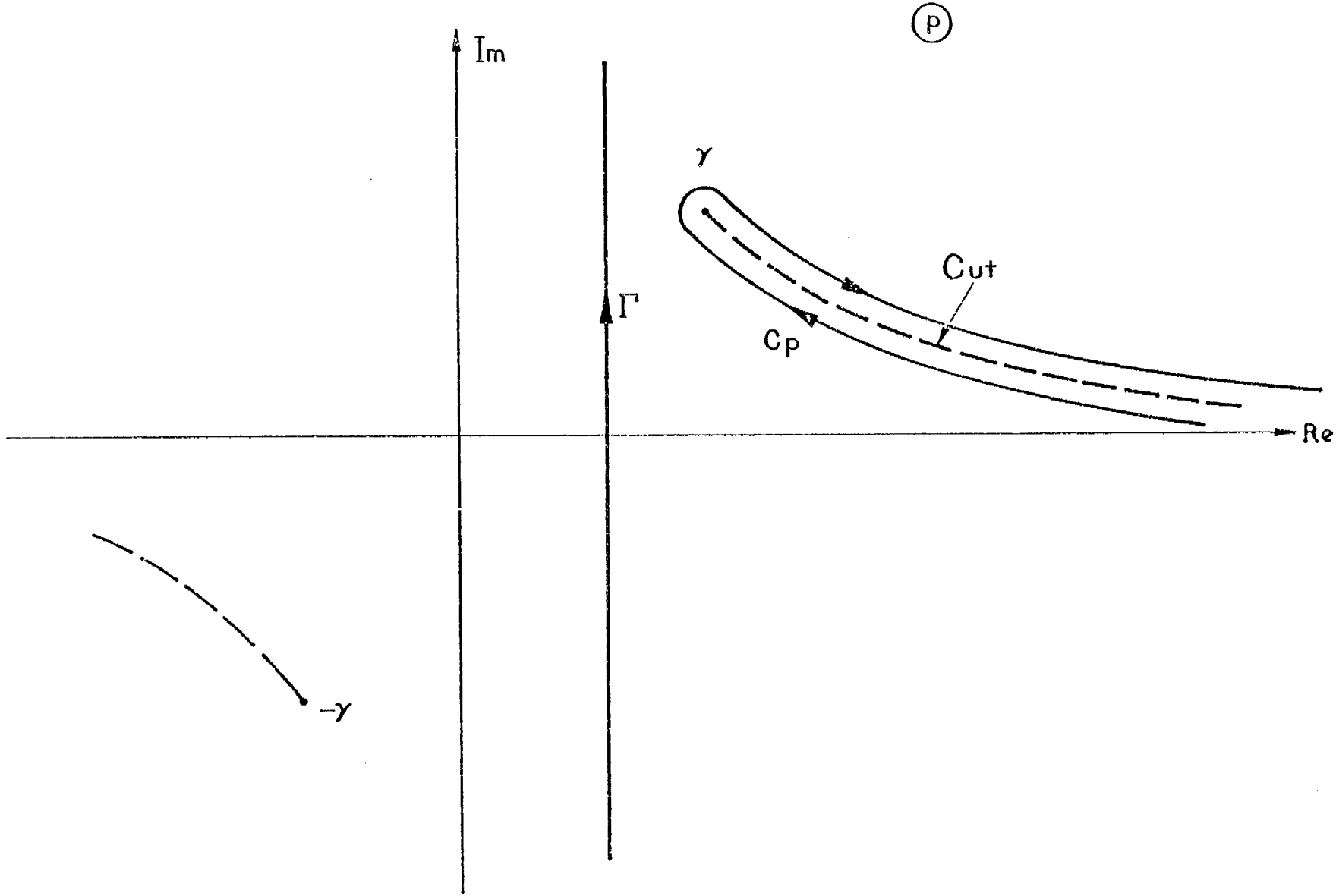

Figure 4. Paths of integration in the branch of $\zeta = \sqrt{\gamma^2 - p^2}$ where $\zeta = -\gamma$ at $p = 0$.

From the asymptotic expressions for the modified Bessel functions one immediately sees that there exists a p_r such that $K_o(pa) \pm K_o(pd)$ has no zeros for $\mathrm{Re}\{p\} \geq p_r$. By choosing the path of integration C_γ such that $\mathrm{Re}\{\gamma\} > p_r$ when γ belongs to C_γ we can deform the path of integration C_p to Γ since $\mathrm{Re}\{(\gamma^2 - p^2)^{1/2}\} \geq 0$ in the branch under consideration. Here, Γ is parallel to the imaginary axis and such that $p_r < \mathrm{Re}\{p\} < \gamma_r$ when p belongs to Γ (see Figure 4). Since Γ is independent of γ we can interchange the order of integration and obtain (c.f. [15])

$$F_\pm(\rho,z,t) = (2\pi i)^{-1}\int_\Gamma H_\pm(p,\rho)\left[(2\pi i)^{-1}\int_{C_\gamma}(\gamma^2 - p^2)^{-1/2}\exp[c\gamma t - z(\gamma^2 - p^2)^{1/2}]d\gamma\right]dp$$

$$= \begin{cases} 0, & ct < z \\ (2\pi i)^{-1}\int_\Gamma H_\pm(p,\rho)I_o(p\tau)dp, & ct > z \end{cases} \tag{23}$$

where $\tau^2 = (ct)^2 - z^2$. Note that $F_\pm(\rho,z,t)$ is uniquely defined by the two quantities ρ and τ. Therefore, we get

$$F_\pm(\rho,z,t) \equiv F_\pm(\rho,\tau) = (2\pi i)^{-1}\int_\Gamma H_\pm(p,\rho)I_o(p\tau)\,dp\,. \tag{24}$$

Since $H_\pm(p,\rho)$ has no singularities to the right of Γ and since

$$H_\pm(p,\rho)I_o(p\tau) \sim \exp[-p(\rho - a - \tau)] \quad \text{as} \quad p \to \infty$$

in the right half plane it follows that $F_\pm(\rho,\tau) = 0$ for $\tau < \rho - a$ or $ct < [(\rho - a)^2 + z^2]^{1/2}$ as expected from causality requirements.

To evaluate $F_\pm(\rho,\tau)$ for $\tau > \rho - a$ we observe that (c.f. [16]) $i\pi I_o(p\tau) = K_o(p\tau) - K_o[p\tau\exp(i\pi)]$ and that $i\pi I_o(p\tau) = K_o[p\tau\exp(-i\pi)] - K_o(p\tau)$. Following the procedure used in [4] and [5] we get

$$F_\pm(\rho,\tau) = -(2\pi^2)^{-1}\int_{C_-} H_\pm(p,\rho)K_o(p\tau)dp + (2\pi^2)^{-1}\int_{C_-} H_\pm(p,\rho)K_o[p\tau\exp(i\pi)]dp$$

$$+ (2\pi^2)^{-1}\int_{C_+} H_\pm(p,\rho)K_o(p\tau)dp - (2\pi^2)^{-1}\int_{C_+} H_\pm(p,\rho)K_o[p\tau\exp(-i\pi)]dp$$

where $C_\pm = \Gamma_\pm \cup R_\pm$. The integration path $\Gamma_+(\Gamma_-)$ is the part of Γ for which $\mathrm{Im}\{p\}$ is positive (negative) and $L_+(L_-)$ is the part of the real axis that is located between Γ and the origin and taken in the positive (negative) direction (see Figure 5). Making use of the Cauchy integration formula we get (c.f. [4] and [5])

$$F_\pm(\rho,\tau) = R_\pm(\rho,\tau) + T_\pm(\rho,\tau) + S_\pm(\rho,\tau) \tag{25}$$

where

$$R_\pm(\rho,\tau) = \frac{\rho}{a}\int_0^\infty \frac{L_\pm(\xi)[L_\pm(\xi)K_1(\xi\rho/a)+M_\pm(\xi)I_1(\xi\rho/a)]}{M_\pm(\xi)[M_\pm^2(\xi)+\pi^2L_\pm^2(\xi)]} K_o(\xi\tau/a)d\xi \tag{26}$$

$$L_\pm(\xi) = I_o(\xi) \pm I_o(\xi d/a), \qquad M_\pm(\xi) = K_o(\xi) \pm K_o(\xi d/a) \tag{27}$$

$$T_+(\rho,\tau) = 0, \quad T_-(\rho,\tau) = [2\ \ln(d/a)]^{-1} \tag{28}$$

$$S_\pm(\rho,\tau) = \frac{2\rho}{\pi}\sum_{n=1}^{\infty} \mathrm{Im}\left\{\mathrm{Res}_{p_n^\pm}\left\{\frac{K_1(p\rho)K_o[p\tau\ \exp(-i\pi)]}{K_o(pa) \pm K_o(pd)}\right\}\right\} \tag{29}$$

and $p_n^\pm$ are the solutions of the equation

$$K_o(pa) \pm K_o(pd) = 0 \tag{30}$$

for which $\mathrm{Im}\{p_n^\pm\} > 0$.

Setting $\rho = a$ in (26) and making use of the Wronskian for the modified Bessel functions we arrive at the following expression, which is useful when calculating the induced current on each wire,

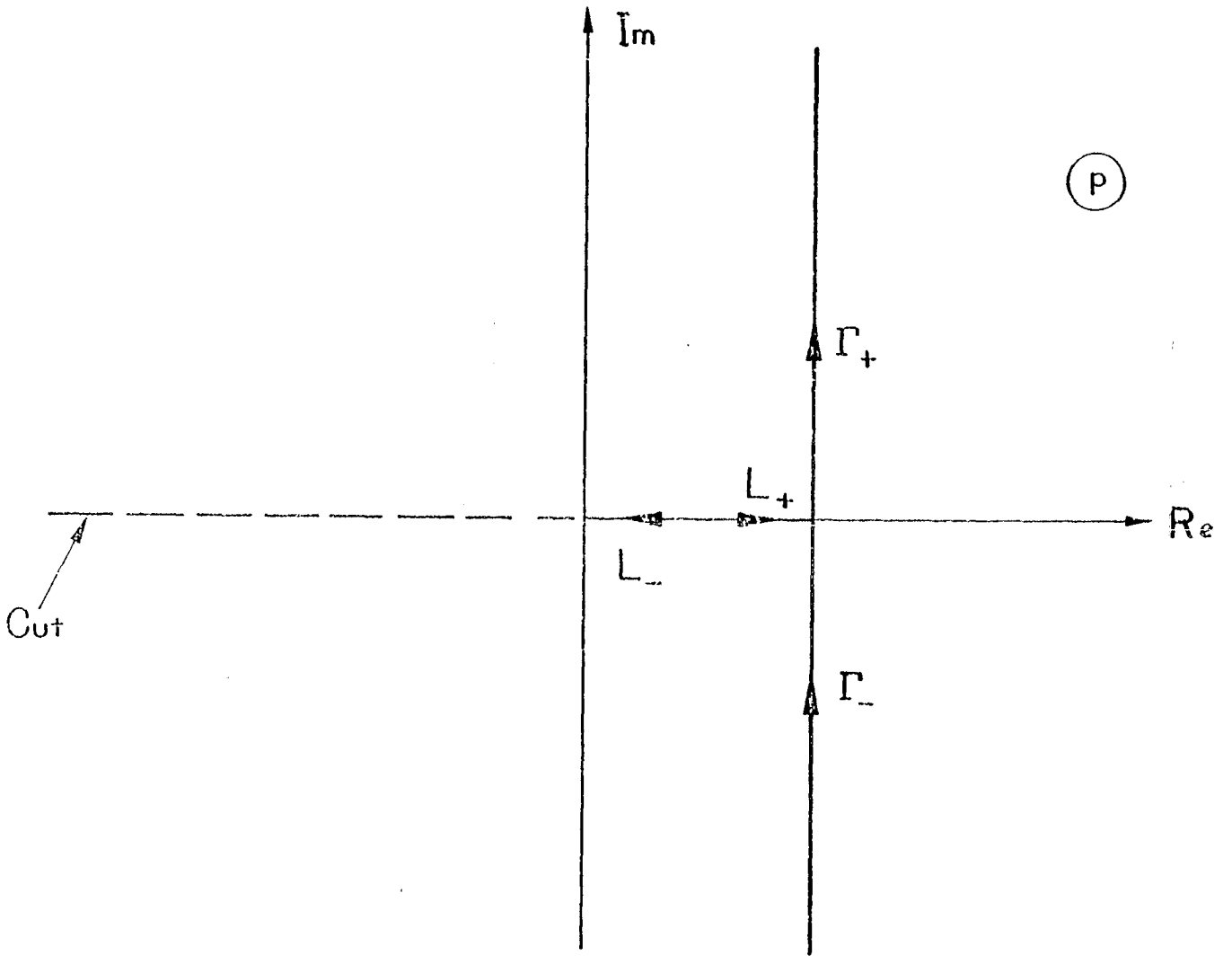

Figure 5. Paths of integration in the complex p-plane. The cut is introduced to make the Bessel functions uniquely determined.

$$R_{\pm}(a,\tau) = \int_0^{\infty} \frac{L_{\pm}(\xi)[1\pm\xi K_1(\xi)I_0(\xi d/a)\pm\xi I_1(\xi)K_0(\xi d/a)]}{\xi M_{\pm}(\xi)[M^2(\xi)+\pi^2 L_{\pm}^2(\xi)]} K_0(\xi\tau/a)d\xi. \qquad (31)$$

The term $R_{\pm}(\rho,\tau)$ in (25) is the combined contribution along the positive and negative real axes, after deforming the paths of integration of the four integrals in (19), respectively, in the fourth, third, first and second quadrant of the complex p-plane and it can be interpreted as due to the continuous part of the spectrum.

The quantity $T_{\pm}(\rho,\tau)$ in (25) is the contribution to $F_{+}(\rho,\tau)$ from a small circle around the origin in the p-plane. From (5) it can be seen that the longitudinal components of both the electric field and the magnetic field associated with $T_{-}(\rho,\tau)$ are zero. Moreover, from (20) and (28) it follows that the current on each wire associated with this term is a step-function wave travelling along the wire. Therefore, the contribution $T(\rho,\tau)$ can be interpreted as the TEM-mode contribution to the total field. A more detailed analysis of this term will be given in Section VII.

Mathematically, the term $S_{+}(\rho,\tau)$ in (25) is due to the poles of $A_{\pm}(p)$. Using the spectral notation, $T_{\pm}(\rho,\tau) + S_{\pm}(\rho,\tau)$ is the contribution from the discrete part of the spectrum. Physically, $S_{\pm}(\rho,\tau)$ can be interpreted as the contribution from the higher-order TM modes to the field. Some properties of each term in the sum will be discussed in Section VI. It should be pointed out here that due to the excitation we have chosen, only transverse magnetic fields (with respect to the z-direction) are generated.

We wish to point out in passing that all the properties of the field in the space-time domain are determined by the analytical properties of the field in the complex p-plane. Thus, when solving transient waveguide problems the complex p-plane plays the same role as the complex frequency (s) plane does in solving transient scattering problems involving finite sized scatterers.

Before we go on with the numerical evaluation of $F_{\pm}(\rho,\tau)$ as given by (25) through (31) we will in the next section determine some analytical properties of $R_{\pm}(\rho,\tau)$ and $S_{\pm}(\rho,\tau)$.

IV. Some Analytical Properties of the Radiated Field

In this section we will determine some of the analytical properties of the radiated field. As we have seen in Section II this is equivalent to investigating the analytical properties of $F_{\pm}(\rho,\tau)$, given by (c.f. (25))

$$F_{\pm}(\rho,\tau) = R_{\pm}(\rho,\tau) + S_{\pm}(\rho,\tau) + T_{\pm}(\rho,\tau) \tag{25'}$$

Since all properties of $T_{\pm}(\rho,\tau)$ are known (c.f. (28)) we only have to investigate the functions $R_{\pm}(\rho,\tau)$ and $S_{\pm}(\rho,\tau)$ and we will start with the asymptotic behavior of $R_{\pm}(\rho,\tau)$ for small values of τ.

A. Asymptotic Behavior of $R_{\pm}(\rho,\tau)$ for Early Time

From (26) it can be shown that $R_{\pm}(\rho,\tau)$ is a continuous function for all $\rho \geq a$ and all $\tau > 0$. We will here investigate $R_{\pm}(\rho,\tau)$ as $\tau \to \rho-a$. Early time for the radiated field can be defined as $\varepsilon = (\tau - \rho + a)/a << 1$. To find the early time behavior of $R_{\pm}(\rho,\tau)$ we split $R_{\pm}(\rho,\tau)$ into two parts,

$$R_{\pm}(\rho,\tau) = R'_{\pm}(\rho,\tau) + R''_{\pm}(\rho,\tau) \tag{32}$$

where

$$\begin{aligned} R'_{\pm}(\rho,\tau) &= \int_0^{\Xi} I_{\pm}(\xi,\rho) K_0(\xi\tau/a)\,d\xi \\ R''_{\pm}(\rho,\tau) &= \int_{\Xi}^{\infty} I_{\pm}(\xi,\rho) K_0(\xi\tau/a)\,d\xi \end{aligned} \tag{33}$$

and

$$I_{\pm}(\xi,\rho) = \frac{\rho}{a} \frac{L_{\pm}(\xi)[L_{\pm}(\xi)K_1(\xi\rho/a)+M_{\pm}(\xi)I_1(\xi\rho/a)]}{M_{\pm}(\xi)[M_{\pm}^2(\xi)+\pi^2 L_{\pm}^2(\xi)]} \tag{34}$$

(c.f. (26)). The quantity Ξ is a finite but large number such that we can use asymptotic expansions of $I_{\pm}(\xi,\rho)$ and $K_0(\xi\tau/a)$, when evaluating $R''_{\pm}(\rho,\tau)$ for $\rho >> a$. Since Ξ is finite it follows that $R'_{\pm}(\rho,\tau)$ is finite for $\rho > a$. Using

asymptotic expansions of the modified Bessel functions we get

$$R''_{\pm}(\rho,\tau) \sim [2ad/(\pi^5\tau\rho)]^{1/2} \int_{\Xi}^{\infty} \{\exp[-\xi(1 + \varepsilon + d/a)] \pm (a/d)^{1/2} \exp[-\xi(\varepsilon + 2\rho/a)]\}\xi^{-1/2}\, d\xi \qquad (35)$$

and it can easily be seen from (35) that $R''_{\pm}(\rho,\tau)$ is finite for all $\varepsilon = (\tau - \rho + a)/a \geq 0$. Thus, $R_{\pm}(\rho,\tau)$ is finite for all times, provided that $\rho >> a$.

Some care has to be exercised in evaluating the asymptotic form of $R_{\pm}(a,\tau)$. In this case we define the early time as $\tau/a = \varepsilon << 1$. For small values of ε we can always find a Ξ such that $\Xi >> 1$ but $\varepsilon\Xi << 1$. Using asymptotic expansions for the integrands in (33) one obtains

$$R'_{\pm}(a,\varepsilon) \sim -\int_0^{\Xi} I_{\pm}(\xi,a)\ln(\xi\varepsilon\Gamma/2)d\xi \sim -\ln\varepsilon \int_0^{\Xi} I_{\pm}(\xi,a)d\xi \qquad (36)$$

and

$$R''_{\pm}(a,\varepsilon) \sim \pi^{-2}(d/\varepsilon)^{1/2} \int_{\Xi}^{\infty} \exp[-\xi(1 + \varepsilon + d/a)]K_0(\varepsilon\xi)d\xi \sim \pi^{-2}(d/\varepsilon)^{1/2} \ln(1 + d/a).$$

From (32) and (36) we get the following early time behavior of $R_{\pm}(a,\tau)$,

$$R_{\pm}(a,\tau) \sim [\pi^{-2} \ln(1 + d/a)]d^{1/2}[(ct)^2 - z^2]^{-1/4} \quad \text{as} \quad ct - z \to 0+. \qquad (37)$$

B. Asymptotic Behavior of $R_{\pm}(\rho,\tau)$ for Late Time

The late time is defined as $\tau >> a$. To estimate $R_{\pm}(\tau,\rho)$ for late time we make use of an integral representation of the Bessel function $K_0(x)$ to get

$$R_{\pm}(\rho,\tau) = \int_0^{\infty} I_{\pm}(\rho,\xi)K_0(\xi\tau/a)d\xi = \int_1^{\infty} (u^2 - 1)^{-1/2}\, du \int_0^{\infty} I_{\pm}(\rho,\xi)\exp(-\xi u\tau/a)d\xi \qquad (38)$$

The analysis presented in Appendix A enables us to derive the following asymptotic expression, valid for large values of τ,

$$\int_0^\infty I_+(\rho,\xi)\exp(-\xi u\tau/a)d\xi = \ln^{-2}(\alpha u\tau) + O[\ln^{-4}(\alpha u\tau)] \tag{39}$$

where $\alpha = 2/[\Gamma(ad)^{1/2}]$ and $\Gamma = 1.781072...$ (the exponential of Euler's constant). Making use of this estimate of the inner integral in (39) and the analysis in Appendix A we get the following late time behavior of $R_\pm(\rho,\tau)$

$$R_+(\rho,\tau) = \frac{1}{4}\ln^{-1}\left[\frac{2\tau}{\Gamma(ad)^{1/2}}\right] + O[\ln^{-2}(\tau)] \quad \text{as} \quad \tau \to \infty. \tag{40}$$

This asymptotic expression can be compared with the result obtained in [5] on the late time behavior of the field of a perfectly conducting, circularly cylindrical antenna excited by a step function delta gap generator.

Similarly, it is easy to show that

$$\int_0^\infty I_-(\rho,\xi)\exp(-\xi u\tau/a)d\xi = 3(d^2 - a^2)[(d^2 - a^2) - 2\rho^2 \ln(d/a)][16 \ln^3(d/a)]^{-1}(u\tau)^{-4} + O[(u\tau)^{-6} \ln(u\tau)] \tag{41}$$

from which it follows that

$$R_-(\rho,\tau) = (d^2 - a^2)[(d^2 - a^2) - 2\rho^2 \ln(d/a)][8 \ln^3(d/a)]^{-1} \tau^{-4} + O(\tau^{-6} \ln \tau) \quad \text{as} \quad \tau \to \infty. \tag{42}$$

C. Some Analytical Properties of $S_-(\rho,\tau)$

We will here investigate the convergence of the sum (29) that defines $S_-(\rho,\tau)$. To do this we split $S_-(\rho,\tau)$ into two parts

$$S_-(\rho,\tau) = \mathrm{Im}\{S'_-(\rho,\tau)\} + \mathrm{Im}\{S''_-(\rho,\tau)\} \tag{43}$$

where

$$S_-'(\rho,\tau) = \sum_{n=1}^{N-1} K_-(p_n^-,\rho,\tau)$$

$$S_-''(\rho,\tau) = \sum_{n=N}^{\infty} K_-(p_n^-,\rho,\tau) \tag{44}$$

$$K_-(p_n^-,\rho,\tau) = (2\rho/\pi)\underset{p_n^-}{\text{Res}}\{K_1(p\rho)K_o[p\tau\exp(-i\pi)]/[K_o(pa) - K_o(pb)]\} \tag{45}$$

The quantities p_n^- are given by the solutions of

$$K_o(pa) - K_o(pd) = 0 \tag{46}$$

for which $\text{Im}\{p_n^-\} > 0$ and N is chosen so that $|p_N^- a| >> 1$. In Appendix B it is shown that all the solutions, p_n^-, of equation (46) are located within a band around the imaginary axis and that for $n > N$ we have

$$p_n^- d = i2\pi n/(1 - \delta) + \ln \delta/[2(1 - \delta)] - i(1 - \delta)/(16\pi n) + O(n^{-2}) \tag{47}$$

where $\delta = a/d$. Using this asymptotic expression it is easy to show that p_n^- is a simple zero of (46) for $n > N$. After some lengthy and tedious algebraic manipulations we get the following asymptotic expression, valid for $n > N$,

$$K_-(p_n^-,\rho,\tau) = A(\rho,\tau)(2\pi n)^{-1/2}\exp(i2\pi nT)[1 + B(\rho,\tau)/(2\pi n) + O(n^{-2})] \tag{48}$$

where

$$A(\rho,\tau) = (1 + i)\{\rho/[\pi\tau(1 - \delta)]\}^{1/2}\ \delta^{T/2}$$

$$B(\rho,\tau) = i[\tfrac{1}{4}\ln\delta - (1 - \delta)/8 - (1 - \delta)^2\ T/(8\delta) - (1 - \delta)d(3\tau + \rho)/(\rho\tau)] \tag{49}$$

and

$$T = T(\rho,\tau) = (\tau - \rho + d)/(d - a).$$

Here, T can be interpreted as a normalized time, and $T \to 1$ as $\tau \to 0$. Thus, we have

$$S''_{-}(\rho,\tau) = A(\rho,\tau)S_{-}(T,0,N) + A(\rho,\tau)B(\rho,\tau)S_{-}(T,1,N) + O(N^{-3/2}) \qquad (50)$$

where

$$S_{-}(T,m,N) = \sum_{n=N}^{\infty} (2\pi n)^{-m-1/2} \exp(i2\pi nT). \qquad (51)$$

In reference [10] the following integral representation of $S_{-}(T,m,N)$ has been derived,

$$S_{-}(T,m,N) = I(T,m,2N) \qquad (52)$$

where

$$I(T,m,M) = [\Gamma(m - \tfrac{1}{2})]^{-1} \exp(i\pi MT) \int_0^{\infty} \{x^{m-1/2} \exp(-\pi Mx)/[1 - \exp(i2\pi T - 2\pi x)]\}dx \qquad (53)$$

and $\Gamma(z)$ is the complete Γ-function[16]. Moreover,

$$S_{-}(T,m,N) = S_{-}(T,m,1) - R_{-}(T,m,N) \qquad (54)$$

where

$$R_{-}(T,m,N) = \sum_{n=1}^{N-1} (2\pi n)^{-m-1/2} \exp(i2\pi nT) \qquad (55)$$

and $R_{-}(T,m,N)$ is finite for all values of T. The integral that defines $S_{-}(T,m,1)$ can be evaluated by the method of residues[10]

$$S_{-}(T,m,1) = [4\Gamma(m + \tfrac{1}{2})]^{-1} \sum_{k=0}^{\infty} \varepsilon_k |T - k|^{m-1/2} \exp[-i(m - \tfrac{1}{2})(\pi/2)\mathrm{sgn}(T - k)]$$

$$+ |T + k|^{m-1/2} \exp[-i(m - \tfrac{1}{2})(\pi/2)\mathrm{sgn}(T + k)] \qquad (56)$$

where $\varepsilon_o = 1$ and $\varepsilon_k = 2$, $k \geq 1$ and $\text{sgn}(x) = -1$ for $x < 0$ and $\text{sgn}(x) = 1$ for $x > 0$. The sum (56) is absolutely convergent for all values of T when $m \geq 1$ and it is absolutely convergent for $m = 0$ provided that $T \neq n$, $n = 0, \pm 1, \pm 2, \ldots$ From (56) we can derive the following asymptotic expression for $S_-(T,0,1)$ that is valid when T is in a neighborhood of n.

$$S_-(T,0,1) = \frac{1}{2}\pi^{-1/2} \exp[i\pi/4 \ \text{sgn}(T - n)]|T - n|^{-1/2} + O(1). \quad (57)$$

From (43) through (57) it can be seen that $S_-(\rho,\tau)$ is a continuous function of τ and ρ except at $\tau - \rho + a = n(d - a)$, n being an integer. In order to investigate $S_-(\rho,\tau)$ around its singularities we introduce ε defined by $\varepsilon = [\tau - \rho + a - n(d - a)]/a$ and $|\varepsilon| << 1$. Equation (57) then enables us to get the following asymptotic expression for $S_-(\rho,\tau)$, valid in a neighborhood of $\tau - \rho = n(d - a) - a$ when $n \neq 1$,

$$S_-(\rho,\tau) = \begin{cases} O(1), & |\varepsilon| << 1 \text{ and } \varepsilon < 0 \\ [\rho\delta^n/(2\pi|\rho - a - na\ nd|)]^{1/2}\ \varepsilon^{-1/2} + O(1), & |\varepsilon| << 1 \text{ and } \varepsilon > 0. \end{cases} \quad (58)$$

For $n = 1$ we have

$$S_-(\rho,\tau) = \begin{cases} O(1), & |\varepsilon| << 1 \text{ and } \varepsilon < 0 \\ \{\rho/[2\pi(\rho - a)]\}^{1/2}\ \varepsilon^{-1/2} + O(1), & |\varepsilon| << 1 \text{ and } \varepsilon > 0 \end{cases} \quad (59)$$

provided that $\rho - a >> a$. For $n = 1$ and $\rho = a$ we have

$$S_-(\rho,\tau) = \begin{cases} O(1), & |\varepsilon| << 1 \text{ and } \varepsilon < 0 \\ (2\pi)^{-1/2}\ \varepsilon^{-1}, & |\varepsilon| << 1 \text{ and } \varepsilon > 0. \end{cases} \quad (60)$$

D. Some Analytical Properties of $S_+(\rho,\tau)$

We will here investigate the sum that defines $S_+(\rho,\tau)$, by following the procedure used in the analysis of $S_-(\rho,\tau)$. Thus,

$$S_+(\rho,\tau) = \mathrm{Im}\{S'_+(\rho,\tau)\} + \mathrm{Im}\{S''_+(\rho,\tau)\} \tag{61}$$

where

$$S'_+(\rho,\tau) = \sum_{n=1}^{N-1} K_+(p_n^+,\rho,\tau)$$

$$S''_+(\rho,\tau) = \sum_{n=N}^{\infty} K_+(p_n^+,\rho,\tau) \tag{62}$$

and

$$K_+(\gamma_n^+,\rho,\tau) = (2\rho/\pi)\mathrm{Res}_{p_n^+}\{K_1(p\rho)K_o[p\tau\exp(-i\pi)]/K_o(pa) - K_o(pd)]\} . \tag{63}$$

The quantities p_n^+ are given by the solutions of

$$K_o(\rho a) + K_o(pd) = 0 \tag{64}$$

for which $\mathrm{Im}\{p_n^+\} > 0$, and N is such that $|p_N^+ a| >> 1$. In Appendix B it is shown that we have the following asymptotic form of p_n^+, valid for $n > N$,

$$p_n^+ d = i\pi(2n - 1)/(1 - \delta) + \ln \delta/[2(1 - \delta)] - i(1 - \delta)/[8\pi(2n - 1)] + O(n^{-2}). \tag{65}$$

From (65) we can derive the following asymptotic expression for $K_+(p_n^+ d)$, valid for large n,

$$K_+(p_n^+,\rho,\tau) = -A(\rho,\tau)[\tau(2n - 1)]^{-1/2}\exp[i\pi(2n - 1)T]\{1 + B(\rho,\tau)/[\pi(2n - 1)] + O(n^{-2})\} \tag{66}$$

where $A(\rho,\tau)$, $B(\rho,\tau)$ and $T = T(\rho,\tau)$ are given by (49). Equation (66) enables us to get the following asymptotic representation of $S''_{+}(\rho,\tau)$,

$$S''_{+}(\rho,\tau) = -A(\rho,\tau)S_{+}(T,0,N) - A(\rho,\tau)B(\rho,\tau)S_{+}(T,1,N) + O(N^{-3/2}) \quad (67)$$

where

$$S_{+}(T,m,N) = \sum_{n=N}^{\infty} [\pi(2n - 1)]^{-m-1/2} \exp[i\pi(2n - 1)T]. \quad (68)$$

We also have the integral representation of $S_{+}(T,m,N)$,

$$S_{+}(T,m,N) = I(T,m,2N - 1) \quad (69)$$

where $I(T,m,M)$ is given by (53). From (61) through (69) it can be shown that $S_{+}(\rho,\tau)$ is a continuous function of τ and ρ except at $\tau = \rho - a + n(d - a)$, where n is an integer. In the vicinity of its singularities, i.e., when $\tau - \rho + a - n(d - a) = \varepsilon a$ we have

$$S_{+}(\rho,\tau) = \begin{cases} O(1), & |\varepsilon| << 1 \text{ and } \varepsilon < 0 \\ (-1)^{n+1}[\rho\delta^{n}/(2\pi|\rho - a - na - nd|)]^{1/2}\ \varepsilon^{-1/2} + O(1), & |\varepsilon| << 1 \text{ and } \varepsilon > 0 \end{cases} \quad (70)$$

except for $n = 1$ and $\rho = a$ in which case we have

$$S_{+}(a,\tau) = \begin{cases} O(1), & |\varepsilon| << 1 \text{ and } \varepsilon < 0 \\ (2\pi)^{-1/2}\ \varepsilon^{-1}, & |\varepsilon| << 1 \text{ and } \varepsilon > 0. \end{cases} \quad (71)$$

E. Some Analytical Properties of $F_{\pm}(\rho,\tau)$

To sum up, we have shown in this section that $F_{\pm}(\rho,\tau)$ is a continuous function of ρ and τ, $\rho \geq a$ and $\tau > 0$ except at $\tau - \rho + a = n(d - a)$, n nonnegative integer, where $F_{\pm}(\rho,\tau)$ has a square root singularity. These

singularities occur because of the assumption of the delta-gap generator. For $a \ll d$ these singularities occur at $\tau - \rho \approx nd$. Physically, they can be understood as being due to the wavefront being reflected at one of the two wires (see Figure 6). The strength of these singularities is proportional to $(a/d)^n$ so they are very weak for thin wires. If we had replaced the delta gap by a feeding gap of finite width Δ the field would have been finite for all times. However, if $\Delta/a \ll 1$ maxima and minima would occur in the field around $T = n$. These extreme values will be more pronounced the smaller Δ/a is and the smaller n is.

For early time, defined as $\tau - \rho + a = \varepsilon a$, $\varepsilon \ll 1$, we have from (15), (38), (58), (59), (60), (70), and (71)

$$\rho Z_o H_\ell(\rho_\ell, z, t) \sim \frac{1}{\pi\sqrt{2}} \sqrt{\frac{\rho}{\rho - a}} \frac{1}{\sqrt{\varepsilon}} V_\ell, \qquad \rho \gg a, \qquad \ell = 1,2 \tag{72}$$

and

$$I_\ell(z,t) \sim \frac{2a}{\sqrt{(ct)^2 - z^2}} \frac{V_\ell}{Z_o}, \qquad ct - z \to 0+, \tag{73}$$

which, of course, agree with the asymptotic forms derived previously[6] for one wire. Unfortunately these asymptotic expansions are only valid for early times in a time scale using a/c as a unit and hence for a very short time compared to the transient time between the wires.

Since $\mathrm{Re}\{p_n^{\pm}\} < 0$ it follows immediately from (45) and (63) that each term, $K_{\pm}(p_n^{\pm}, \rho, \tau)$, in $S_{\pm}(\rho,\tau)$ is exponentially attenuated so that for τ large and $\tau - \rho + a \neq n(d - a)$, we have

$$F_{\pm}(\rho,\tau) \sim R_{\pm}(\rho,\tau) + T_{\pm}(\rho,\tau). \tag{74}$$

Thus,

$$F_+(\rho,\tau) \sim 1/\ln[4\tau^2/(\Gamma^2 ad)]$$

$$F_-(\rho,\tau) \sim [2\ln(d/a)]^{-1} + (d^2 - a^2)[(d^2 - a^2) - 2\rho^2 \ln(d/a)][8\ln^3(d/a)]^{-1} \tau^{-4} \tag{75}$$

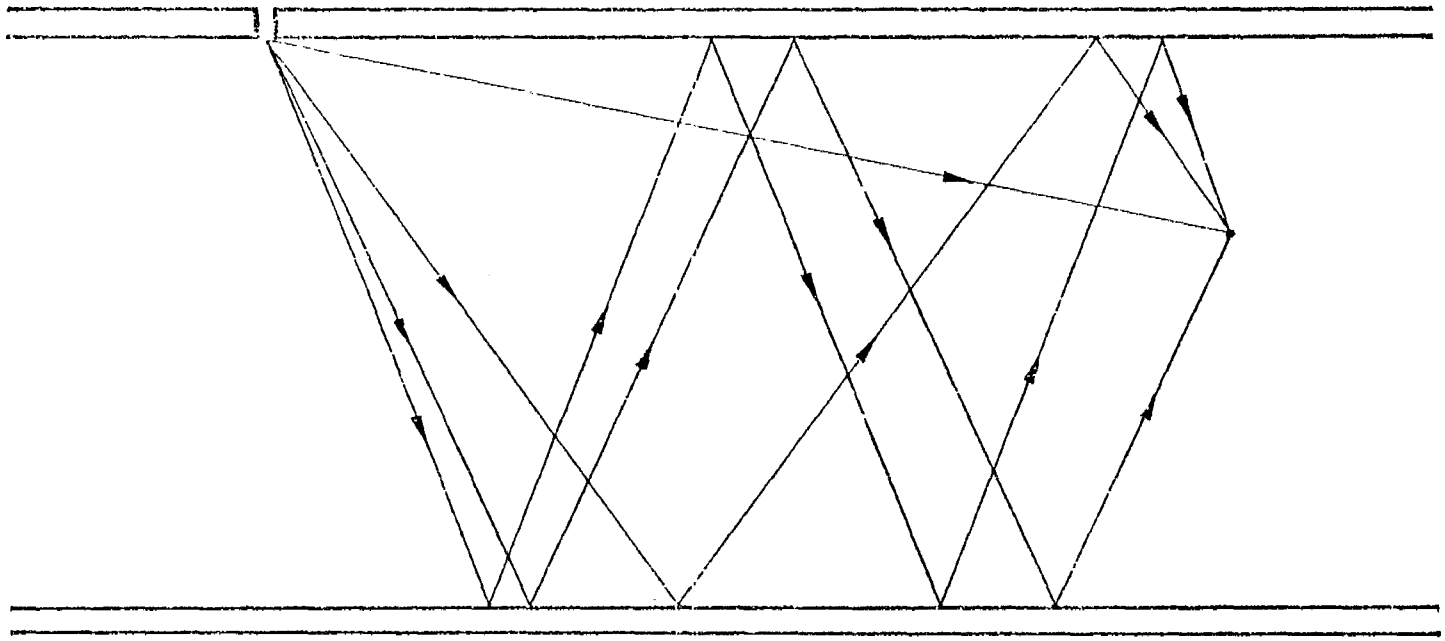

Figure 6. A ray model describing the reflections of the wavefront.

as $\tau \to \infty$. The expression (75) for $F_+(\rho,\tau)$ can be compared with the late-time expression for the transverse magnetic field of an infinitely long, perfectly conducting, cylindrical antenna excited by a step function slice generator [5]. It can also be seen from the asymptotic form (75) of $F_-(\rho,\tau)$ that the TEM mode quickly becomes the dominant part of the field when the two wires are fed unsymmetrically, i.e., when $V_2 = -V_1$, so that $V_+ = 0$ and $V_- = V_1 = -V_2$.

V. An Alternative Representation of $F_{\pm}(\rho,\tau)$

In this section we will derive an alternative representation of $F_{+}(\rho,\tau)$ which is useful for early time computations. We begin with (24):

$$F_{\pm}(\rho,\tau) = (2\pi i)^{-1} \int_{\Gamma} \rho K_1(p\rho) I_o(p\tau)/[K_o(pa) \pm K_o(pd)]\,dp \qquad (76)$$

The asymptotic expression of the modified Bessel functions implies that there exists a $p_r > 0$ such that $|K_o(pd)/K_o(pa)| < 1$ when $\mathrm{Re}\{p\} > p_r$. We now choose the path of integration, Γ, in (61) such that $\mathrm{Re}\{p\} > p_r$ when p belongs to Γ. The following series expansion is valid,

$$F_{\pm}(\rho,\tau) = \sum_{m=0}^{\infty} (2\pi i)^{-1} \varepsilon_{\pm}^{m} \rho \int_{\Gamma} K_1(p\rho) I_o(p\tau) K_o^m(pd)/K_o^{m+1}(pa)\,dp \qquad (77)$$

where $\varepsilon_{\pm} = \mp 1$. Since the integrand in (77) has no singularities to the right of Γ and since

$$K_1(p\rho) I_o(p\tau) K_o^m(pd)/K^{m+1}(pa) \sim \exp\{-p[\rho - a - \tau - m(d - a)]\} \quad \text{as } p \to \infty$$

in the right half plane it follows that

$$F_{\pm}(\rho,\tau) = \sum_{m=0}^{M} (2\pi i)^{-1} \varepsilon_{\pm}^{m} \rho \int_{\Gamma} K_1(p\rho) I_o(p\tau) K_o^m(pd)/K_o^{m+1}(pa)\,dp \qquad (78)$$

where $M = M(\rho,\tau) = \mathrm{int}\{\tau - \rho + a)/(d - a)\}$ and $\mathrm{int}\{x\}$ denotes the integer part of x. For $\tau - \rho + a < d - a$ we have

$$F_{+}(\rho,\tau) = F_{-}(\rho,\tau) = (2\pi i)^{-1} \rho \int_{\Gamma} K_1(p\rho) I_o(p\tau)/K_o(pa)\,dp \qquad (79)$$

and in this case the electromagnetic field around the two wires is the same as from two noninteracting, cylindrical antennas[5].

The integral in (78) can be transformed into a real integral by employing the methods used in Section III. Thus,

$$F_{\pm}(\rho,\tau) = \sum_{m=0}^{M} \pi^{-2}\, \rho\varepsilon_{\pm}^{m} \int_{o}^{\infty} H_{\pm}(\rho,\tau,\xi,m)d\xi \tag{80}$$

where

$$H_{\pm}(\rho,\xi,m) = K_1(\xi\rho)K_o^m(\xi d)K_o^{-m-1}(\xi a)K_o(\xi\tau)$$

$$-\mathrm{Re}\{[K_1(\xi\rho) + \pi i I_1(\xi\rho)][K_o(\xi\rho) - \pi i I_o(\xi\rho)]^m[K_o(\xi a)$$

$$-\pi i I_o(\xi a)]^{-m-1}\, K_o(\xi\tau)\} \tag{81}$$

For m = 0 this expression reduces to the one given in [5]. Each term in the sum (80) has a square-root singularity at its "turn-on time", i.e.,

$$\pi^{-2}\, \rho\varepsilon_{\pm}^{m} \int_{o}^{\infty} H_{\pm}(\rho,\tau,\xi,m)d\xi \sim \varepsilon_{\pm}^{m+1}[\rho(a/d)^m/(2\pi|\rho - a - ma - md|)]^{1/2}\, \varepsilon^{-1/2} \tag{82}$$

where $\varepsilon = \tau-\rho + a - m(d - a)$, and $0 < \varepsilon << 1$. This is the same singularity that was derived from another representation in Section V. Physically, the singularities can be understood as due to reflections of the wavefront at each wire when using a δ-gap generator. The time at which the different reflections of the wavefront arrive at a point can be determined from a ray model of the wavefront (see Figure 6).

The representation (78) is useful mostly for earlier times, i.e., for $\tau - \rho < 3d$. It is especially useful for $\tau - \rho < d$ when the two wires radiate like two independent wires in free space. The representation (25) is useful mostly for later times, i.e., $\tau - \rho > 3d$. It is especially useful for late times when the wires are fed in a push-pull manner so that the TEM mode is the dominant part of the electromagnetic field.

In the next section we will present some numerical results that were obtained from the theory outlined in Sections II through V.

VI. The Time History of the Field

In this section we will present the numerical results obtained from the theory outlined in Sections II through V.

A. Solution of $K_o(pa) \pm (K_o(pd)$

The roots, $p_n^{\pm}$, of the equations

$$K_o(pa) \pm K_o(pd) = 0 \tag{30'}$$

were found numerically and the results of these numerical calculations are presented in Figure 7 and Tables 1 and 2. As a comparison we have also included in Table 1 and 2 the asymptotic expressions of $p_n^{\pm}$ as given by equations (47) and (65). It is observed that the larger a/d is the faster the solution of (30) converges to the asymptotic expressions (47) and (65). This is obvious since the asymptotic expressions (47) and (65) are derived under the assumption that $p_n^{\pm}a >> 1$. We also observe that the absolute value of the real part of $p_n^{\pm}$ is a monotonically decreasing function of a/d, and all the $p_n^{\pm}$ belong to one branch for fixed a/d.

B. The Time History of the Current on Each Wire

The time history of the current along each wire can be determined from the two functions $F_-(a,\tau)$ and $F_+(a,\tau)$ (c.f. (20)). These two functions were evaluated numerically by using the representation (25) of $F_{\pm}(a,\tau)$. The integral (26) was evaluated by using a Gaussian quadrature formula, and in evaluating the sum (29) the asymptotic expressions (50) and (67) were used with N = 12. From the representation (79) it is noted that[5]

$$F_-(a,\tau) = F_+(a,\tau) = \int_o^{\infty} \frac{I_o(\xi)K_o(\xi\tau/a)}{\xi K_o(\xi)[K_o^2(\xi)+\pi^2 I_o^2(\xi)]}\, d\xi, \qquad \tau < d - a \tag{83}$$

and this function is tabulated in [18]. Equation (83) provided a good check on the numerical calculations and agreement within .5% between the results reported in [18] and our numerical results was found for $.5 < \tau/d < .99 - a/d$.

In Figures 8 through 11 we have graphed the τ-dependence of the two quantities $I_-(\tau)$ and $I_+(\tau)$,

$$I_\pm(\tau) = 2\pi F_\pm(a,\tau) \tag{84}$$

for a/d = .1, .01, .001. In order to show the strength of each singularity we have graphed the functions $I_-(\tau)$ and $I_+(\tau)$ for $n(d - a) + .01 < \tau < (n+1)(d - a)$, n being a nonnegative integer. It can be seen from the graphs that the singularities are very weak when a/d < .01.

The time history of the current at different points on each wire can be determined from $I_-(\tau)$ and $I_+(\tau)$. The currents due to two step functions of arbitrary amplitude and polarization can be obtained by superposition of two cases, namely, (1) when $V_1 = -V_2 = V_o$, i.e., $V_- = V_o$ and $V_+ = 0$ (push-pull) and (2) when $V_1 = V_2 = V_o$, i.e., $V_- = 0$ and $V_+ = V_o$ (push-push). From symmetry considerations it is clear that when the wires are fed in a push-pull manner we have

$$I_1(z,t) = -I_2(z,t) = I_-(z,t) \tag{85}$$

where $I_1(z,t)$ denotes the current on the upper wire and $I_2(z,t)$ the current on the lower wire. Similarly, symmetry considerations imply that

$$I_1(z,t) = I_2(z,t) = I_+(z,t) \tag{86}$$

when the wires are excited in a push-push manner. In Figures 12 through 17 we have graphed $I_\pm(z,t)$ as a function of t for z = 0, 1, 2, 5 and a/d = .1, .01, .001. From these graphes one observes that the larger the distance z is and the smaller a/d is the sooner the current approaches the late time behavior. In the push-pull excitation one quantity of interest is the elaps time, t', between the arrival time of the current wavefront at a given observation point and the time when the current at the same point has decayed to less than 10% of the TEM field. Of course this time can be determined from the smallest τ such that $|I_-(\tau) - I_-(\infty)|/I_-(\infty) < .1$. Figure 18 shows the variation of t' with z for a/d = .1, .01, .001.

Table 1. The roots, $\bar{p}_n$, of the equation $K_o(pa) - K_o(pd) = 0$.

The quantity $\bar{p}_{na}$ is the asymptotic form given by (47).

a/d	n	Re{$\bar{p}_n$d}	Im{$\bar{p}_n$d}	Re{$\bar{p}_{na}$d}	Im{$\bar{p}_{na}$d}
.1	1	-1.232	6.85	-1.279	6.96
	2	-1.261	13.88	-1.279	13.95
	3	-1.270	20.89	-1.279	20.94
	4	-1.273	27.88	-1.279	27.92
	5	-1.275	34.87	-1.279	34.90
	6	-1.276	41.86	-1.279	41.88
	7	-1.277	48.84	-1.279	48.87
	8	-1.278	55.83	-1.279	55.85
	9	-1.278	62.81	-1.279	62.83
	10	-1.278	69.80	-1.279	69.81
	11	-1.278	76.78	-1.279	76.79
	12	-1.278	83.76	-1.279	83.77
.01	1	-1.923	5.94	-2.326	6.33
	2	-2.061	12.38	-2.326	12.68
	3	-2.129	18.78	-2.326	19.03
	4	-2.171	25.16	-2.326	25.38
	5	-2.199	31.53	-2.326	31.73
	6	-2.219	37.89	-2.326	38.08
	7	-2.235	44.25	-2.326	44.42
	8	-2.247	50.61	-2.326	50.77
	9	-2.257	56.97	-2.326	57.12
	10	-2.265	63.33	-2.326	63.46
	11	-2.272	69.68	-2.326	69.81
	12	-2.277	76.04	-2.326	76.16
.001	1	-2.394	5.68	-3.457	6.27
	2	-2.608	12.06	-3.457	12.57
	3	-2.725	18.39	-3.457	18.86
	4	-2.808	24.71	-3.457	25.15
	5	-2.867	31.02	-3.457	31.44
	6	-2.915	37.33	-3.457	37.73
	7	-2.953	43.63	-3.457	44.02
	8	-2.986	49.94	-3.457	50.31
	9	-3.014	56.24	-3.457	56.60
	10	-3.038	62.54	-3.457	62.89
	11	-3.060	68.83	-3.457	69.18
	12	-3.079	75.13	-3.457	75.47

Table 2. The roots, p_n^+, of the equation $K_o(pa) + K_o(pd) = 0$.

The quantity p_{na}^+ is the asymptotic form given by (65).

a/d	n	Re{$p_n^+ d$}	Im{$p_n^+ d$}	Re{$p_{na}^+ d$}	Im{$p_{na}^+ d$}
.1	1	-1.178	3.27	-1.279	3.46
	2	-1.251	10.37	-1.279	10.46
	3	-1.267	17.39	-1.279	17.45
	4	-1.271	24.38	-1.279	24.43
	5	-1.274	31.38	-1.279	31.41
	6	-1.276	38.37	-1.279	38.39
	7	-1.277	45.35	-1.279	45.38
	8	-1.277	52.34	-1.279	52.36
	9	-1.278	59.32	-1.279	59.34
	10	-1.278	66.31	-1.279	66.32
	11	-1.278	73.29	-1.279	73.30
	12	-1.278	80.27	-1.279	80.28
	13	-1.278	87.25	-1.279	87.26
.01	1	-1.762	2.64	-2.326	3.13
	2	-2.007	9.17	-2.326	9.51
	3	-2.100	15.58	-2.326	15.86
	4	-2.150	21.97	-2.326	22.21
	5	-2.186	28.34	-2.326	28.56
	6	-2.210	34.71	-2.326	34.90
	7	-2.228	41.07	-2.326	41.25
	8	-2.241	47.43	-2.326	47.60
	9	-2.252	53.79	-2.326	53.94
	10	-2.261	60.15	-2.326	60.29
	11	-2.268	66.51	-2.326	66.64
	12	-2.274	72.86	-2.326	72.98
	13	-2.280	79.21	-2.326	79.33
.001	1	-2.177	2.40	-3.457	3.10
	2	-2.520	8.88	-3.457	9.42
	3	-2.674	15.23	-3.457	15.72
	4	-2.767	21.55	-3.457	22.01
	5	-2.839	27.87	-3.457	28.30
	6	-2.892	34.18	-3.457	34.59
	7	-2.935	40.48	-3.457	40.88
	8	-2.970	46.78	-3.457	47.17
	9	-3.000	53.09	-3.457	53.46
	10	-3.027	59.39	-3.457	59.75
	11	-3.049	65.69	-3.457	66.04
	12	-3.070	71.98	-3.457	72.33
	13	-3.088	78.28	-3.457	78.62

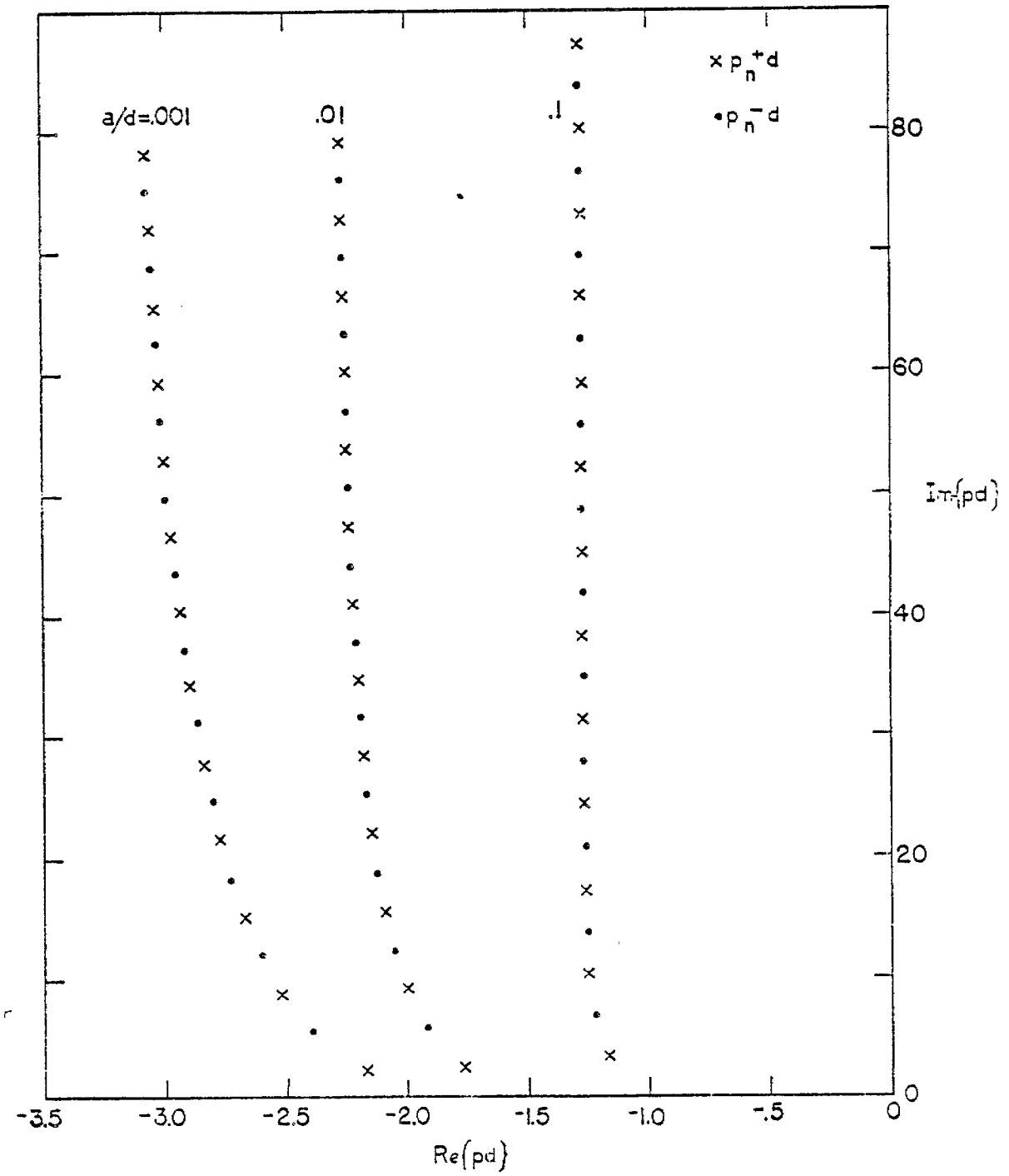

Figure 7. The roots of the equations $K_o(pa) \pm K_o(pd) = 0$.

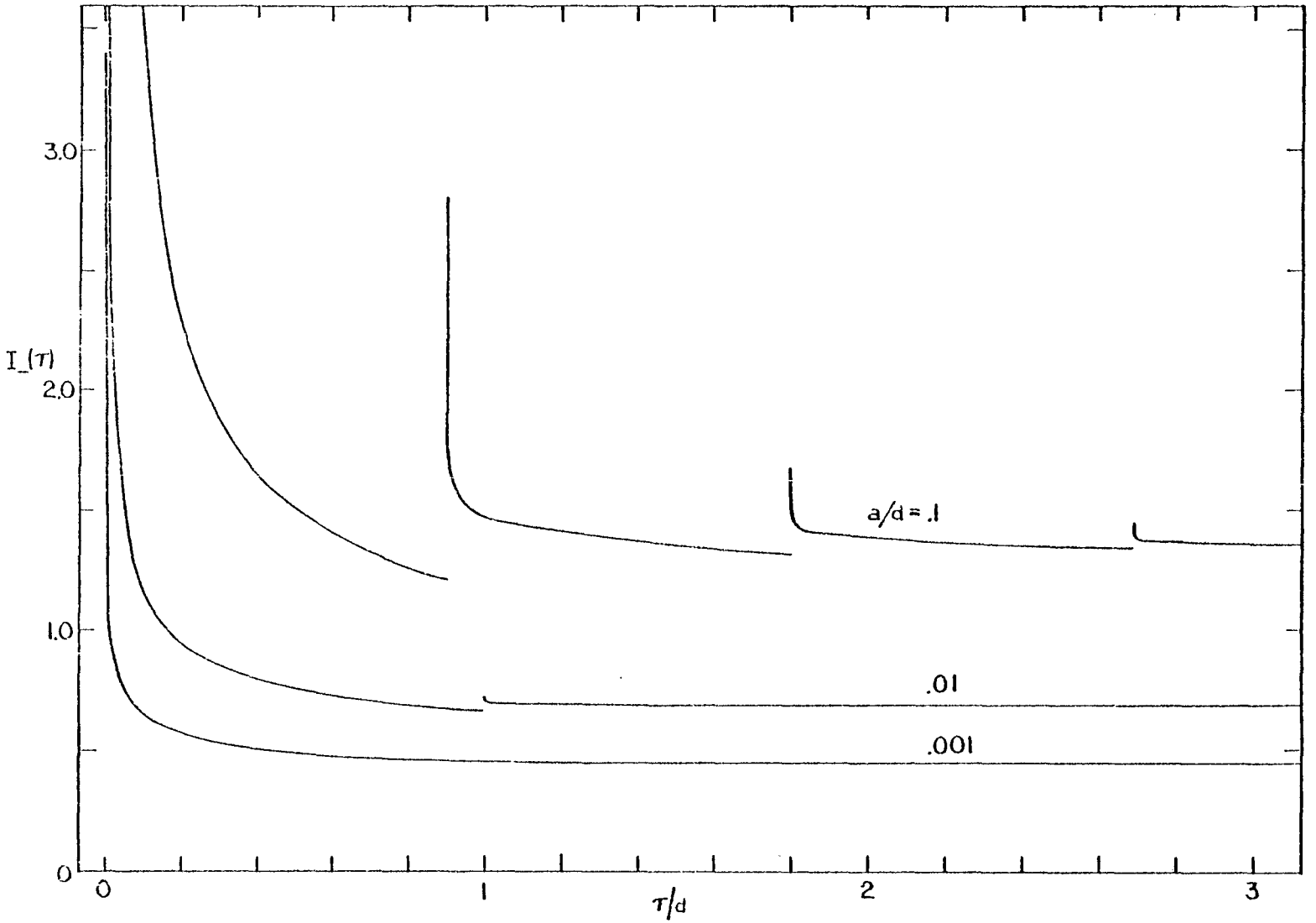

Figure 8. The function $I_-(\tau)$ for $n(d - a) + .01 < \tau < (n + 1)(d - a)$, $n = 0,1,2$.

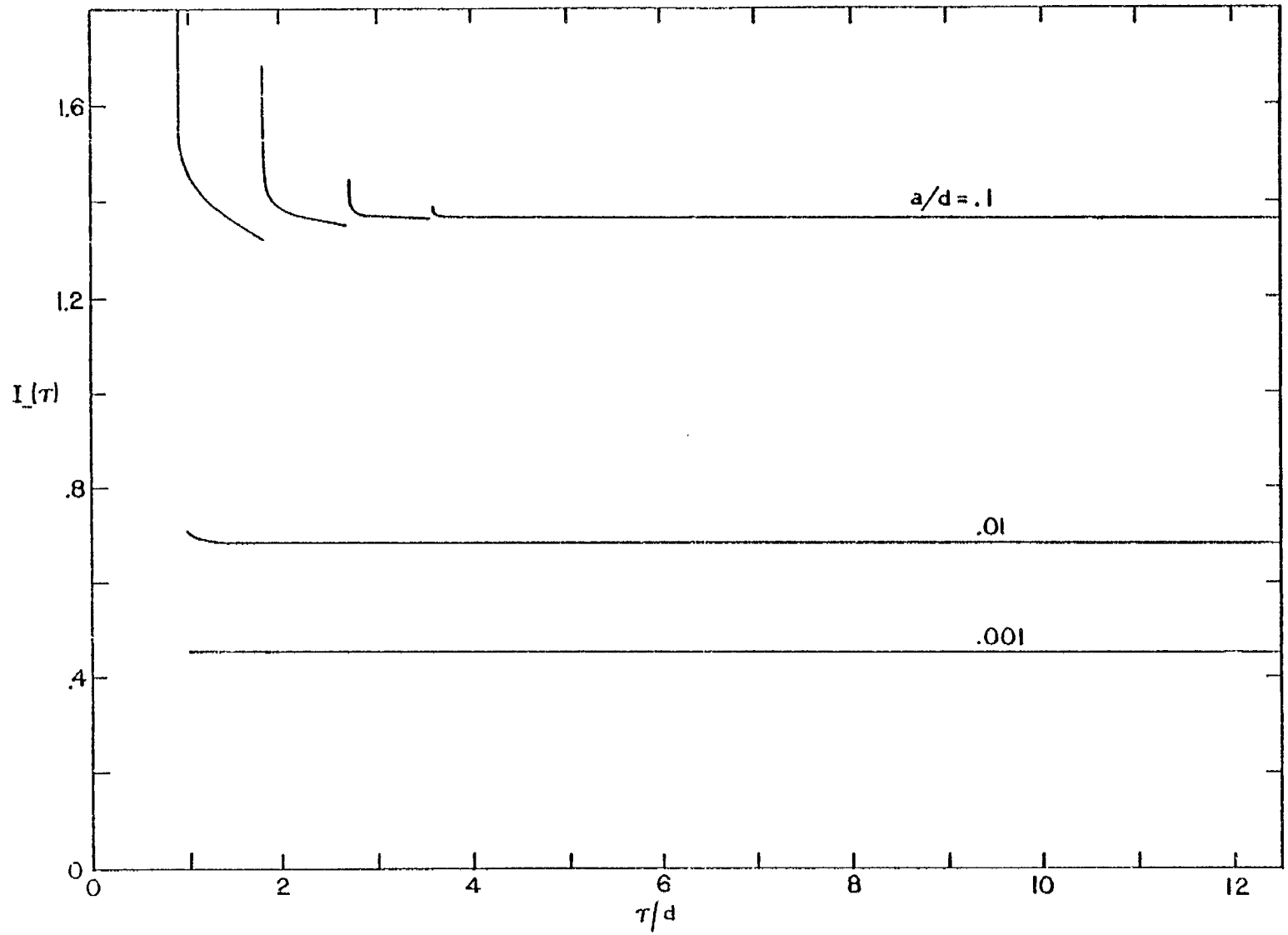

Figure 9. The function $I_{-}(\tau)$ for $n(d - a) + .01 < \tau < (n + 1)(d - a)$, $n = 1,2,\ldots,11,12$.

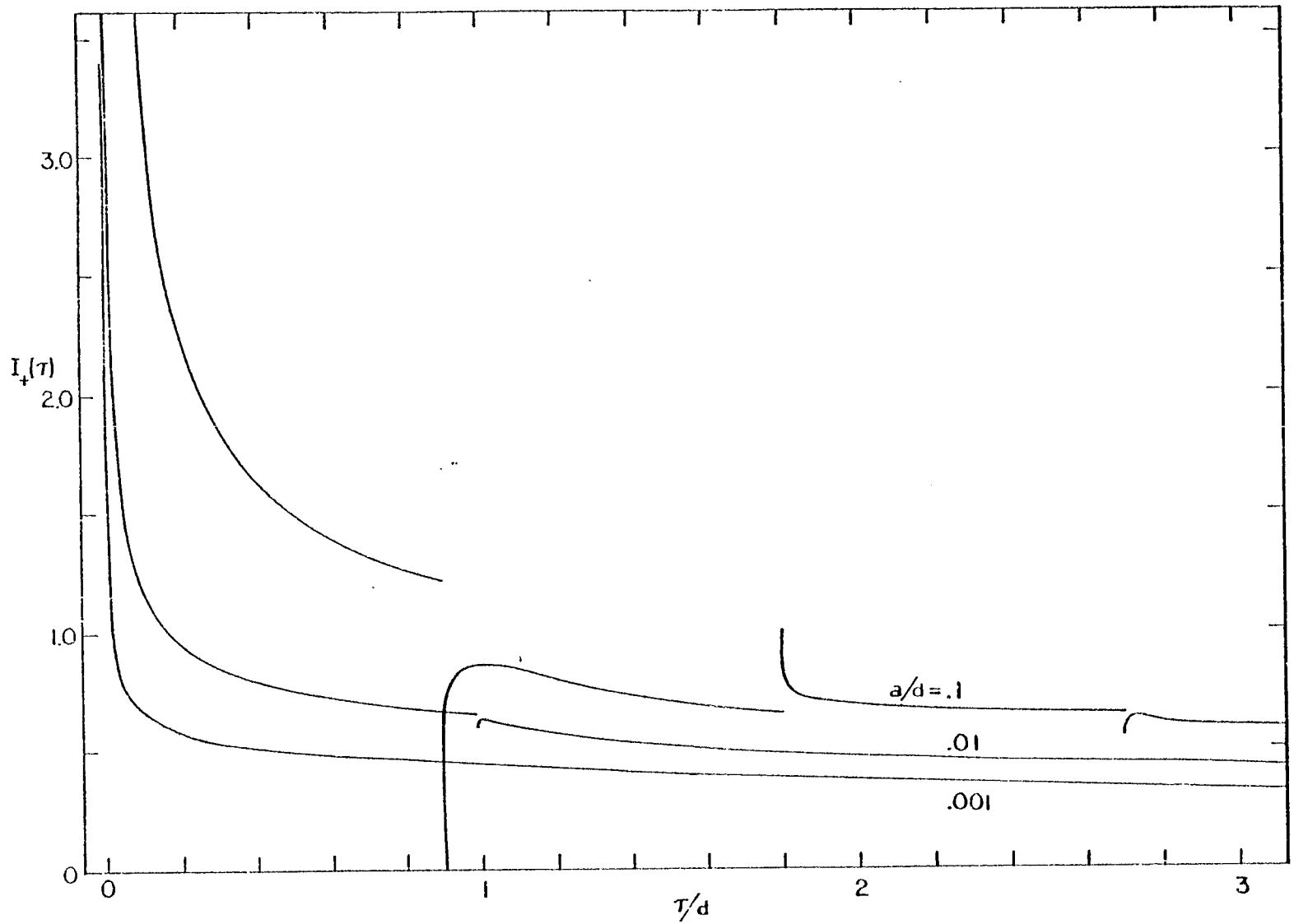

Figure 10. The function $I_+(\tau)$ for $n(d - a) + .01 < \tau < (n + 1)(d - a)$, $n = 0,1,2$.

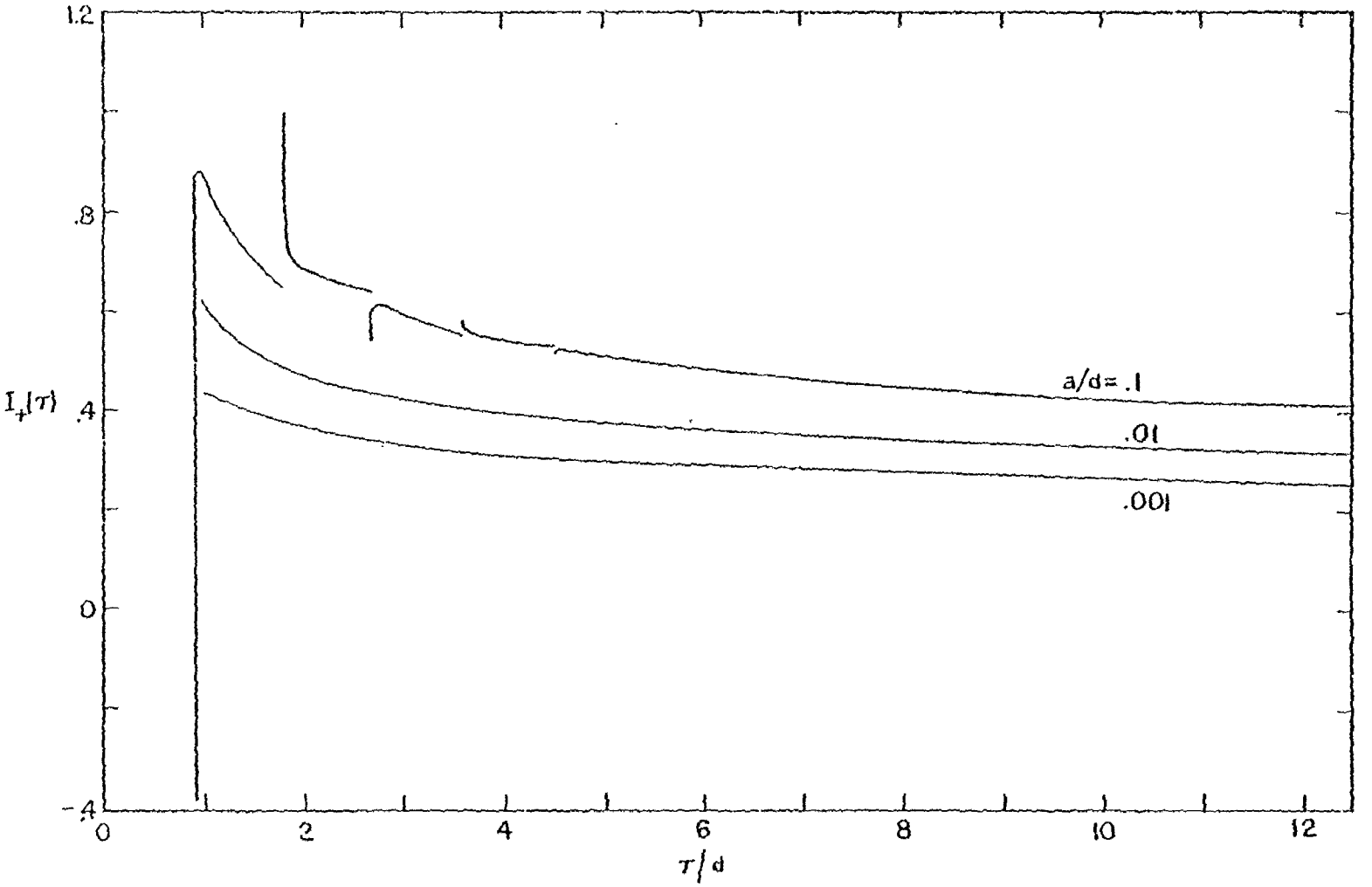

Figure 11. The function $I_+(\tau)$ for $n(d-a)+.01 < \tau < (n+1)(d-a)$, $n = 1,2,\ldots,11,12$.

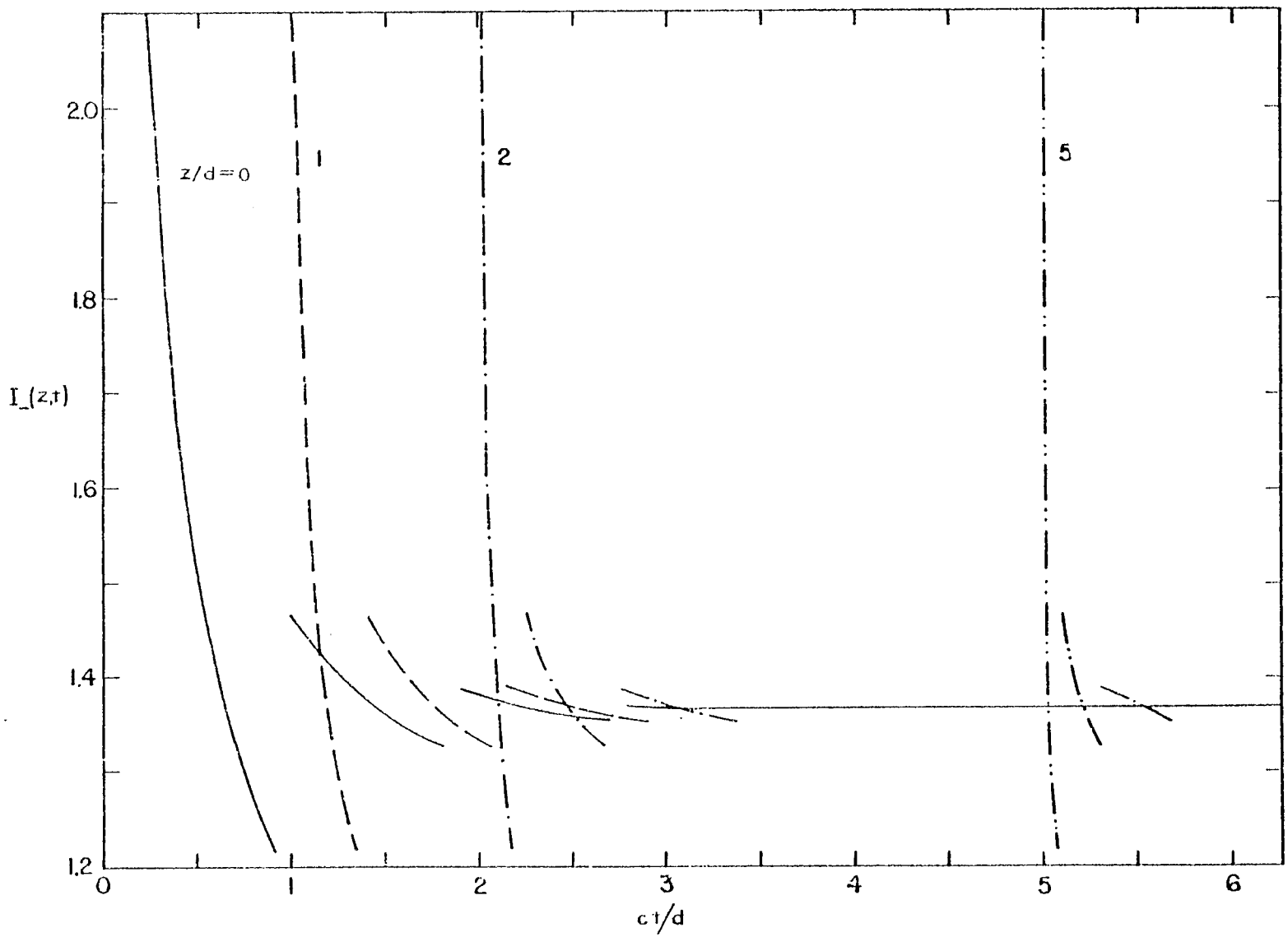

Figure 12. The time history of the current at four points on one wire when the wires are excited in a push-pull manner and a/d = .1.

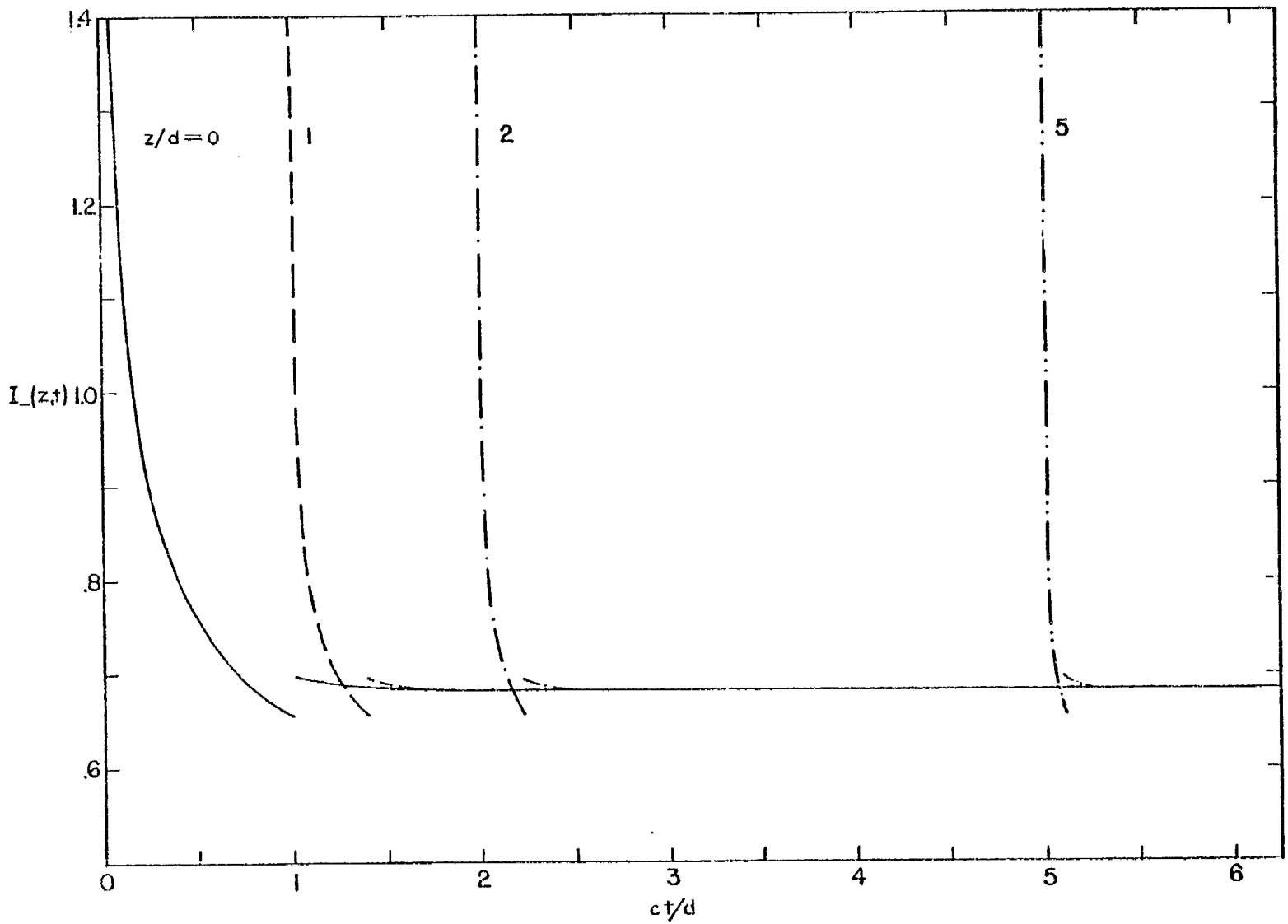

Figure 13. The time history of the current at four points on one wire when the wires are excited in a push-pull manner and a/d = .01.

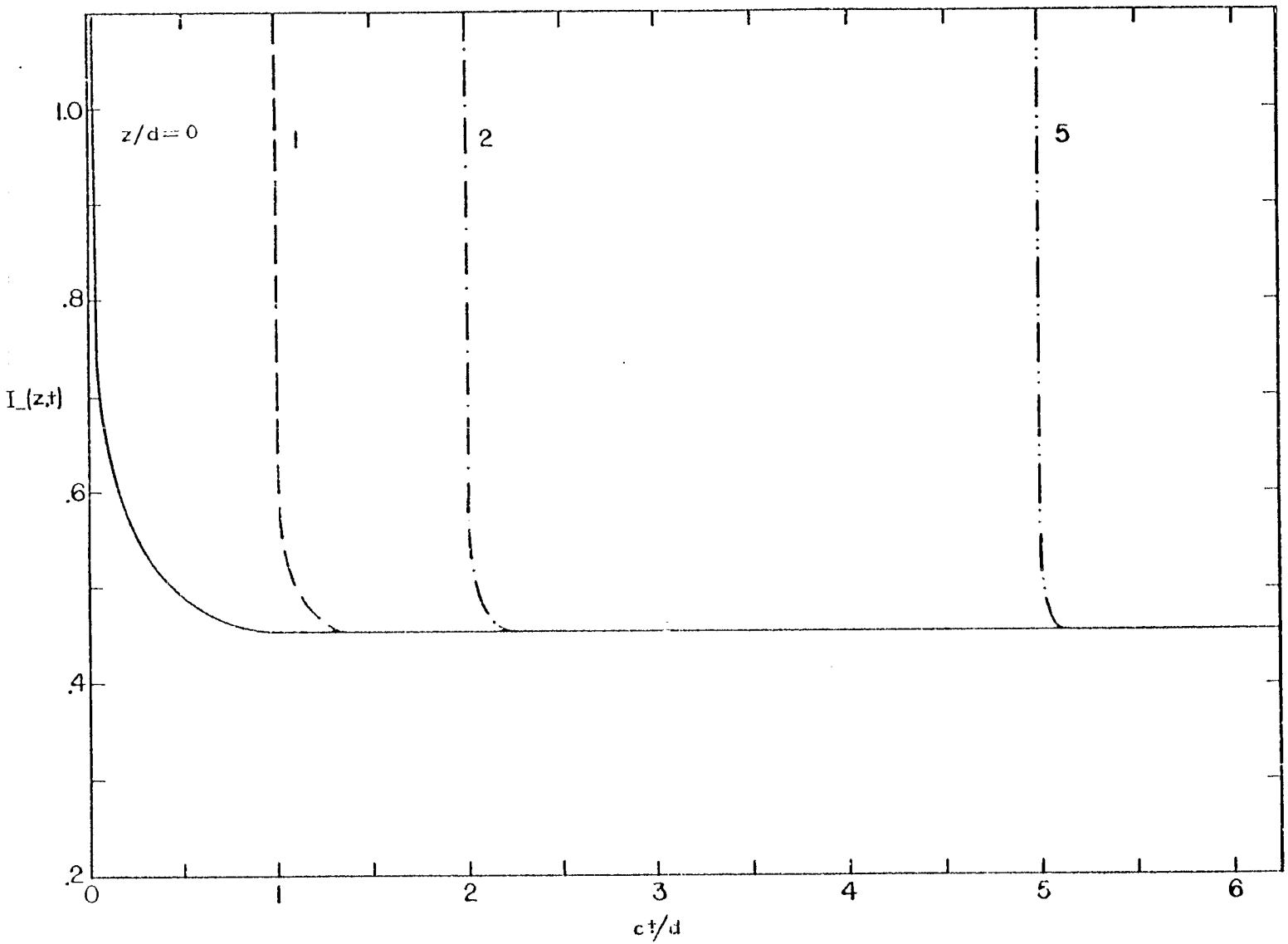

Figure 14. The time history of the current at four points on one wire when the wires are exicted in a push-pull manner and a/d = .001.

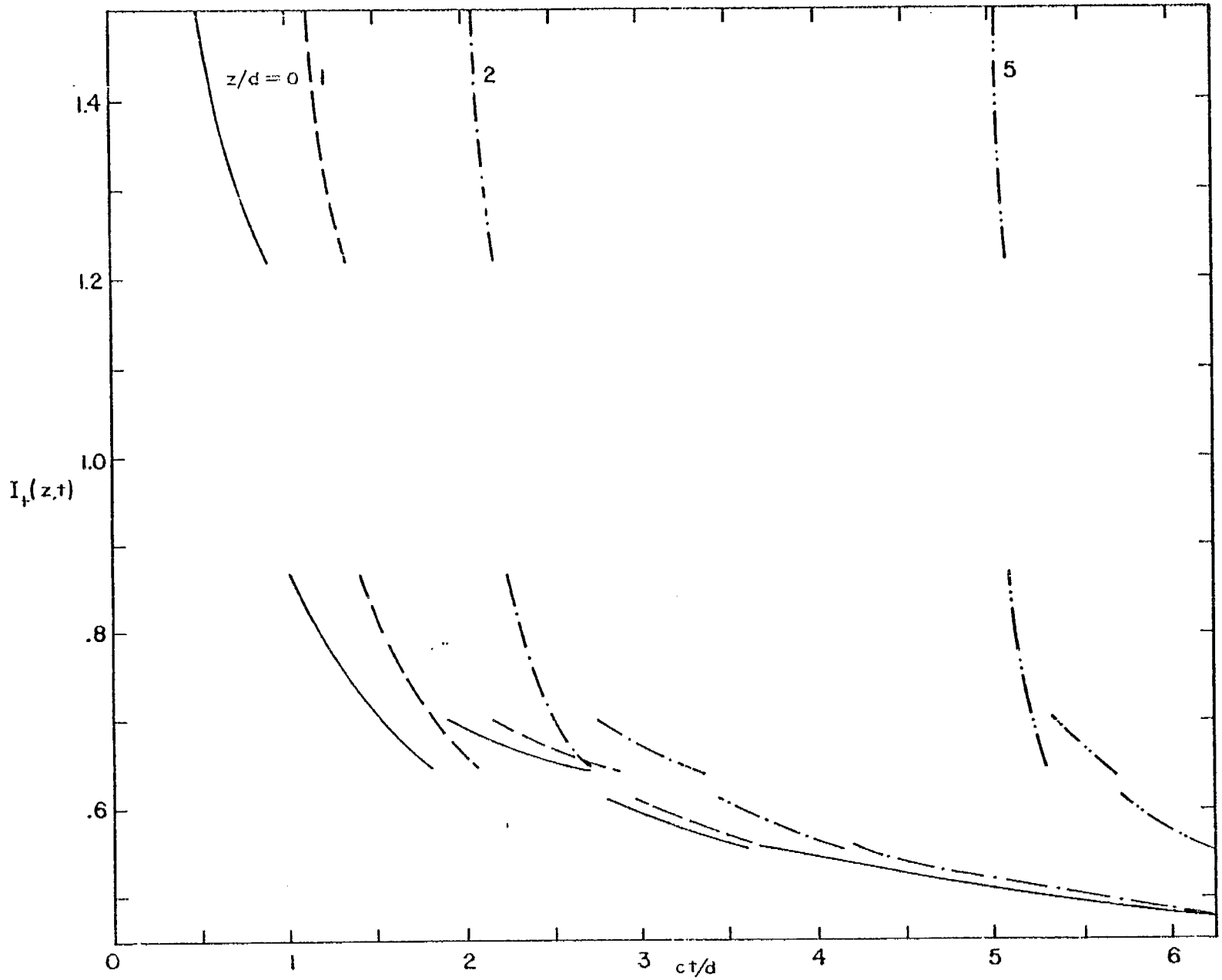

Figure 15. The time history of the current at four points on one wire when the wires are excited in a push-push manner and a/d = .1.

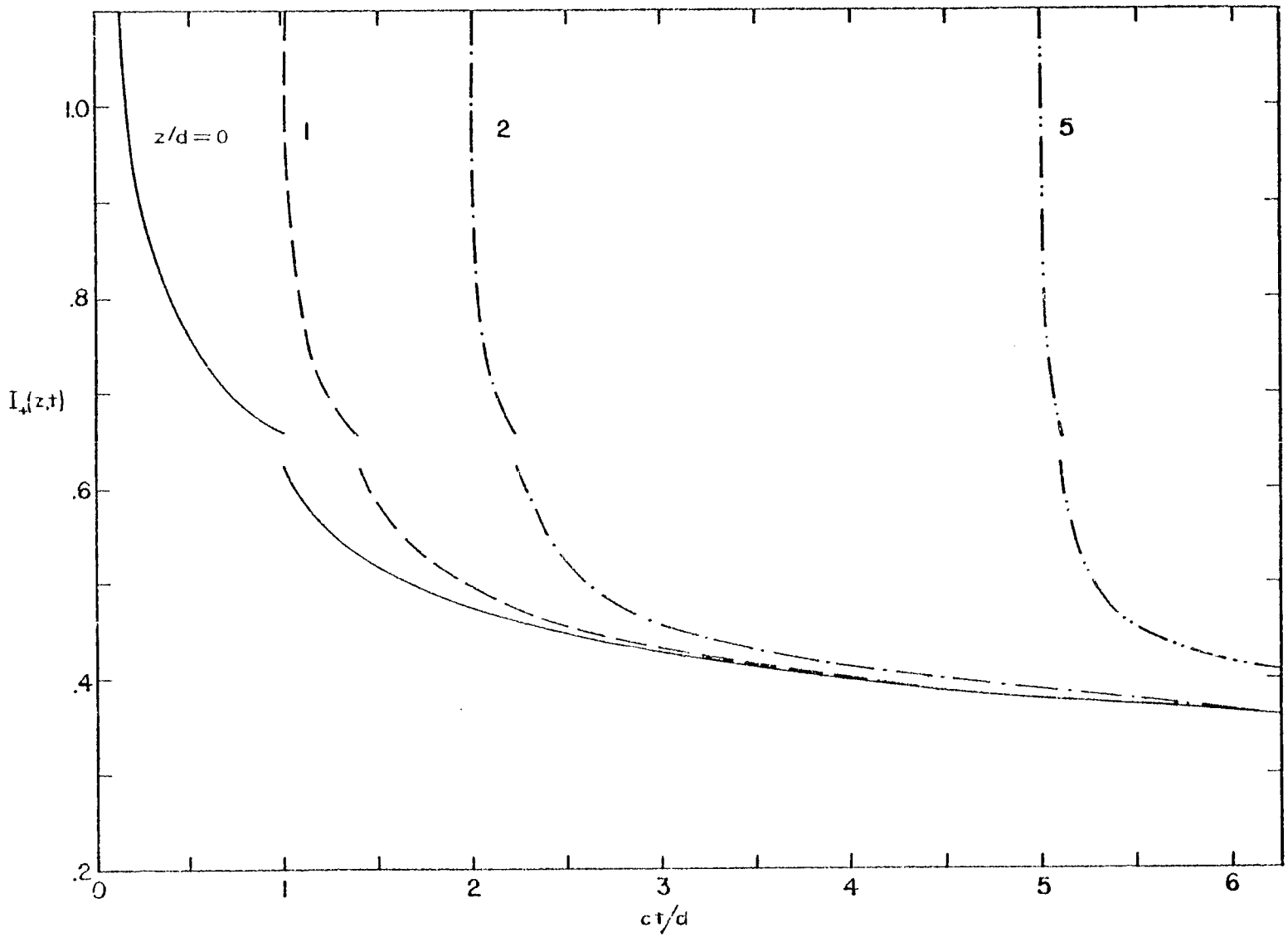

Figure 16. The time history of the current at four points on one wire when the wires are excited in a push-push manner and a/d = .01.

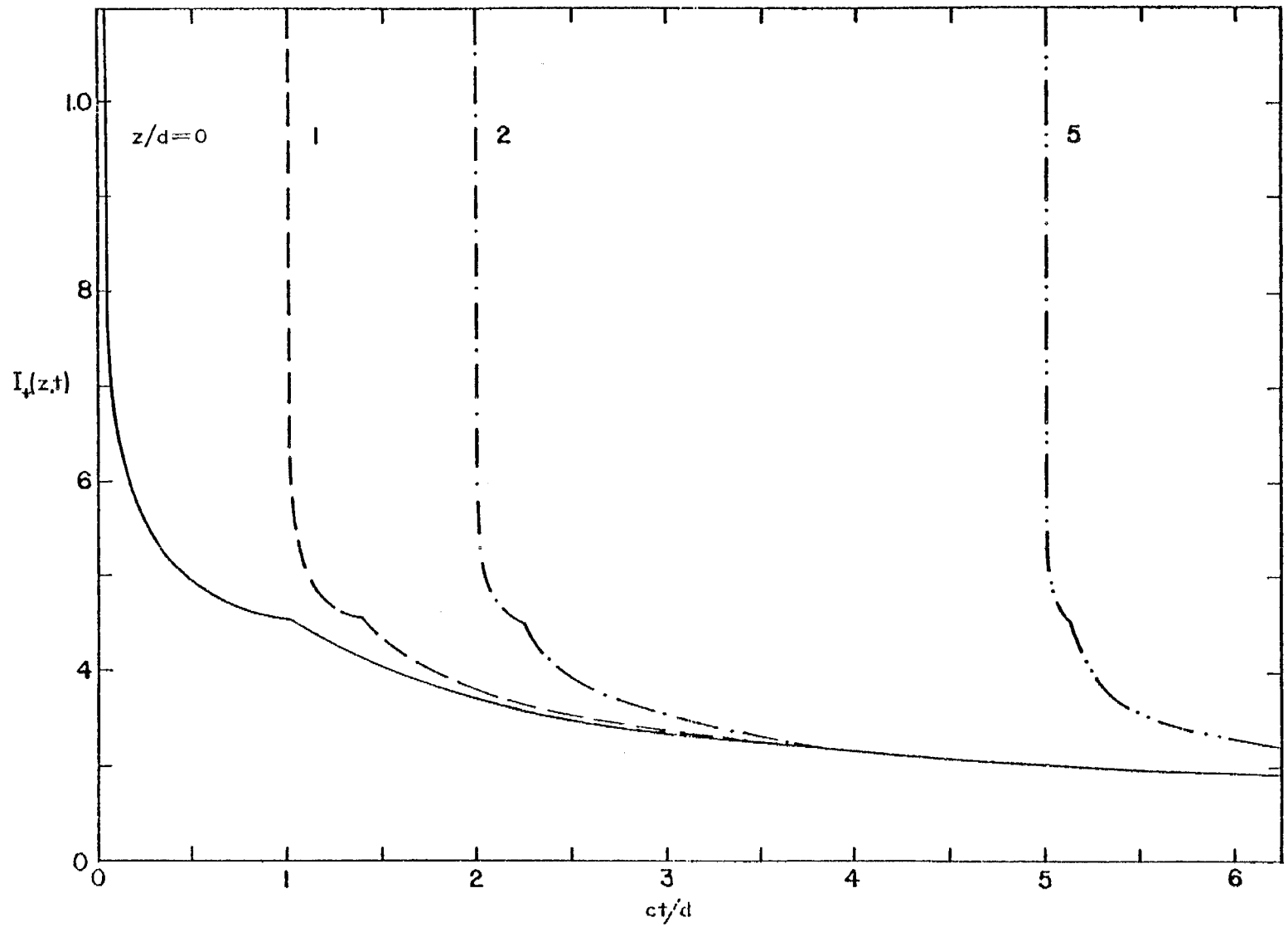

Figure 17. The time history of the current at four points on one wire when the wires are excited in a push-push manner and a/d = .001.

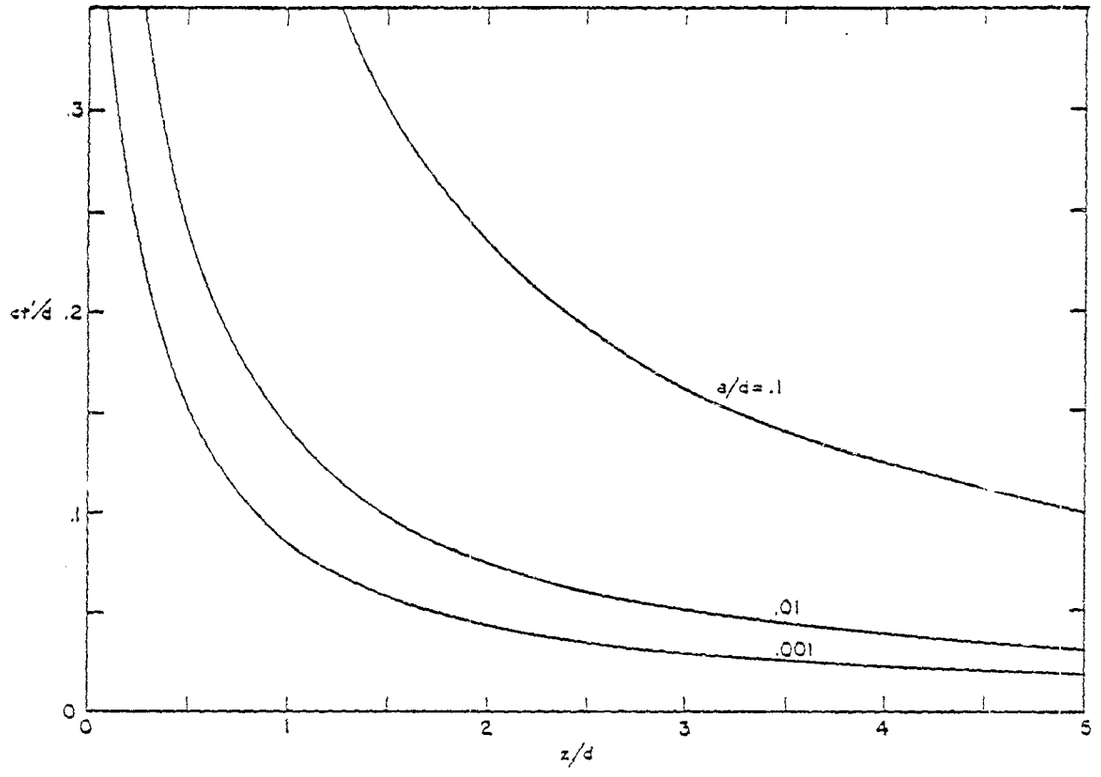

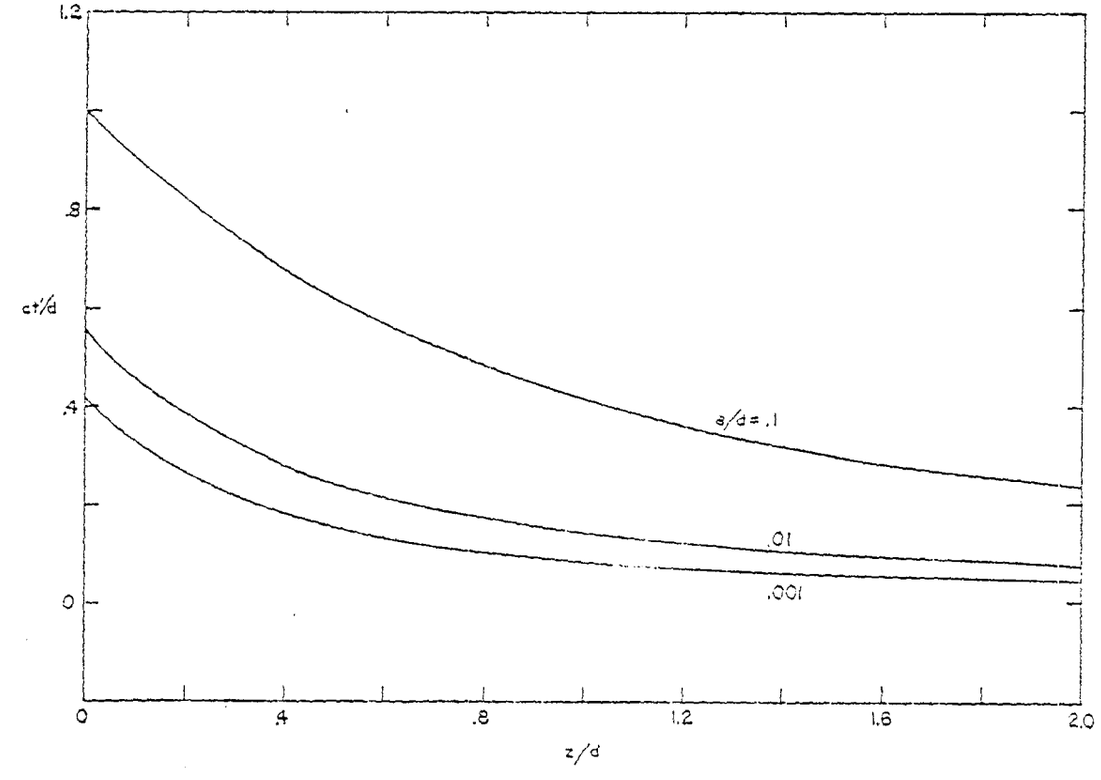

Figure 18. The time that has to elapse after the current wavefront has reached one observation point until the current at the same point differs less than 10% from the TEM current.

In order to get some information on the relative contribution to the field from the TEM mode and the higher order modes when the wires are excited in a push-pull manner we will graphically represent some of the terms in the sum (29) and the term (28). The transverse field distribution of the TEM mode is given by

$$\underline{e}_o(x,y) = \sum_{\ell=1}^{2} (-1)^{\ell}\, d/(4\rho_\ell)[\hat{x}\cos\phi_\ell + \hat{y}\sin\phi_\ell]$$

$$\underline{h}_o(x,y) = \sum_{\ell=1}^{2} (-1)^{\ell}\, d/(4\rho_\ell)[\hat{x}\sin\phi_\ell - \hat{y}\cos\phi_\ell] \qquad (87)$$

and the transverse field distributions of the antisymmetrical higher order modes are given by (c.f. (5)), n = 1,2,3...

$$\underline{e}_n(x,y) = \sum_{\ell=1}^{2} (-1)^{\ell}\, K_1(p_n^-\rho_\ell)[\hat{x}\cos\phi_\ell + \hat{y}\sin\phi_\ell]/[2|K_1(p_n^- d/2)|]$$

$$\underline{h}_n(x,y) = \sum_{\ell=1}^{2} (-1)^{\ell}\, K_1(p_n^-\rho_\ell)[\hat{x}\sin\phi_\ell - \hat{y}\cos\phi_\ell]/[2|K_1(p_n^- d/2)|] \qquad (88)$$

Note that $\underline{e}_n = \hat{z}\times\underline{h}_n$ and that (87) can be obtained from (88) by letting p_n^- tend to zero. We have normalized $\underline{e}_n(x,y)$ such that $|\underline{e}_n(0,0)| = 1$. Since $\mathrm{Re}\{p_n^-\} < 0$ we can see from (88) that the field components of the higher order modes grow exponentially in the transverse direction far away from the wires. This exponential growth does not cause any problems when treating transient problems. However, some care has to be exercised when using these modes in the solution of steady-state problems, since the fields associated with each mode violate the radiation condition at infinity. In the next section we will discuss the region in which these higher order modes are mostly useful in the steady state solution.

A graphical representation of $|\underline{e}_n(0,y)|$, or equivalently, $|\underline{h}_n(0,y)|$ for $0 < y < d$, $a/d = .01$, and $n = 0,1,2,3$ is given in Figure 19. The quantity $|\underline{e}_n(x,0)|$ or $|\underline{h}_n(x,0)|$ is depicted in Figure 20 for $0 < x < d$, $a/d = .01$, and $n = 0,1,2,3$. Note that both $\underline{e}_n(0,y)$ and $\underline{e}_n(x,0)$ are even functions of x and y.

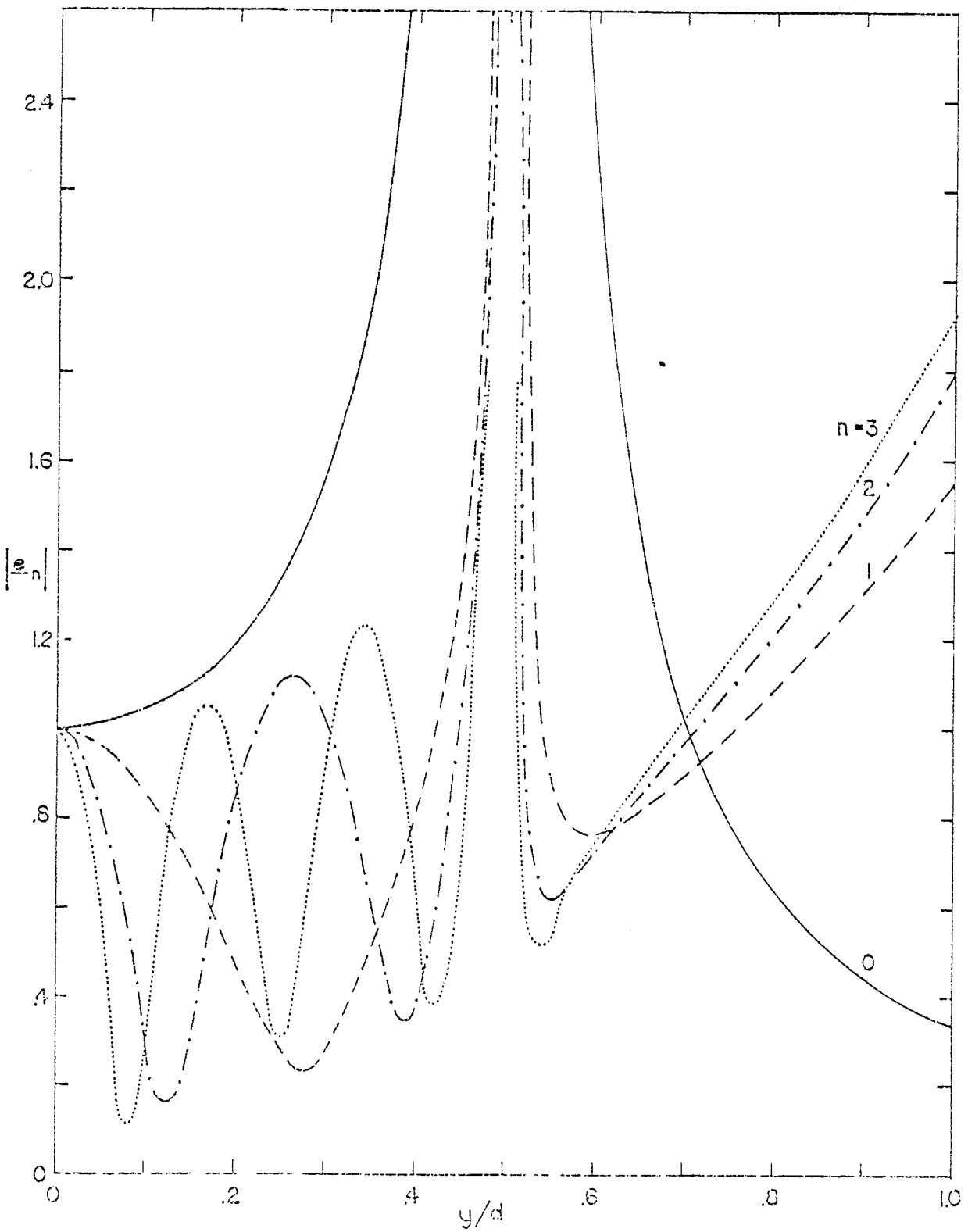

Figure 19. The variations along the y-axis of the normalized electric and magnetic fields for the TEM-mode (n=0) and the lowest antisymmetric TM-modes (n=1,2,3). The axes of the wires are located at x = 0 and y = ±d/2. The radius of each wire is d/100.

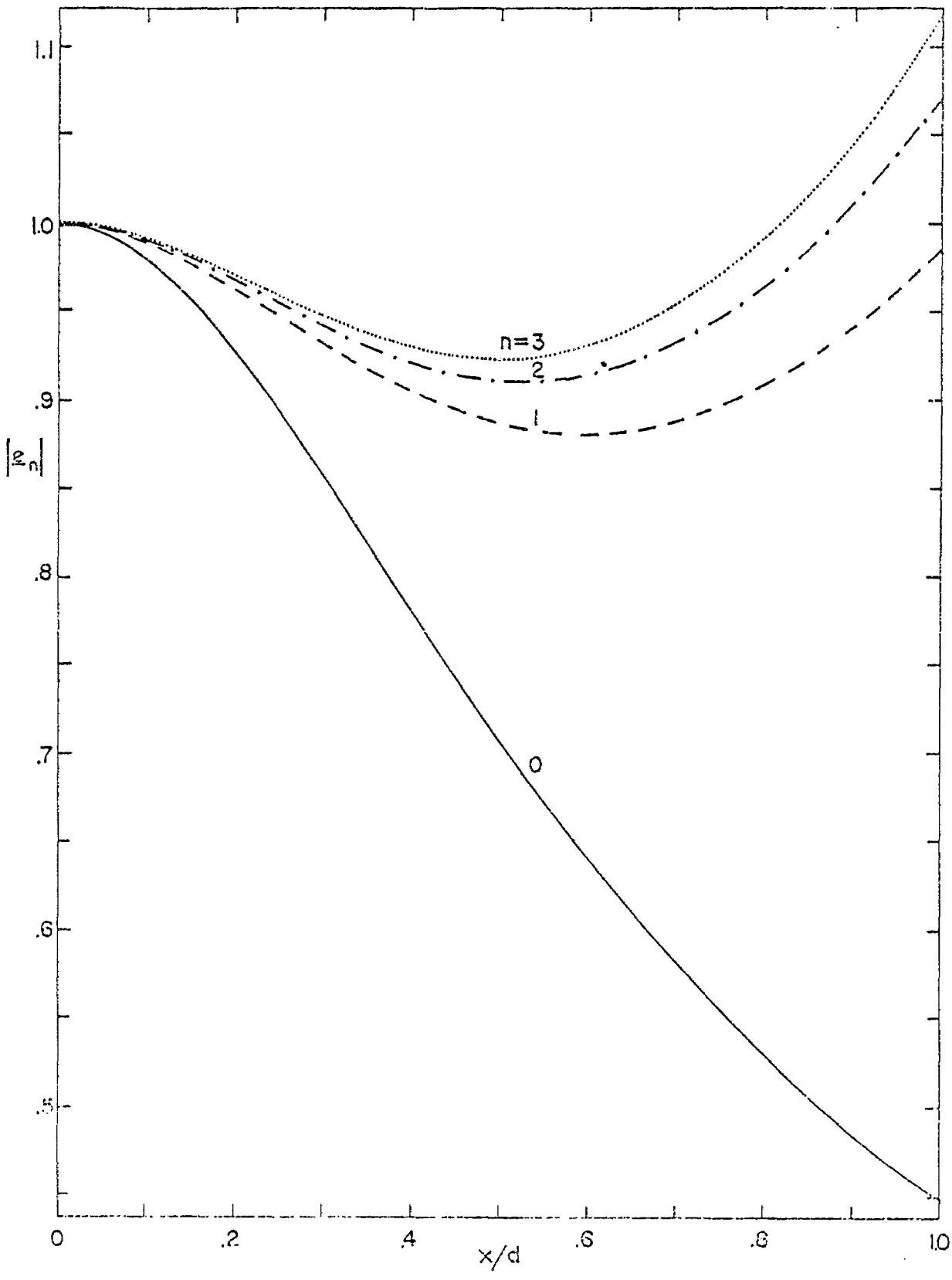

Figure 20. The variation along the x-axis of the normalized electric and magnetic fields for the TEM-mode (n=0) and the lowest antisymmetric TM-modes (n=1,2,3). The axes of the wires are located at x = 0, y = ±d/2.

The time history and spatial variation in the longitudinal direction of each mode are obtained from $f_n(\tau)$, defined by (c.f. (28) and (29))

$$f_o(\tau) = 2/[d \ln(d/a)]^{-1}$$

$$f_n(\tau) = 4(i\pi)^{-1} K_o[p_n^- \tau \exp(-i\pi)]\,|K_o(p_n^- d/2)|/[dK_1(p_n^- d) - aK_1(p_n^- a)], \quad n > 1 \tag{89}$$

Figure 21 shows the variation with τ of $f_n(\tau)$ for n = 0,1,2,3. From this graph we can see that $f_n(\tau)$, $n > 1$ is a monotonically decreasing function of τ and that for $\tau > 5$ the contribution from the higher order modes are negligible. Note that $f_n(\tau)$ gives the time history and longitudinal spatial dependence of the transverse magnetic field of each mode on the z-axis. To obtain this dependence of the transverse electric field requires an extra numerical integration. To sum up (87) through (89) show that we have the following representation of the magnetic field associated with each antisymmetrical mode

$$\underline{H}_n(x,y,z,t) = \mathrm{Re}\{f_n(\tau)\underline{h}_n(x,y)\}, \qquad n = 0,1,2,.... \tag{90}$$

where $f_n(\tau)$ and $\underline{h}_n(x,y)$ are given by (87) through (89).

This concludes our time-domain analysis. In the next section we will derive some frequency domain properties of the field.

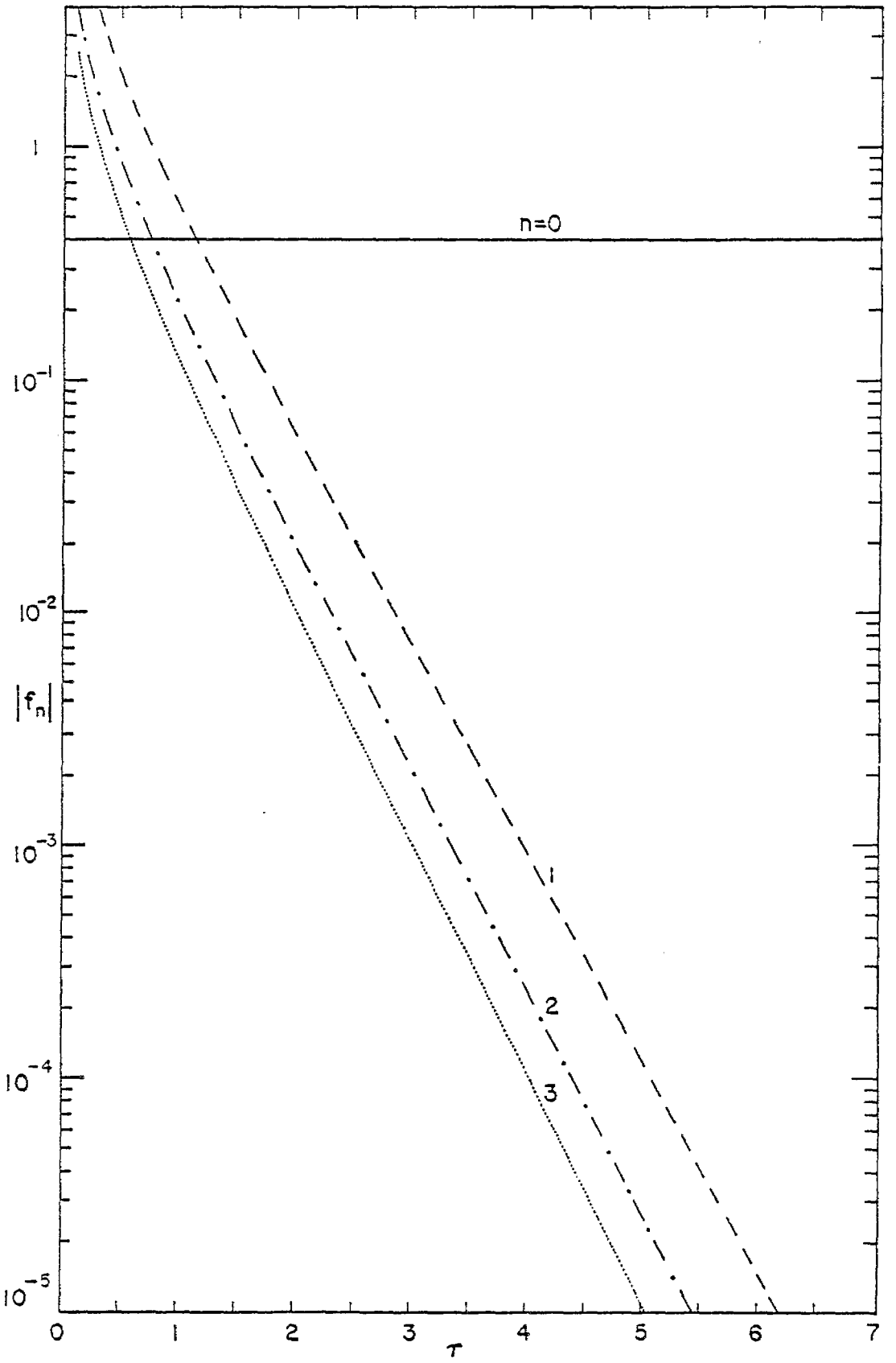

Figure 21. The longitudinal spatial variation and the time history of the magnetic field of the TEM-mode (n=0) and the lowest antisymmetric TM-modes (n=1,2,3).

VII. Some Frequency Domain Considerations

Although the method used in Section II-V to derive a time domain representation of the field is based on first solving the Maxwell equations in the frequency domain, we have not explored any properties of the field in the frequency domain. In this section we will investigate some of these properties.

Our point of departure is equation (11)

$$Z_o\hat{\tilde{H}}_\ell(\rho,\zeta,\gamma) = \gamma p^{-1} K_1(p\rho)[A_+(p)\tilde{V}_+(\gamma) - (-1)^\ell A_-(p)\tilde{V}_-(\gamma)] \tag{11'}$$

where

$$A_\pm(p) = [K_o(pa) \pm K_o(pd)]^{-1}$$

Performing one inverse Laplace transform we get

$$Z_o\tilde{H}_\ell(\rho,z,\gamma) = (2\pi i)^{-1} \gamma \int_{C_\zeta} p^{-1} K_1(p\rho)[A_+(p)\tilde{V}_+(\gamma)$$

$$- (-1)^\ell A_-(p)\tilde{V}_-(\gamma)]\exp(\zeta z)d\zeta \tag{91}$$

For $\gamma = -ik$, k real, the proper branch for $p = i\sqrt{\zeta^2 + k^2}$ in the complex ζ plane, i.e., the branch for which $\mathrm{Re}\{p\} \geq 0$, is depicted in Figure 22. The path of integration C_ζ is along the imaginary axis and "between" the branch-cuts that start at $\zeta = \pm ik$. This choice of branch-cuts makes the integral in (91) converge for all values of ρ and z. Since all zeros of $K_o(pa) \pm K_o(pd)$ are located in the left half plane the integrand is an analytic function of ζ in the proper branch. From the Cauchy integration formula we get

$$Z_o\tilde{H}_\ell(\rho,z,-ik) = -(2\pi)^{-1} k \int_{C_\pm} p^{-1} K_1(p\rho)[A_+(p)\tilde{V}_+(-ik)$$

$$-(-1)^\ell A_-(p)\tilde{V}_-(-ik)]\exp(\zeta z)d\zeta \tag{92}$$

The path $C_+(C_-)$ is around the branch-cut in the right (left) half plane and

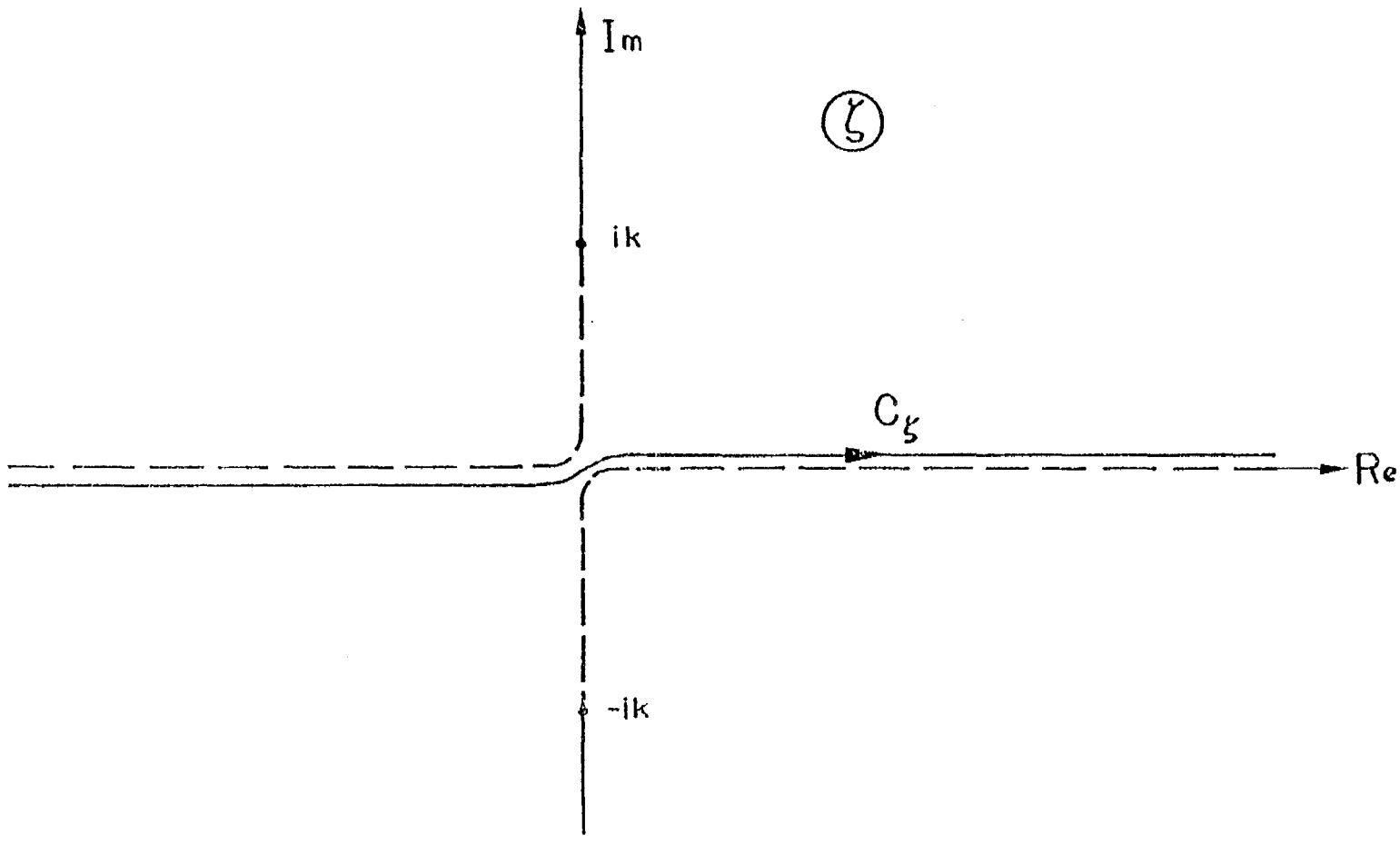

Figure 22. The proper branch of $p = i\sqrt{\zeta^2 + k^2}$ where $\mathrm{Re}\{p\} \geq 0$.

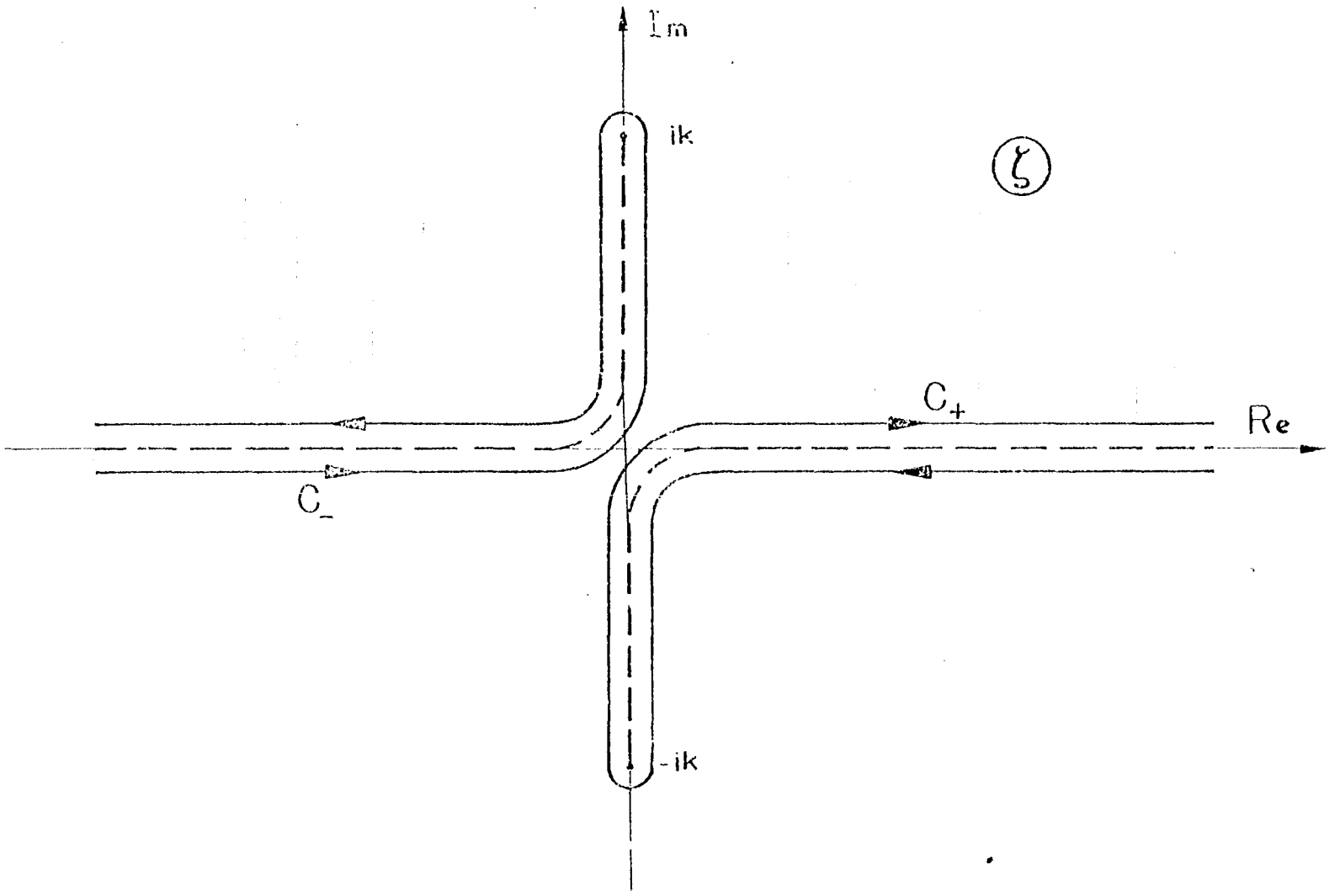

Figure 23. The paths of integration C_+ and C_-.

$C_+(C_-)$ should be chosen for $z < 0 (> 0)$ (see Figure 23). From (92) it follows that $\tilde{H}(\rho,z,\gamma)$ is an even function of z and so there is no loss in generality to only consider the case $z > 0$.

For $z > 0$ equation (92) also has the form

$$Z_o\tilde{H}_\ell(\rho,z,-ik) = kH_+(\rho,z,k)\tilde{V}_+(-ik) - (-1)^\ell kH_-(\rho,z,k)\tilde{V}_-(-ik)$$

$$- (-1)^\ell[2\rho \ln(d/a)]^{-1} \exp(ikz)\tilde{V}_-(-ik) \qquad (93)$$

where

$$H_\pm(\rho,z,k) = -\pi^{-1}\int_o^k F_\pm[(k^2 - \xi^2)^{1/2},\rho]\exp(i\xi z)d\xi$$

$$+ i\pi^{-1}\int_o^\infty F_\pm[(k^2 + \xi^2)^{1/2},\rho]\exp(-\xi z)d\xi$$

$$F_\pm(\sigma,\rho) = \mathrm{Im}\{\sigma^{-1} H_1^{(1)}(\sigma\rho)/[H_o^{(1)}(\sigma a) \pm H_o^{(1)}(\sigma d)]\}.$$

In (93) the first two parts can be interpreted as the contribution from the continuous part of the spectrum and the last part is the contribution from the discrete part of the spectrum.

In order to interpret (93) physically we will evaluate the total current, $I_\ell(z,k)$, on each wire, given by

$$I_\ell(z,k) = 2\pi a\tilde{H}_\ell(a,z,-ik) = [P_+(z,k) + Q_+(z,k)]\tilde{V}_+(-ik)Z_o^{-1}$$

$$- (-1)^\ell[P_-(z,k) + Q_-(z,k)]\tilde{V}_-(-ik)Z_o^{-1}$$

$$- (-1)^\ell \pi \ln^{-1}(d/a)\exp(ikz)\tilde{V}_-(-ik)Z_o^{-1} \qquad (94)$$

where

$$P_{\pm}(z,k) = -2ka \int_0^k G_{\pm}[(k^2 - \xi^2)^{1/2}, a]\exp(i\xi z)d\xi$$

$$Q_{\pm}(z,k) = i2ka \int_0^{\infty} G_{\pm}[(k^2 + \xi^2)^{1/2}, a]\exp(-\xi z)d\xi$$

$$G_{\pm}(\sigma,z) = \frac{2/(\rho\sigma a)\pm[J_1(\sigma a)Y_0(\sigma d)-J_0(\sigma d)Y_1(\sigma a)]}{\sigma\{[J_0(\sigma a)\pm J_0(\sigma d)]^2+[Y_0(\sigma a)\pm Y_0(\sigma d)]^2\}}$$

We first note that $Q_{\pm}(z,k)$ is a purely imaginary function for real values of z and k. Hence the term $Q_{\pm}(z,k)\tilde{V}_{\pm}(-ik)Z_o^{-1}$ represents a stationary wave, i.e., a nonradiating wave. The term $P_{\pm}(z,k)\tilde{V}_{\pm}(-ik)Z_o^{-1}$ can be interpreted as a superposition of traveling waves, each wave being a fast wave, i.e., its phase velocity is greater than the speed of light. The last term in (94) represents a TEM wave and the quantity $Z = Z_o\pi^{-1}\ln(d/a)$ is the characteristic impedance of two parallel wires.

For the special case where $\tilde{V}_1(\gamma) = -\tilde{V}_2(\gamma) = \tilde{V}(\gamma)$ equation (94) becomes

$$I_1(z,k) = -I_2(z,k) = [P_-(z,k) + Q_-(z,k)]Z_o^{-1}\tilde{V}(-ik)$$

$$+ Z^{-1}\exp(ikz)\tilde{V}(-ik). \qquad (95)$$

The output complex power from the two generators is given by $2\tilde{V}(-ik)I_1(\Delta,k) = Y_-^*(k)|2\tilde{V}(ik)|^2$ and $Y_-(k)$ is the input admittance of a parallel pair of wires driven in a push-pull manner. The admittance $Y_-(k)$ can be split up in the following way:

$$Y_-(k) = G + iB_-(k) + Y_-'(k) \qquad (96)$$

where $G = Z^{-1} = \pi[2Z_o\ln(d/a)]^{-1}$ is the conductance of the TEM mode and represents the power guided by the line. The second term is $B_-(k) = (2Z_o)^{-1}Q_-(\Delta,k)$ where Δ is the gap width. This term is a capacitance and represents the stationary field in the vicinity of each generator. It should be noted here that $Q_-(z,k)$ has a logarithmic singularity at $z = 0$. This is the same type of singularity that has been known for one cylindrical antenna in free space fed

by a delta gap. The third term, $Y'_-(k) = (2Z_o)^{-1} P_-(0,k)$, is the radiation admittance and its real part accounts for power radiated from the wires. The imaginary part of $Y'_-(k)$ is small compared to $B(k)$. A similar representation can be found for the input admittance, $Y_+(k)$, of a parallel pair of wires driven symmetrically. In this case we do not have any term corresponding to the contribution from a TEM wave. In Figure 24 we give a graphical representation of the input impedance of two wires for these two different excitations.

The calculations so far have been based on the integral representation (93). This representation is based on a choice of Riemann sheets of $\sqrt{\zeta^2 + k^2}$ such that the radiation condition is satisfied throughout the entire configuration space. However, if we limit our calculations to only certain parts of the configuration space there are other possible choices of Riemann sheets. For example, when calculating the field between the wires we can choose any branch-cut starting at $\pm ik$ as shown in Figure 25. By choosing these branch-cuts we will have $\mathrm{Re}\{p\} < 0$ in part of the Riemann sheet under consideration. One way is to let the branch-cuts coincide with the imaginary axis in the ζ-plane in which case we get

$$Z_o \widetilde{H}_\ell(\rho,z,-ik) = H'_+(\rho,z,k)\widetilde{V}_+(-ik) - (-1)^\ell H'_-(\rho,z,k)\widetilde{V}_-(-ik) \tag{97}$$

where

$$H'_\pm(\rho,z,k) = R'_\pm(\rho,z,k) + S'_\pm(\rho,z,k) + T'_\pm(\rho,z,k) \tag{98}$$

$$R'_\pm(\rho,z,k) = -ika(2\pi)^{-1} \int_k^\infty \frac{L_\pm(\eta)[L_\pm(\eta)K_1(\eta\rho/a) \mp M_\pm(\eta)I_1(\eta\rho/a)]}{\eta M_\pm(\eta)[M_\pm^2(\eta) \mp \pi^2 L_\pm^2(\eta)]} \exp(i\xi z)d\xi \tag{99}$$

$$L_\pm(\eta) = I_o(\eta) \pm I_o(\eta d/a), \qquad M_\pm(\eta) = K_o(\eta d/a) \tag{100}$$

$$\eta = a(\xi^2 - k^2)^{1/2}$$

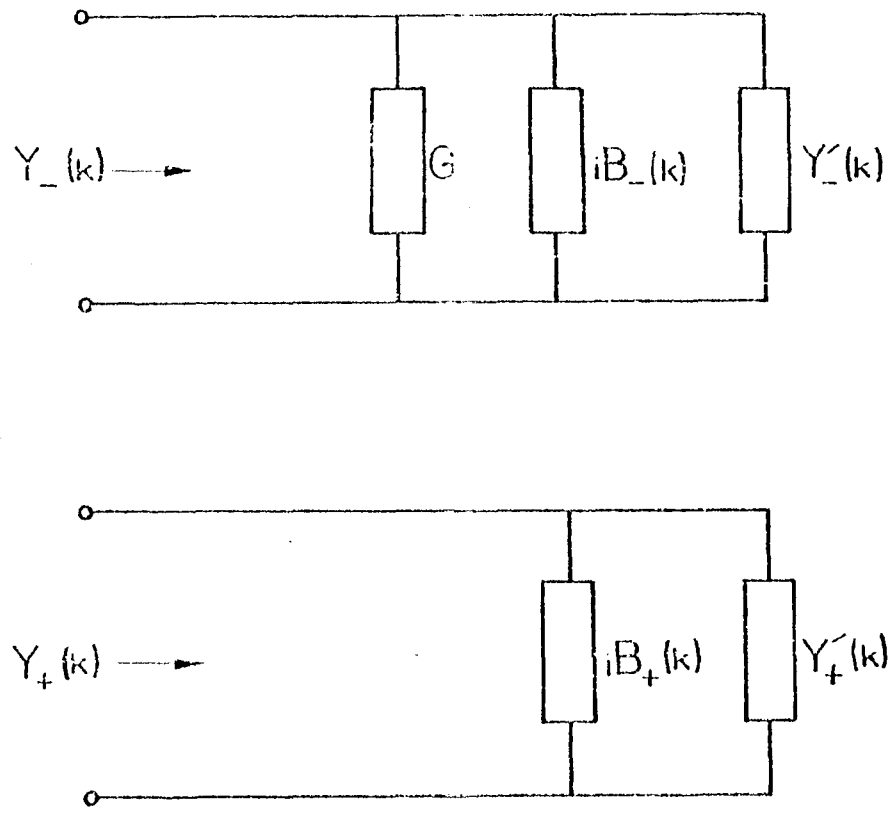

Figure 24. The push-pull, $Y_{-}(k)$, and push-push, $Y_{+}(k)$, input impedances of two parallel wires.

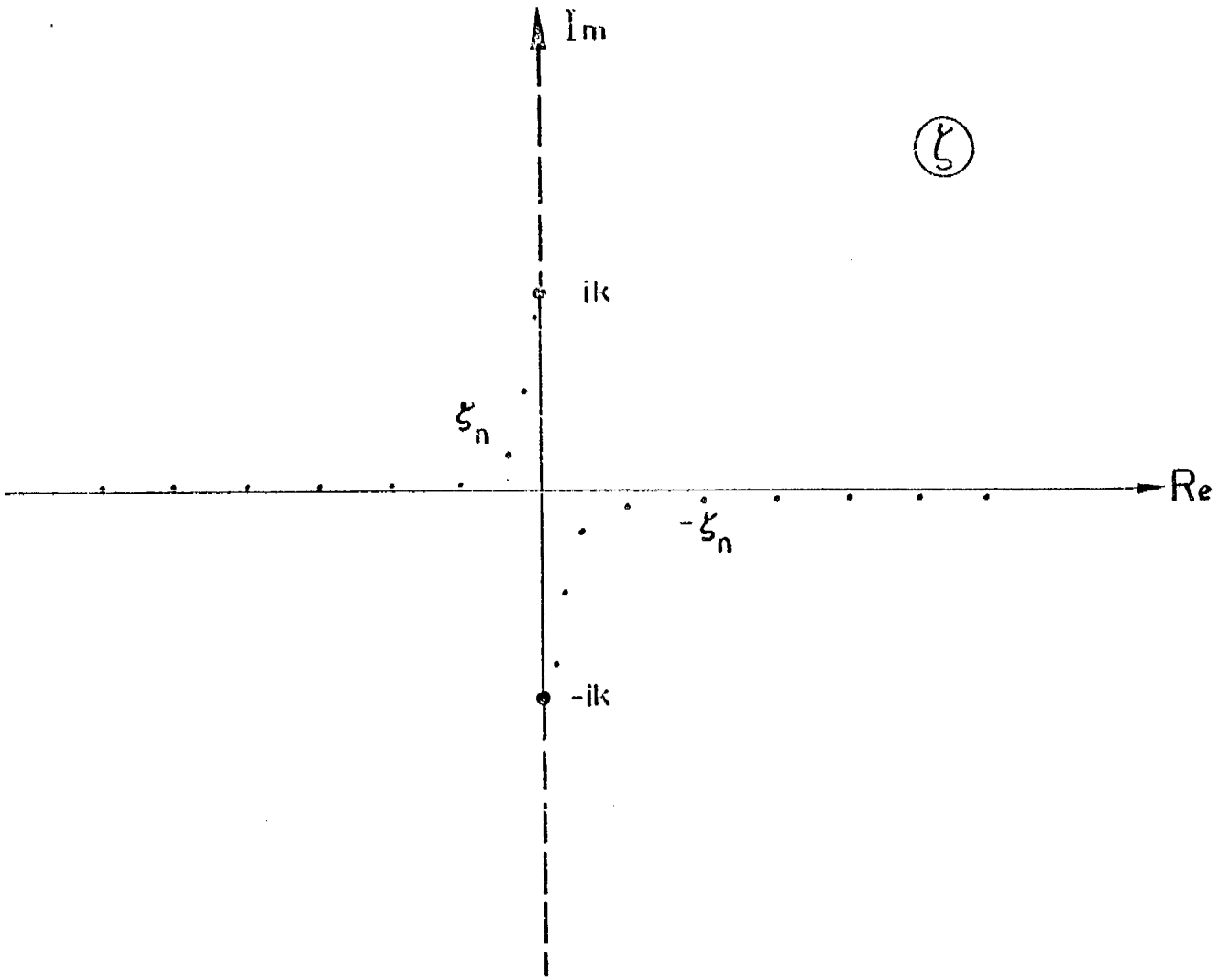

Figure 25. The branch of $p = \sqrt{\zeta^2 + k^2}$ used in the representation (78). In this branch, $\mathrm{Re}\{p\} < 0$ in the second and fourth quandrants and $\mathrm{Re}\{p\} > 0$ in the first and third quadrants.

$$S'_{\pm}(\rho,z,k) = -ik \sum_{n=1}^{\infty} K_1(p_n^{\mp}\rho)[\zeta_n^{\pm}aK_1(p_n^{\pm}a) \pm \zeta_n^{\pm}dK_1(p_n^{\pm}d)]^{-1} \exp(\zeta_n z) \qquad (101)$$

$$T'_{+}(\rho,z,k) = 0, \qquad T'_{-}(\rho,z,k) = [2\rho \ln(d/a)]^{-1} \exp(ikz), \qquad (102)$$

and $p_n^{\pm}$ are the roots of the equation $K_o(pa) \pm K_o(pd) = 0$ such that $\pi \le \arg\{p_n^{\pm}\} \le 0$ and $|\zeta_n^{\pm}| = |k^2 + p_n^{\pm 2}|^{1/2}$, $-\pi \le \arg\{\zeta_n\} \le -3\pi/2$. This representation corresponds to the representation (25) through (29) of the time-domain result.

The quantities $p_n^{\pm}$ have been tabulated in Section VI. From (101) it is clear that $\mathrm{Im}\{\zeta_n^{\pm}\}$ is the propagation constant and $-\mathrm{Re}\{\zeta_n^{\pm}\}$ is the attenuation constant of the higher order modes. Furthermore, the transverse field distribution of each mode is determined by $K_1(p_n^{\pm}\rho)[aK_1(p_n^{\pm}a) \pm dK_1(p_n^{\pm}d)]^{-1}$ and this expression is exponentially growing for large values of ρ, indicating that the representation (95) is not valid in all space. However, as we have said before, (97) is valid in the region between the two wires.

The quantity that determines the relative importance of the contribution of each higher-order mode is $\zeta_n^{\pm}$. It is therefore of value to have the frequency variation of $\zeta_n^{\pm}$. The loci of $\zeta_n^{\pm}$ in the complex plane as the frequency varies is depicted in Figures 26 through 31. Figures 32 through 39 give the variation with kd of the following two normalized quantities

$$\alpha_n^{\pm} = \mathrm{Re}\{\zeta_n^{\pm}d\}, \qquad \beta_n^{\pm} = \mathrm{Im}\{\zeta_n^{\pm}d\}$$

for n = 1, 2, 3, 4, 5 and a/d = .1, .01, .001.

Finally, we will derive a representation which is most useful between the wires and far away from the source point. In this case we draw the branch-cuts from $\pm ik$ to $\pm ik \mp \infty$ parallel to the real axis as indicated in Figure 40. This Riemann sheet enables us to derive the following representation

$$Z_o\tilde{H}_{\ell}(\rho,z,-ik) = H''_{+}(\rho,z,k)\tilde{V}_{+}(-ik) - (-1)^{\ell} H''_{-}(\rho,z,k)\tilde{V}_{-}(-ik) \qquad (103)$$

where

$$H''_{\pm}(\rho,z,k) = R''_{\pm}(\rho,z,k) + S''_{\pm}(\rho,z,k) + T'_{\pm}(\rho,z,k) \qquad (104)$$

$$R''_{\pm}(\rho,z,k) = ika\int_0^{\infty} \frac{L_{\pm}(n)K_1(n\rho/a)+M_{\pm}(n)I_1(n\rho/a)}{2nM_{\pm}(n)[M_{\pm}(n)+i\pi^2 L_{\pm}(n)]} \exp(ikz - \xi z)d\xi \qquad (105)$$

$$|n| = (|\xi^2 - 2ik\xi|a^2)^{1/2}, \qquad \arg\{n\} = \frac{\pi}{4} + \arctan[\xi/(2k)]$$

$$S''_{\pm}(\rho,z,k) = ik \sum_n{}' K_1(\gamma_n^{\pm}\rho)[\zeta_n^{\pm}aK_1(p_n^{\pm}a) \pm \zeta_n^{\pm}dK_1(p_n^{\pm}d)]^{-1} \exp(\zeta_n z) \qquad (106)$$

and Σ' denotes summation over all n such that $\mathrm{Re}\{\zeta_n^{\pm}\} < 0$ and $0 < \mathrm{Im}\{\zeta_n^{\pm}\} < k$. For large values of z, $S''_{\pm}(\rho,z,k)$ is negligable since each term is exponentially attenuated. Moreover, the main contribution of $R''_{\pm}(\rho,z,k)$ comes from small values of ξ when z is large. This enables us to derive an asymptotic expression of the integral (104), valid for large values of z. From this asymptotic expression it can be seen that the current on the antenna, far away from the feeding point z = 0 has the following form,

$$I(z,k) = I_+(z,k) + I_-(z,k) \qquad (107)$$

where

$$I_+(z,k) = \pi \ln^{-2}[2ik\Gamma^2 ad/z]\exp(ikz)\tilde{V}_+(-ik)/Z_o \qquad (108)$$

$$I_-(z,k) = (\pi^3/2)^{1/2}(ik/z)^{3/2} a^2 \ln(d/a)$$

$$- (d^2 - a^2)/4]\ln^{-2}(d/a)\exp(ikz)\tilde{V}_-(-ik)/Z_o \qquad (109)$$

The branch-cut chosen here has been discussed previously in connection with the calculation of the current on a cylindrical antenna and the expression (108) can be compared with the results obtained in [11] through [13]. It should also be noted that the connection between this choice of the branch-cut and the saddle point method is discussed in [14].

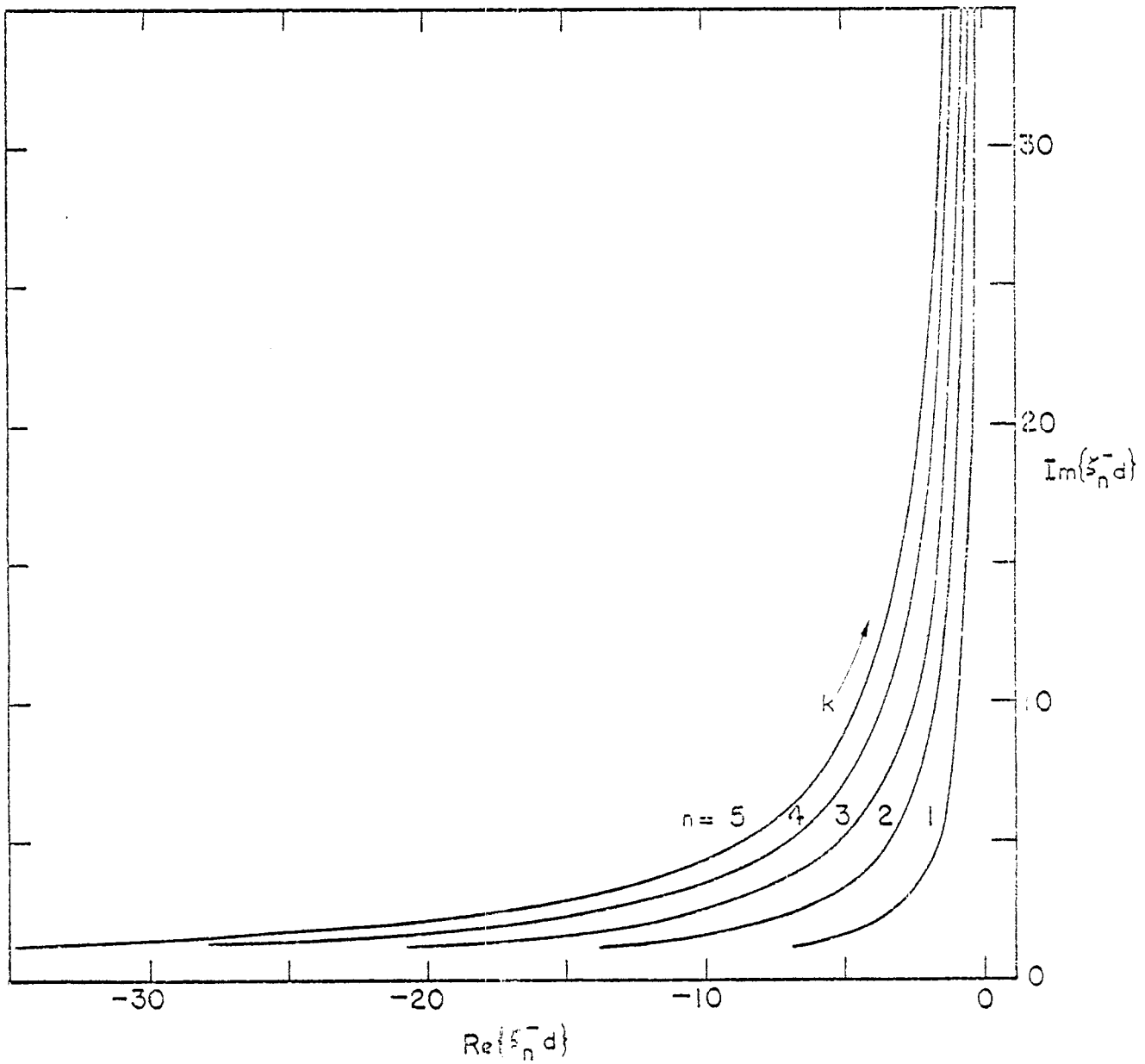

Figure 26. The loci of the complex propagation constants of the five lowest, antisymmetric TM modes on two wires when a/d = .1.

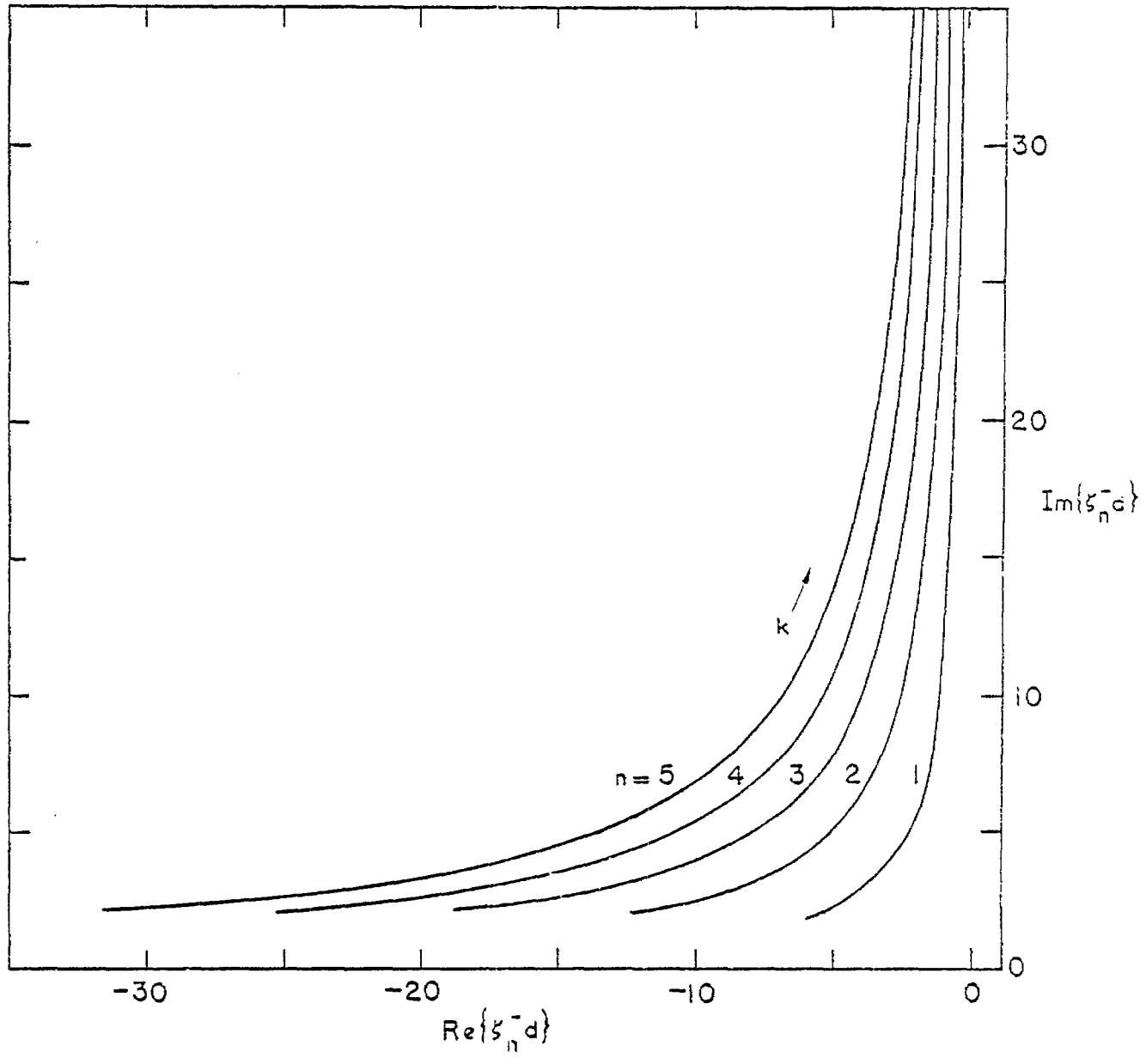

Figure 27. The loci of the complex propagation constants of the five lowest, antisymmetric TM modes on two wires when a/d = .01.

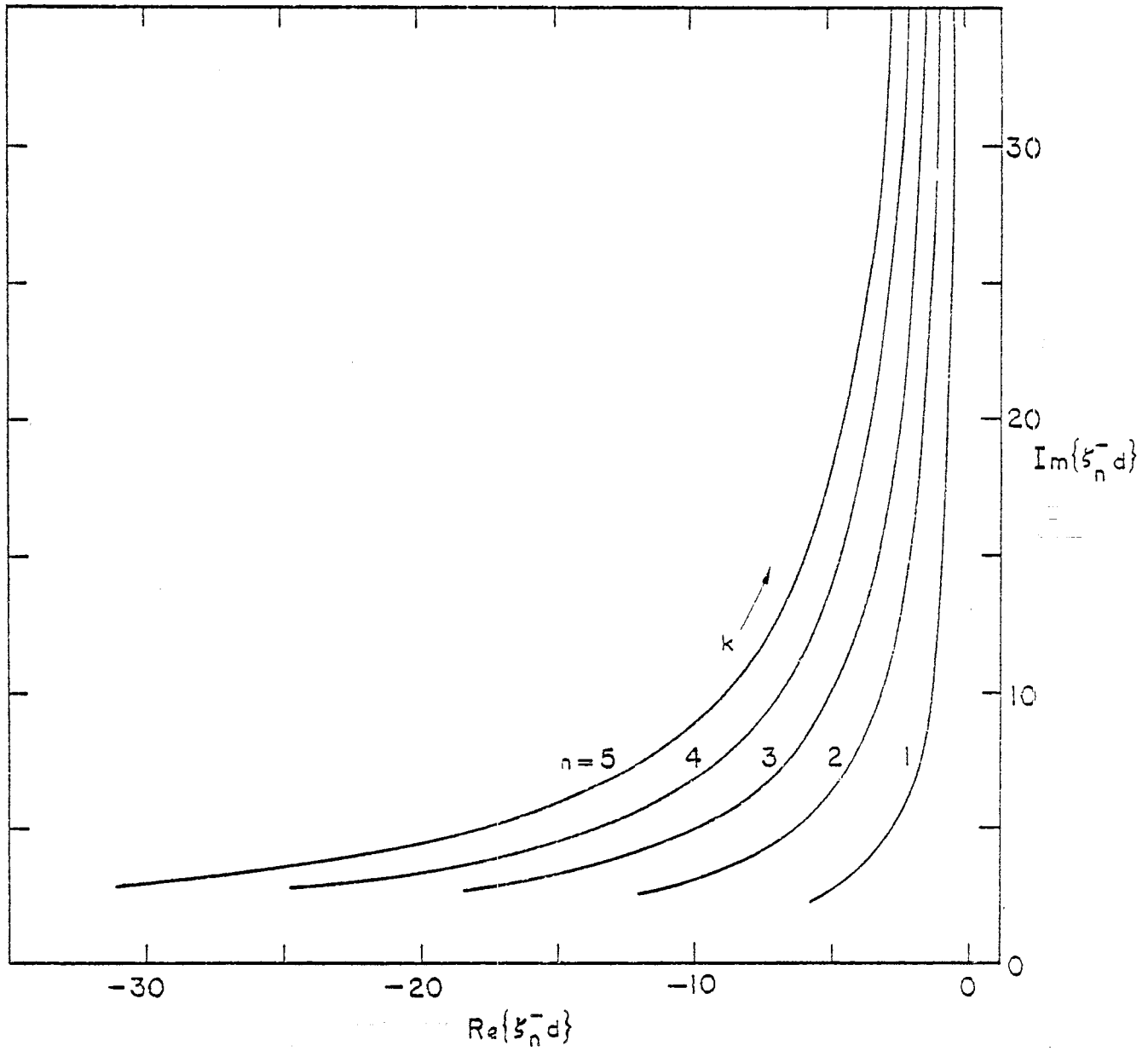

Figure 28. The loci of the complex propagation constants of the five lowest, antisymmetric TM modes on two wires when a/d = .001.

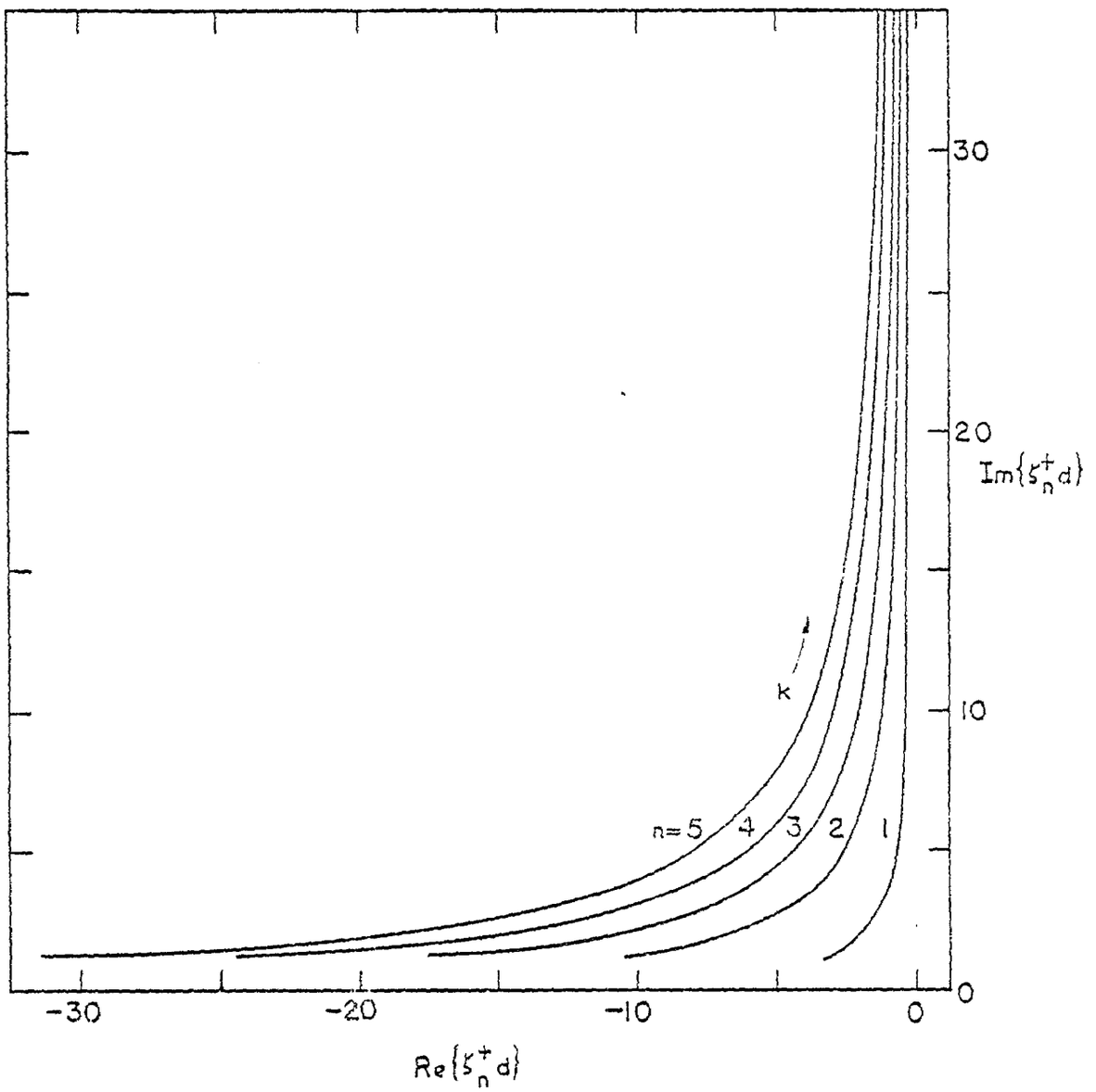

Figure 29. The loci of the complex propagation constants of the five lowest, symmetric TM modes on two wires when a/d = .1.

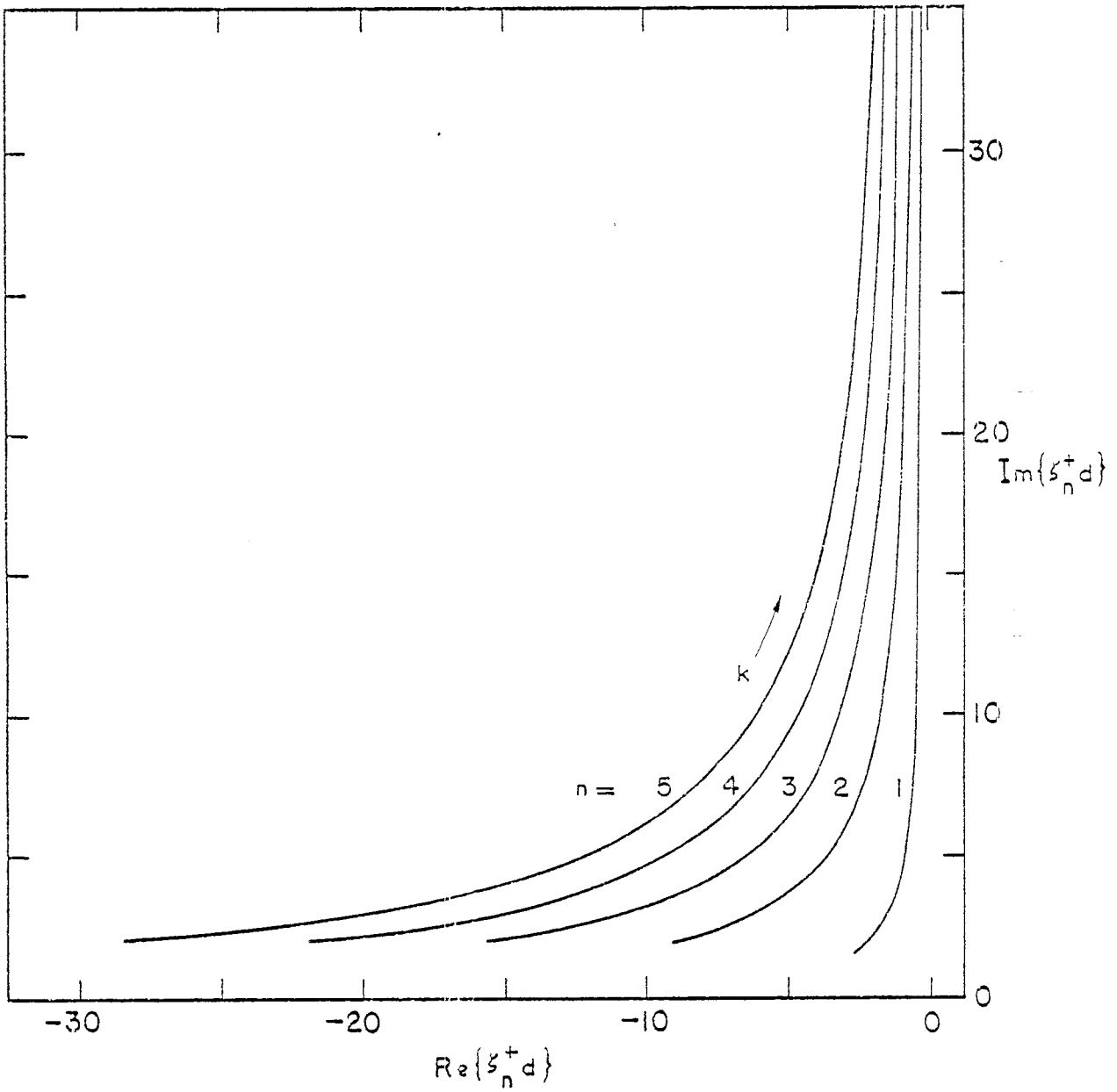

Figure 30. The loci of the complex propagation constants of the five lowest, symmetric TM modes on two wires when a/d = .01.

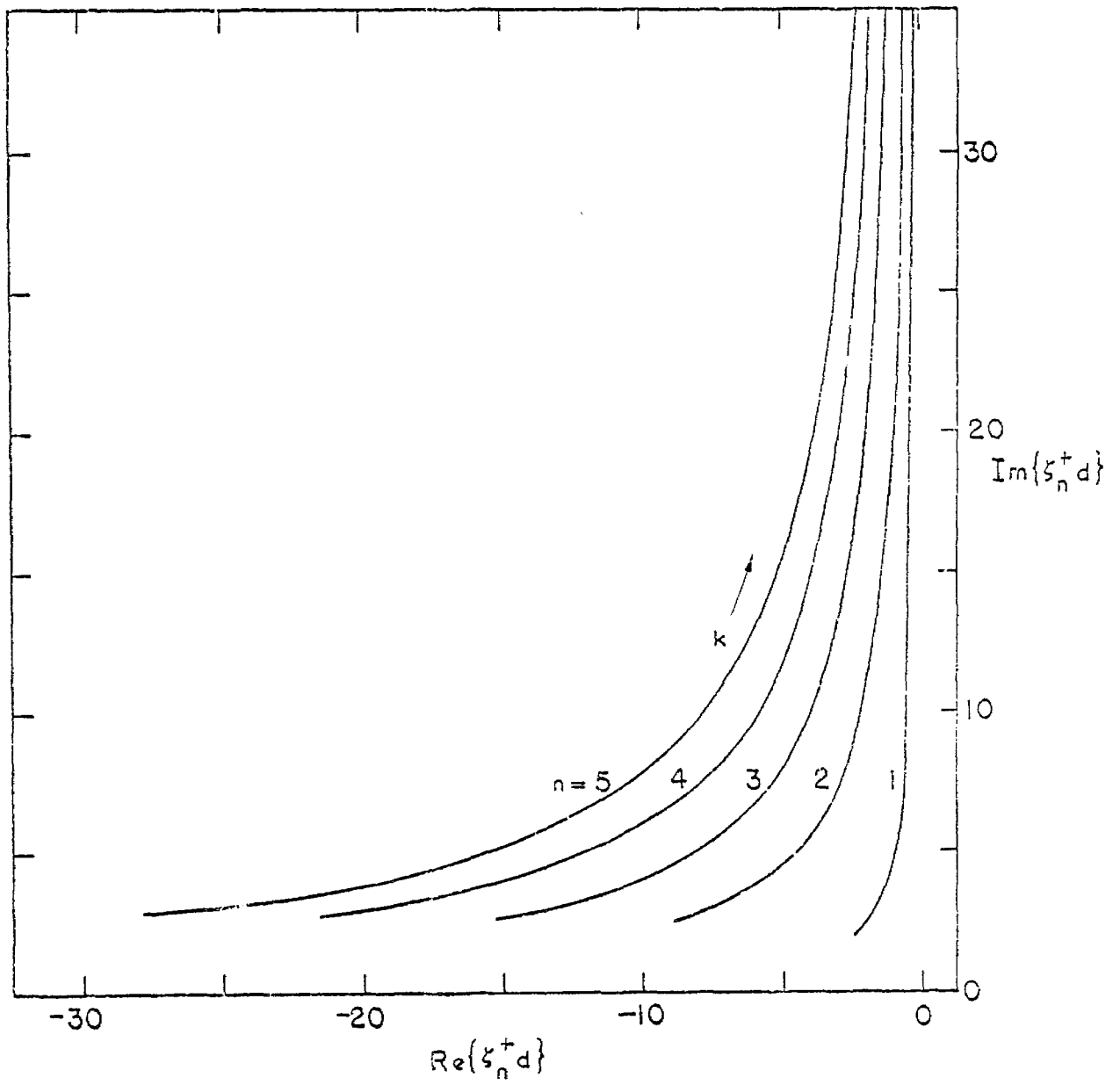

Figure 31. The loci of the complex propagation constants of the five lowest, symmetric TM modes on two wires when a/d = .001.

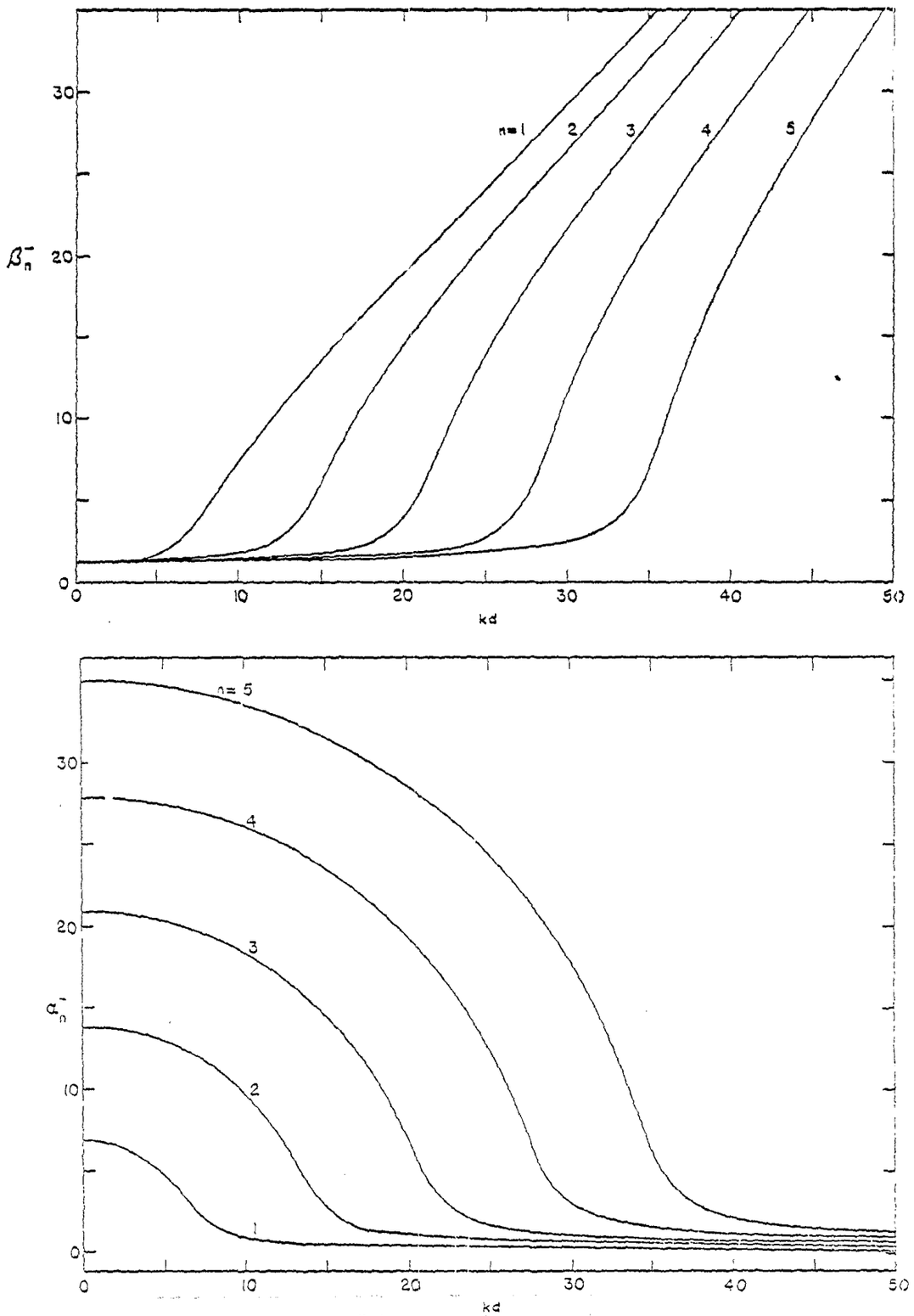

Figure 32. The propagation and attenuation constants of the five lowest antisymmetric TM modes on two wires when a/d = .1.

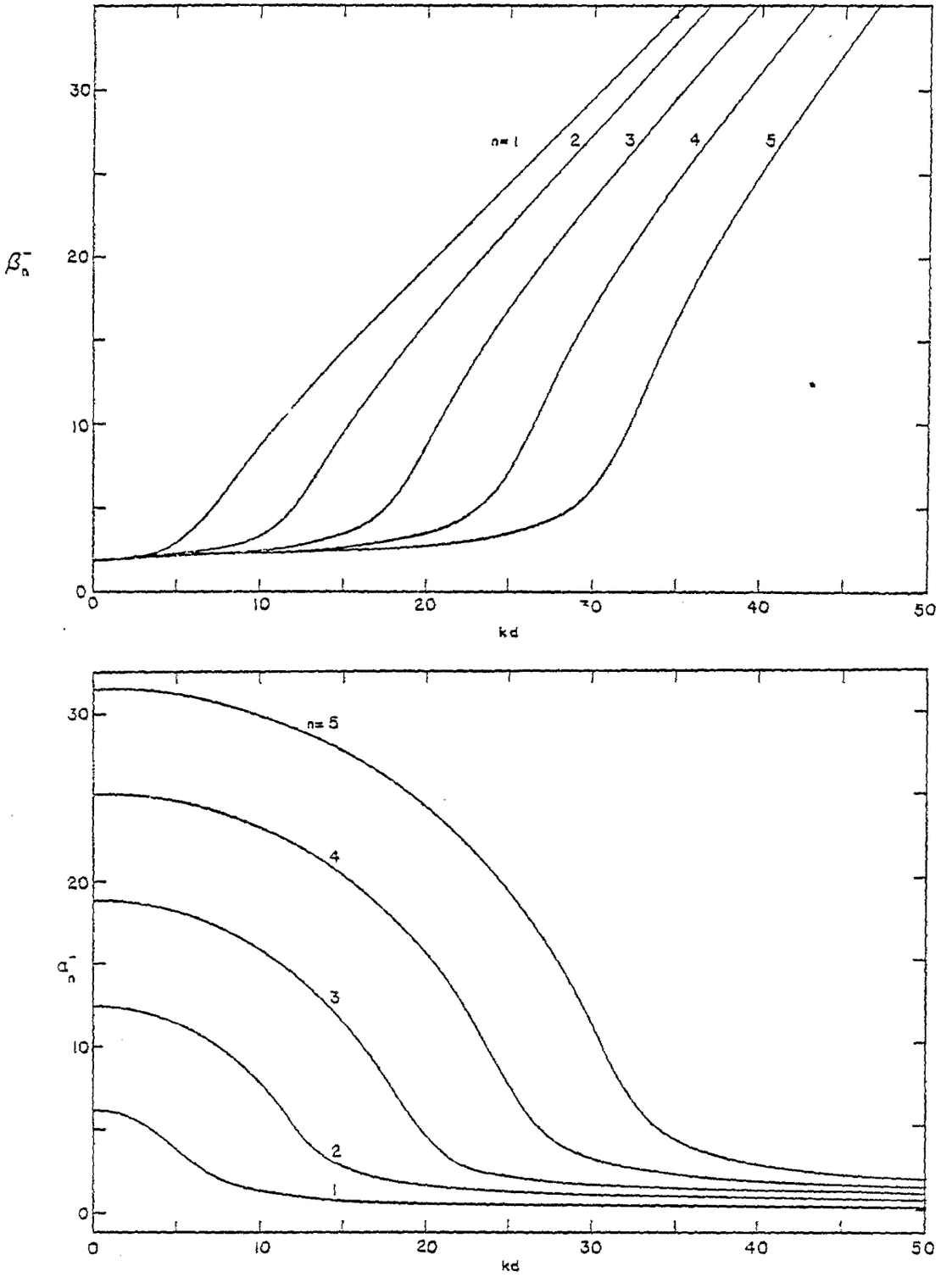

Figure 3 3. The propagation and attenuation constants of the five lowest antisymmetric TM modes on two wires when a/d = .01.

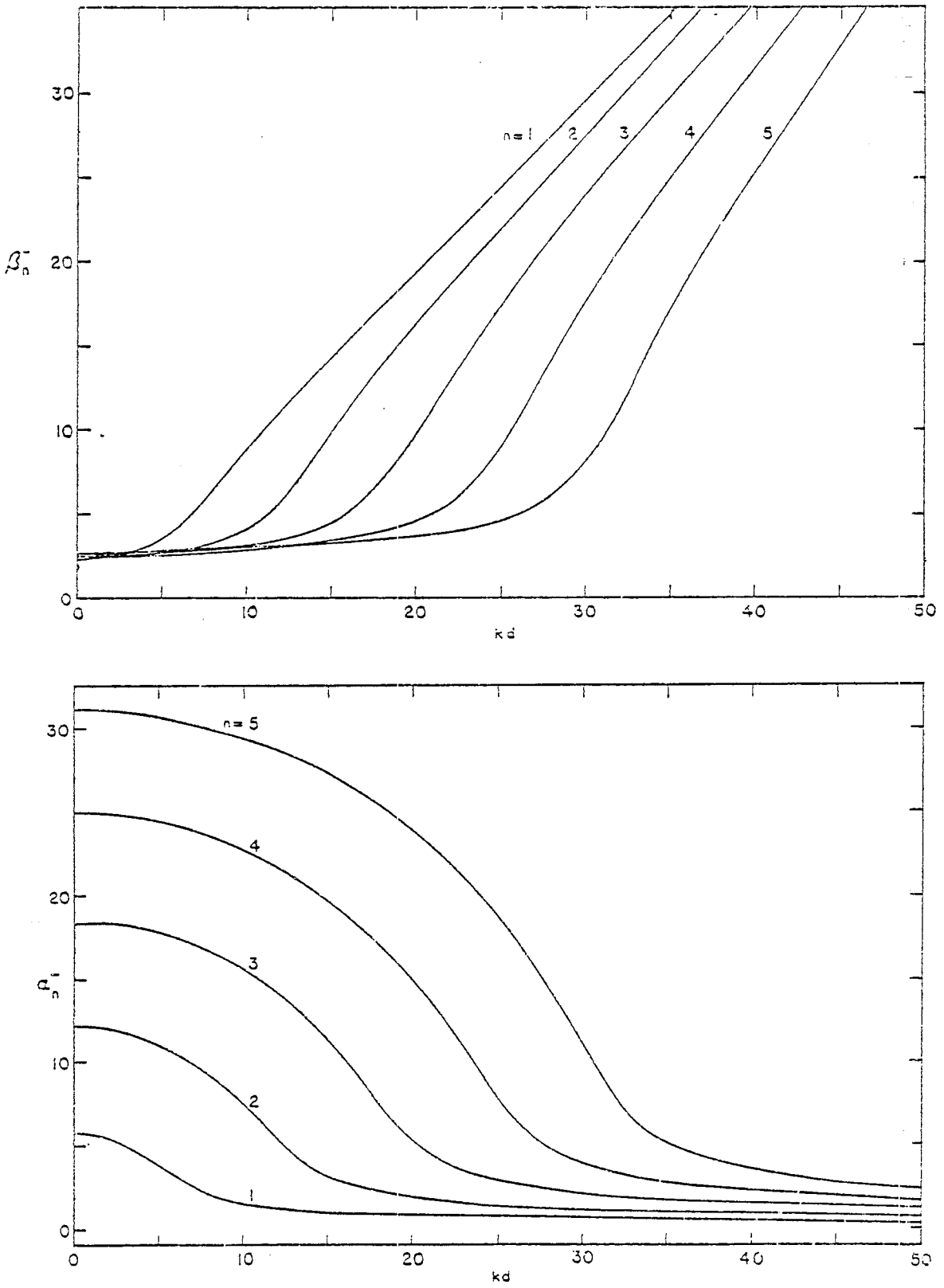

Figure 34. The propagation and attenuation constants of the five lowest antisymmetric TM modes on two wires when a/d = .001.

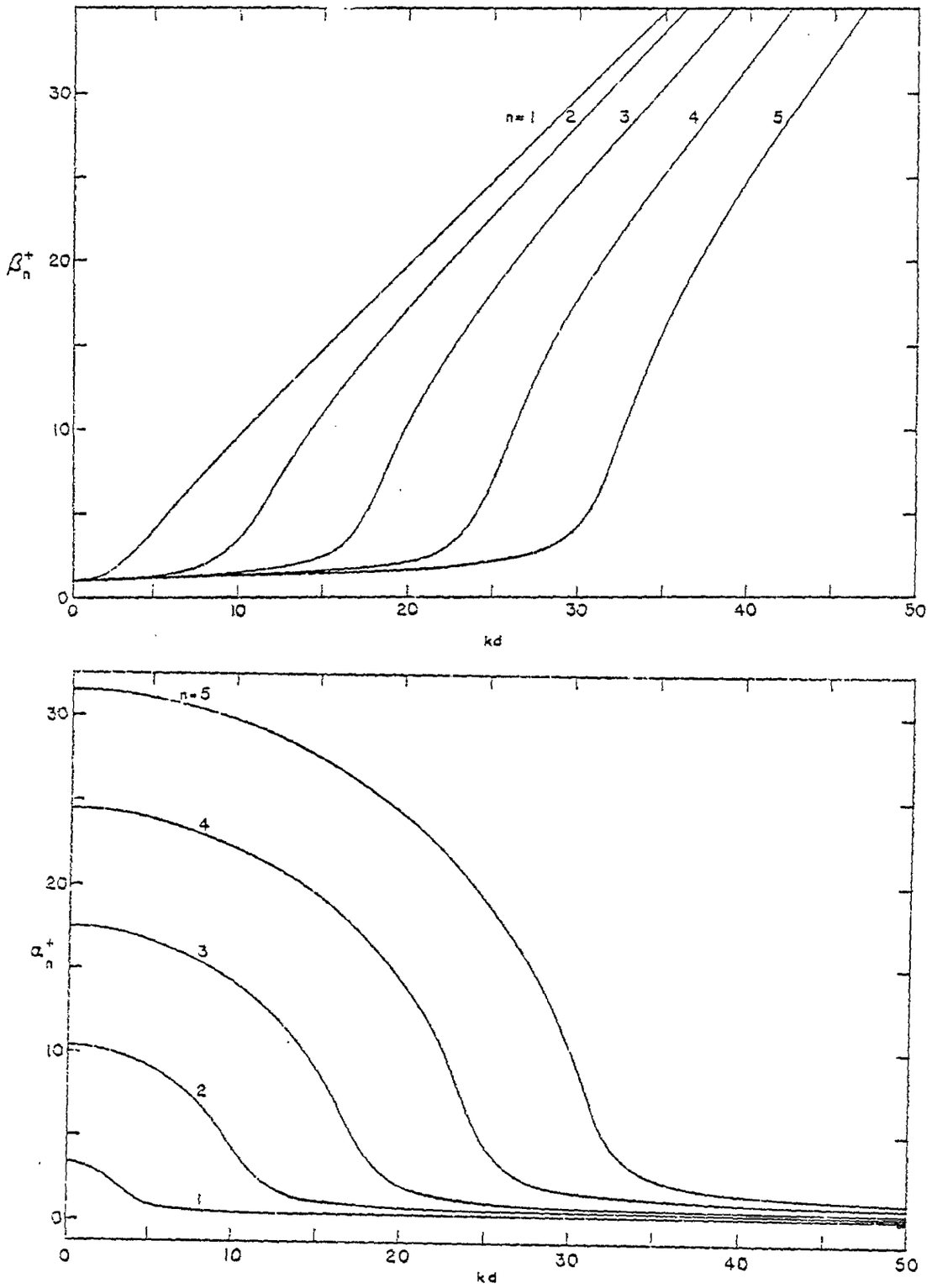

Figure 35. The propagation and attenuation constants of the five lowest symmetric TM modes on two wires when a/d = .1.

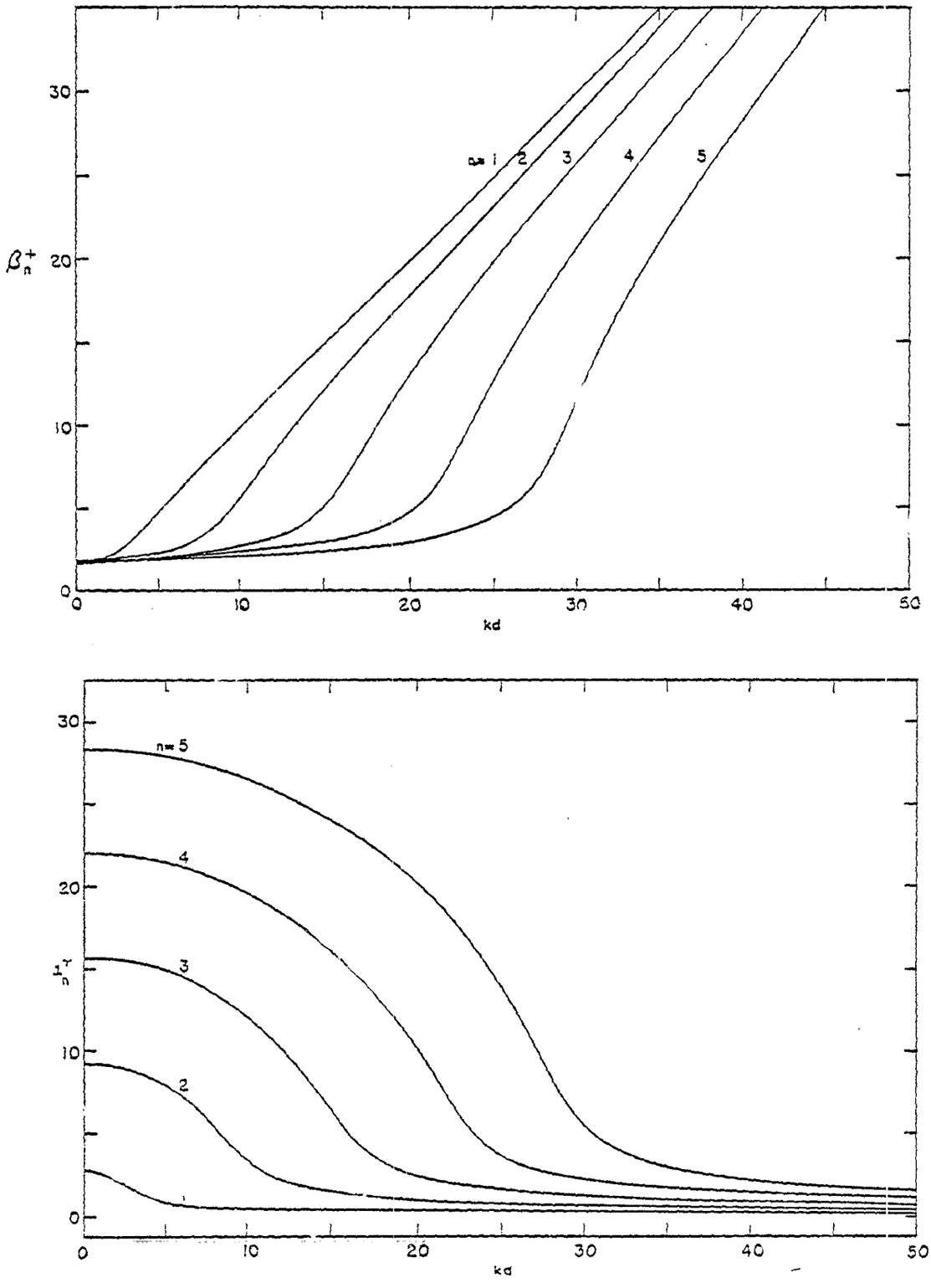

Figure 36. The propagation and attenuation constants of the five lowest symmetric TM modes on two wires when a/d = .01.

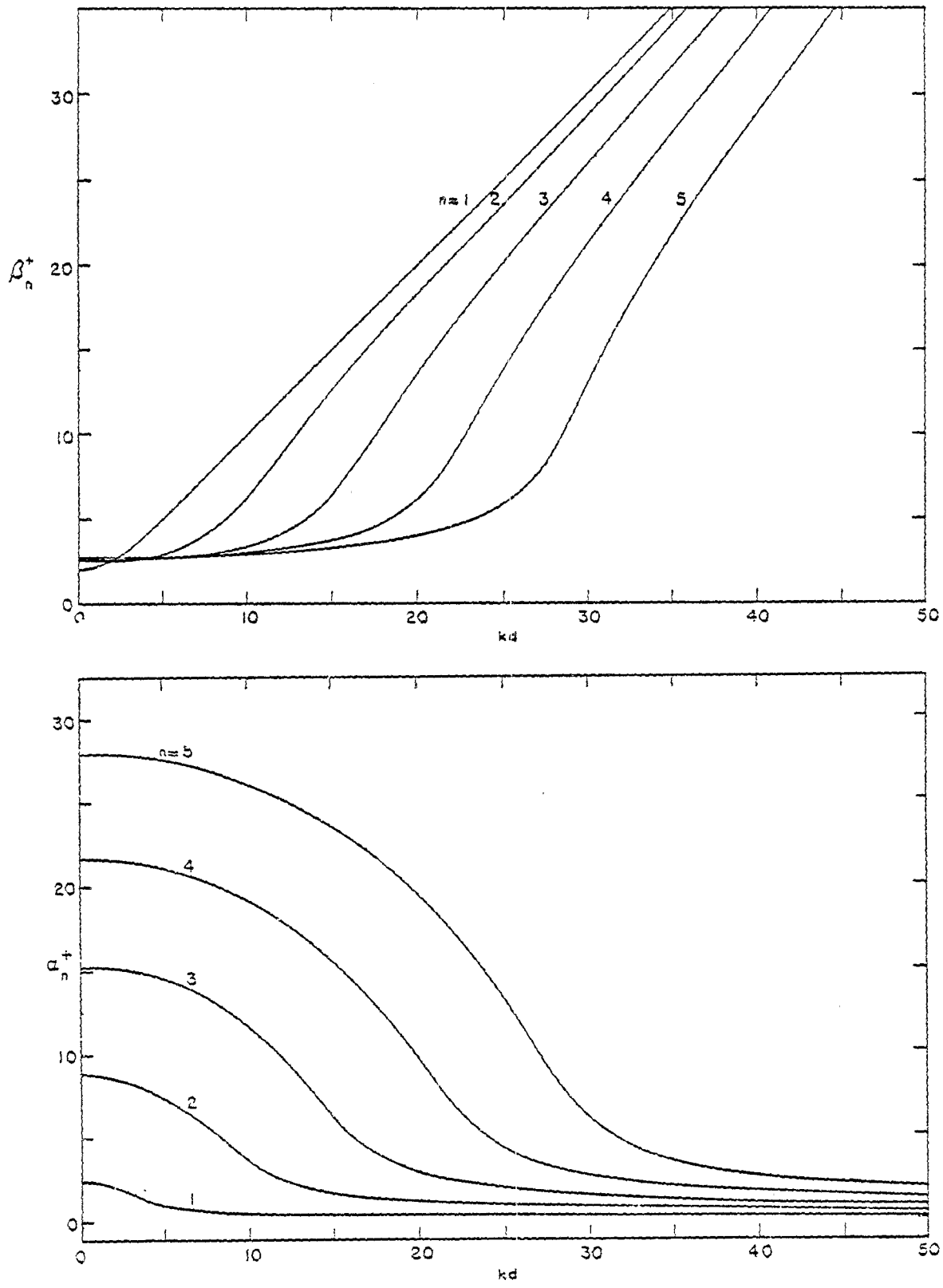

Figure 37. The propagation and attenuation constants of the five lowest symmetric TM modes on two wires when a/d = .001.

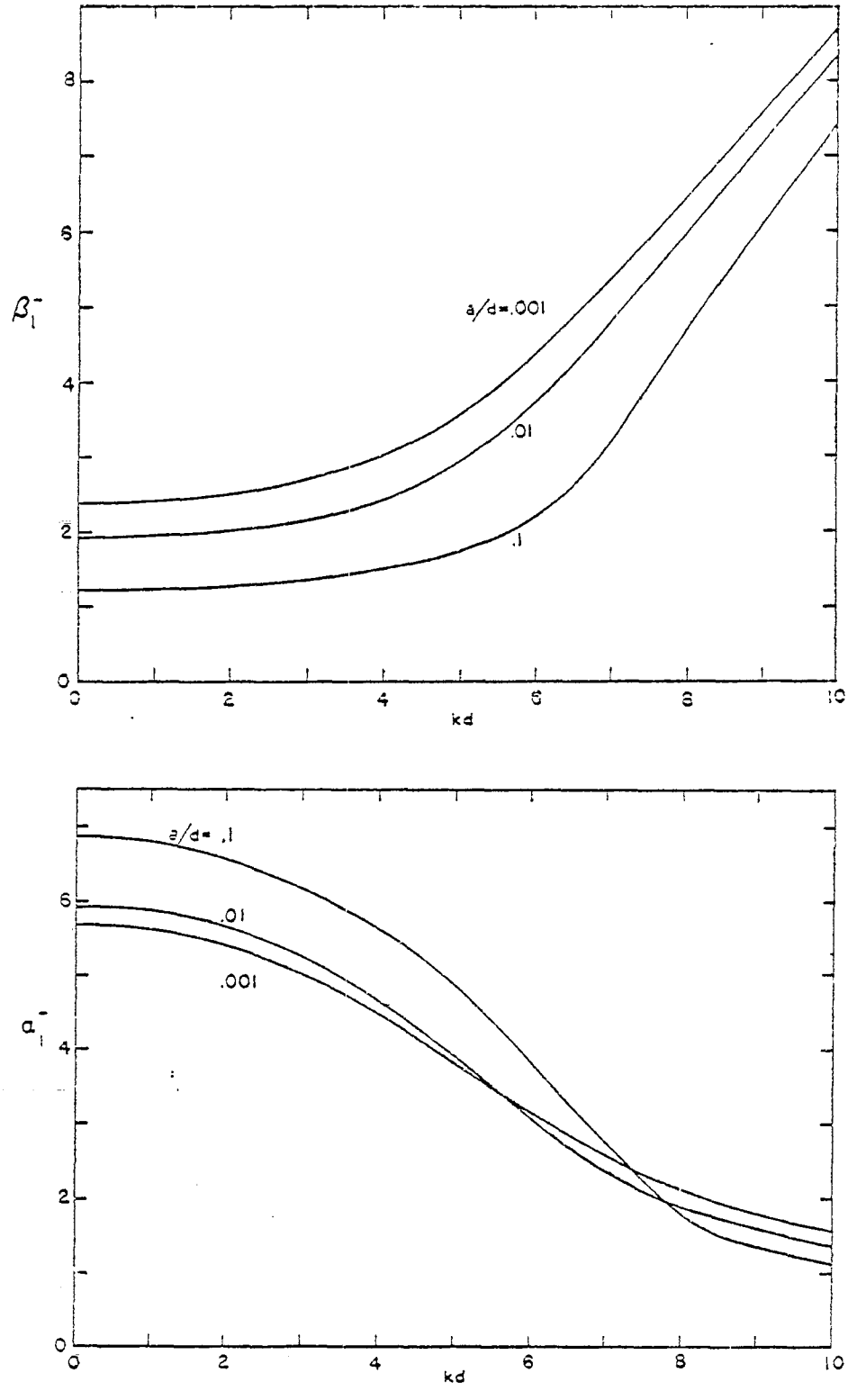

Figure 38. The propagation and attenuation constants of the lowest antisymmetric TM mode on two wires when a/d = .1, .01, .001.

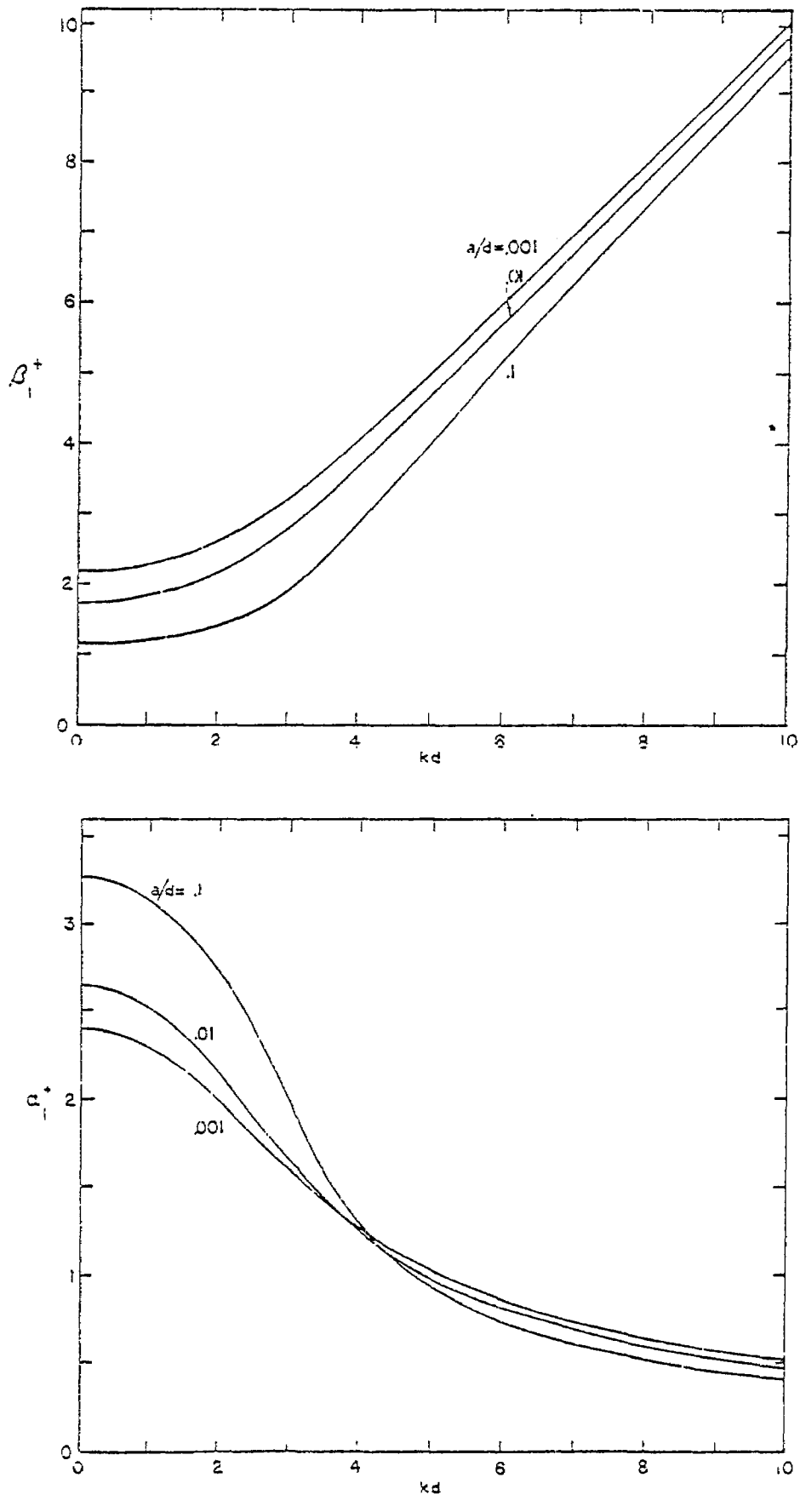

Figure 39. The propagation and attenuation constants of the lowest symmetric TM mode on two wires when a/d = .1, .01., .001.

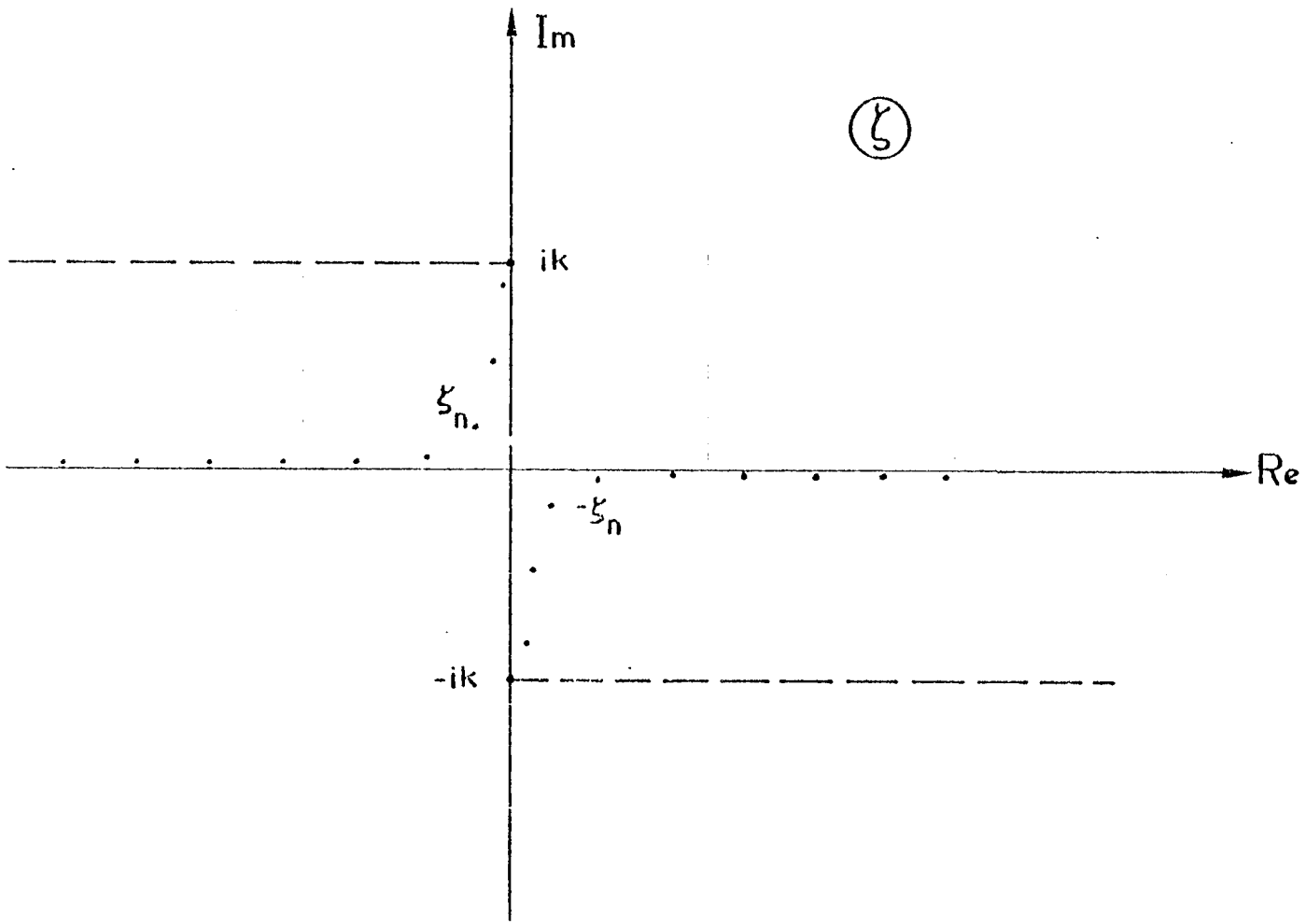

Figure 40. The branch of $p = \sqrt{\zeta^2 + k^2}$ used in the representation (84). In this branch, $\mathrm{Re}\{p\} < 0$ for $\{\zeta : \mathrm{Re}\{\zeta\} > 0$ and $-k < \mathrm{Im}\{\zeta\} < 0\}$ and $\{\zeta : \mathrm{Re}\{\zeta\} < 0$ and $0 < \mathrm{Im}\{\zeta\} < k\}$.

To conclude this section we discuss briefly the analytical properties of the field in the complex frequency plane. As we have seen in Section III the field, when considered as a function of the complex variable p, has a branch point at $p = 0$ and poles at $p = p_n^{\pm}$ where $K_o(p_n^{\pm}a) \pm K_o(p_n^{\pm}d) = 0$. The analytical properties of the field in the complex p-plane completely determine the space-time behavior of the scattered field (c.f. (23)). From the analysis in this section (c.f. (89)) it can be seen that the field has branch points in the complex frequency plane and that the locations of these branch points are given by $s = cp_n^{\pm}$. These branch points may be compared with the branch points of the field scattered from an object located in a parallel-plate region [21].

VIII. Concluding Remarks

The transient electromagnetic field around two wires can be expressed in terms of a discrete spectrum and a continuous spectrum. The discrete part of the spectrum can be interpreted as modes. The propagation and attenuation constants of these modes have been calculated for a wide range of frequencies and for different values of the radius-to-separation ratio. The field of each mode grows exponentially in the transverse direction far away from the wires thereby violating the radiation condition. Thus, the usefulness of the modes in the frequency domain is limited to a region near the two wires.

The time history of the current on the wires has been calculated when each wire is fed by a step-function slice generator. The current due to two step-function voltage sources of arbitrary amplitude and polarity has been obtained by superposition of two linearly independent cases: (1) when the two voltage generators have the opposite polarity (push-pull), and (2) when they have the same polarity (push-push). When the wires are fed in a push-pull manner and when the radius-to-separation ratio is less then .01 it was found that the current on the wires can be described accurately by the TEM mode alone after one transient time or so between the wires. This, of course, means that transmission line theory is applicable for times larger than the transit time across the structure.

There are other wave guiding structures that can be analyzed with the methods used in this note. For example, the properties of the electromagnetic field supported by any number of parallel, thin wires can be determined by employing exactly the same methods. However, due to the rather complicated expressions that will result, the number of wires cannot be too large.

Two perfectly conducting plates of finite width is another example of a structure where Laplace transform methods are suitable. In the parallel plate problem it is impossible to derive an explicit expression for the current induced on the plates due to step-function slice generators. Instead, an integral equation of the first kind for the induced current density can be derived. After a suitable transformation this integral equation can be transformed into an integral equation of the second kind. This integral equation can be further transformed into a set of algebraic equations by expanding the current density

in a Fourier series with the Chebyshev polynomials as basis functions. Standard numerical methods can then be applied to solve this set of equations. The TM modes can be determined from the nontrivial solution of the homogeneous integral equation. Furthermore, it can be shown from this set of equations that in the limit when the width-to-separation ratio is small, the propagation and attenuation constants of the TM modes of the parallel plates are the same as those of two parallel, circular wires. Hopefully, we will be able to report some results on the two plates problem in the near future.

Appendix A

In this appendix we will derive asymptotic forms of some integrals. These asymptotic forms are used in Section IV to evaluate the late time behavior of the field.

A. Asymptotic Evaluation of $\int_o^\infty I_+(\xi)\exp(-v\xi)d\xi$

First, we will find an asymptotic form of the integral

$$J_+(v) = \int_o^\infty I_+(\xi)\exp(-v\xi)d\xi \tag{A1}$$

valid for large values of v. The function $I_+(\xi)$ is given by

$$I_+(\xi) = \frac{L_+(\xi)[L_+(\xi)K_1(\alpha\xi)+M_+(\xi)I_1(\alpha\xi)]}{M_+(\xi)[M_+^2(\xi)+\pi^2L_+^2(\xi)]}\,, \tag{A2}$$

$$L_+(\xi) = I_o(\xi) + I_o(\delta\xi), \qquad M_+(\xi) = K_o(\xi) + K_o(\delta\xi)$$

where $\alpha > 1$, $\delta < 1$ and $I_o(x)$ and $K_o(x)$ are modified Bessel functions.

The main contribution to $J_+(v)$ comes from small values of ξ. Asymptotically, for small values of ξ we have

$$I_+(\xi) = -1/\{2\xi\ \ln(\sigma\xi)[\pi^2 + \ln^2(\sigma\xi)]\} + O(\xi^2\ \ln\ \xi) \tag{A3}$$

where

$$\sigma = \Gamma\delta^{1/2}/2, \qquad \Gamma = 1.78102.....\text{(the exponential of Euler's constant)}.$$

From (A3) it follows that

$$J_+(v) = -\int_o^\infty \{2\xi\ \ln(\sigma\xi)[\pi^2 + \ln^2(\sigma\xi)]\}^{-1}\ \exp(-v\xi)d\xi + O(v^{-3}\ \ln\ v) \tag{A4}$$

as $v \to \infty$. Integration by parts give

$$J_+(v) = J_+'(v) + J_+''(v) + J_+'''(v) + O(v^{-3} \ln v) \tag{A5}$$

where

$$J_+'(v) = \int_0^{\kappa'} I(\xi,v)\exp(-\xi)d\xi,$$

$$J_+''(v) = \int_{\kappa'}^{\kappa''} I(\xi,v)\exp(-\xi)d\xi,$$

$$J_+'''(v) = \int_{\kappa''}^{\infty} I(\xi,v)\exp(-\xi)d\xi, \tag{A6}$$

$$I(\xi,v) = (2\pi)^{-2} \ln\{(\ln \xi - \ln \kappa)^2/[(\ln \xi - \ln \kappa)^2 + \pi^2]\},$$

$$\kappa = 2v/(\Gamma\delta^{1/2}).$$

The limits of integration κ' and κ'' are chosen so that $\kappa' << 1$ but $\kappa'\kappa >> 1$, and $\kappa'' >> 1$ but $\kappa''/\kappa << 1$. These choices of κ' and κ'' are obviously possibly when v is large. We can now derive the following asymptotic forms for $J_+'(v)$, $J_+''(v)$ and $J_+'''(v)$, valid for large values of v

$$J_+'(v) = O(v^{-1} \ln^{-1} v),$$

$$J_+''(v) = \frac{1}{4} \ln^{-2}[2v/(\Gamma\beta^{1/2})] + O[\ln^{-4}(v)], \tag{A7}$$

$$J_+'''(v) = O\{\exp[-2v/(\Gamma\beta^{1/2})]\}.$$

Thus, we have

$$J_+(v) = \frac{1}{4} \ln^{-2}[2v/(\Gamma\beta^{1/2})] \tag{A8}$$

as $v \to \infty$.

B. Asymptotic evaluation of $\int_o^\infty I_-(\xi)\exp(-v\xi)d\xi$

Next, we will find an asymptotic form of the integral

$$J_-(v) = \int_o^\infty I_-(\xi)\exp(-v\xi)d\xi \tag{A9}$$

valid for large values of v. The function $I_-(\xi)$ is given by

$$I_-(\xi) = \frac{L_-(\xi)[L_-(\xi)K_1(\alpha\xi)+M_-(\xi)I_1(\alpha\xi)]}{M_-(\xi)[M_-^2(\xi)+\pi^2L_-^2(\xi)]}\,, \tag{A10}$$

$$L_-(\xi) = I_o(\xi) - I_o(\delta\xi), \qquad M_-(\xi) = K_o(\xi) - K_o(\delta\xi).$$

Asymptotically, for small values of ξ we have

$$I_-(\xi) = \{(1 - \delta^2)[(1 - \delta^2) + 2\alpha^2 \ln \alpha]/(32 \ln^3 \alpha)\}\xi^3 + O(\xi^5 \ln \xi) \tag{A11}$$

from which it follows that

$$J_-(v) = 3\{(1 - \delta^2)[(1 - \delta^2) + 2\alpha^2 \ln \alpha]/(16 \ln^3 \alpha)\}v^{-4} + O(v^{-6} \ln v) \tag{A12}$$

as $v \to \infty$.

C. Asymptotic Evaluation of $\int_1^\infty (u^2-1)^{-1/2} \ln^{-n}(vu)du$

Finally, we will find an asymptotic form of the integral

$$F_n(v) = \int_1^\infty (u^2 - 1)^{-1/2} \ln^{-n}(vu)du \tag{A13}$$

valid for large values of v and for n being an integer, $n \geq 2$. A change of variables enables us to cast the integral into the following form

$$F_n(v) = F_n'(v) + F_n''(v) \tag{A14}$$

where

$$F'_n(v) = \int_0^{\varepsilon} P_n(v,u)\,du,$$

$$F''_n(v) = \int_{\varepsilon}^{1} P_n(v,u)\,du, \tag{A15}$$

$$P_n(v,u) = u(1 - u^2)^{1/2}\ \ln^n(v/u)$$

and ε is a small but finite quantity such that $\varepsilon << 1$ but $v\varepsilon >> 1$. We can now derive the following asymptotic forms for $F'_n(v)$ and $F''_n(v)$,

$$F'_n(v) = (n - 1)^{-1}\ \ln^{n-1}(v) + O[\ln^n(v)],$$

(A16)

$$F''_n(v) = O[\ln^n(v)]$$

Thus,

$$F_n(v) \sim (n - 1)^{-1}\ \ln^{n-1}(v) \tag{A17}$$

as $v \to \infty$.

Appendix B

In this appendix we will determine certain properties of the zeros of the functions $K_o(w) \pm K_o(\delta w)$, where δ is a real, positive number such that $\delta < 1$. $K_o(w)$ is the modified Bessel function of the second kind and $-\pi < \arg\{w\} < \pi$.

Firstly, we will show that all zeros are located within a band around the imaginary axis. For $\mathrm{Re}\{w\} >> 1$ we have

$$K_o(w) \pm K_o(\delta w) = \pm K_o(\delta w)[\pm 1 + K_o(w)/K_o(\delta w)] \tag{B1}$$

and the asymptotic expansion for large arguments implies the existance of a finite $w_r' > 0$ such that $|K_o(w)/K_o(\delta w)| < 1$ for $\mathrm{Re}\{w\} > w_r'$. Moreover, since $K_o(\delta w)$ has no zeros it follows immediately that $K_o(w) \pm K_o(\delta w)$ has no zeros for $\mathrm{Re}\{w\} > w_r'$. Next, for $-\mathrm{Re}\{w\} >> 1$ we have

$$K_o(w) \pm K_o(\delta w) = K_o(w)[1 \pm K_o(\delta w)/K_o(w)] \tag{B2}$$

and again from the asymptotic expansion it is clear that there exists a finite $w_r'' < 0$ such that $|K_o(\delta w)/K_o(w)| < 1$ for $\mathrm{Re}\{w\} < w_r''$. Thus, $K_o(w) \pm K_o(\delta w)$ has no zeros for $\mathrm{Re}\{w\} < w_r''$. It is now obvious that all zeros of $K_o(w) \pm K_o(\delta w)$ are located within a band around the imaginary axis in the complex w-plane.

Secondly, we will deduce an asymptotic expression for the zeros, $w_n^{\pm}$, of $f_{\pm}(w) = K_o(w) \pm K_o(\delta w)$, valid when $|w_n^{\pm}| >> 1$. Using the asymptotic expressions for $K_o(w)$, valid when $|w| >> 1$ we have

$$f_{\pm}(w) = [\pi/(2w)]^{1/2} \exp(-w)\{1 - 1/(8w) \pm \delta^{-1/2} \exp[(1 - \delta)w][1 - 1/(8\delta w)] + O(w^{-2})\}. \tag{B3}$$

Making use of a method due to Stokes[17] we get the following asymptotic form of $w_n^{\pm}$,

$$w_n^{\pm} = i(1 - \delta)\beta_n^{\pm} + \ln \delta/[2(1 - \delta)] - i(1 - \delta)/(8\delta\beta_n^{\pm}) + O[(\beta_n^{\pm})^2] \tag{B4}$$

where $\beta_n^- = (2n - 1)\pi$, $\beta_n^+ = 2n\pi$, n integer.

Since $\delta < 1$ equation (B4) implies that $\mathrm{Re}\{w_n^{\pm}\} < 0$. It is our contention that $\mathrm{Re}\{w_n^{\pm}\} < 0$ for all zeros of $f_{\pm}(w)$. This is true for all cases that have been investigated numerically. It is also true for all those zeros for which $|w_n^{\pm}| >> 1$ and $|\delta w_n^{\pm}| << 1$. The last statement follows from an investigation of the variation of the argument of the function,

$$g_{\pm}(w) = [2/(\pi w)]^{1/2} \exp(-w) \pm \ln[2/(\Gamma \delta w)],$$

around a closed contour in the right half plane.

Acknowledgment

We wish to thank Dr. K. S. H. Lee for his valuable technical advice and remarks, Dr. C. E. Baum for his kind interest in this problem, Dr. T. K. Liu for his help in the numerical calculations and Mrs. T. Abramian for her preparation of the manuscript.

References

1. C. E. Baum, "Impedances and Field Distributions for Symmetrical Two Wire and Four Wire Transmission Line Simulators," Sensor and Simulation Note 27, October 1966.
2. T. T. Wu, "Theory of the Dipole Antenna and the Two-Wire Transmission Line," J. Math. Phys., Vol. 2, pp. 550-574, 1961.
3. S. A. Schelkunoff, Electromagnetic Waves, D. van Nostrand, New York, 1943.
4. P. O. Brundell, "Transient Electromagnetic Waves Around a Cylindrical Transmitting Antenna," Ericsson Techniques, Sweden, Vol. 16, No. 1, pp. 137-162, 1960.
5. R. W. Latham and K. S. H. Lee, "Waveforms Near a Cylindrical Antenna," Sensor and Simulation Note 89, June 1969.
6. T. T. Wu, "Transient Response of a Dipole Antenna," J. Math. Phys., Vol. 2, pp. 892-894, 1961.
7. S. P. Morgan, "Transient Response of a Dipole Antenna," J. Math. Phys., Vol. 3, pp. 564-565, 1962.
8. N. Marcuvitz, "On Field Representations in Terms of Leaky Modes or Eigenmodes," IRE Trans. Antennas Propagat., Vol. AP-4, pp. 192-194, 1956.
9. A. Hessel, "General Characteristics of Travelling-Wave Antennas," Chapter 19 in Antenna Theory edited by R. E. Collin and F. J. Zucker, McGraw Hill, New York, 1969.
10. L. Marin, "Radiation From a Resistive Tubular Antenna Excited by a Step Voltage," Sensor and Simulation Note 101, March 1970.
11. C. H. Papas, "On the Infinitely Long Cylindrical Antenna," J. Appl. Phys., Vol. 20, pp. 437-440, 1949.
12. T. T. Wu, "Input Admittance of Linear Antennas Driven From a Coaxial Line," J. Research Natl. Bur. Std., Vol. 67D, pp. 83-89, 1963.
13. K. S. Kuntz, "Asymptotic Behavior of Current on an Infinite Cylindrical Antenna," J. Research Nat. Bur. Std., Vol. 67D, pp. 417-431, 1963.
14. B. L. van der Waerden, "On the Method of Saddle Points," Appl. Sci. Res., Sect. B, Vol. 2, pp. 33-45, 1950.
15. W. Magnus, F. Oberhettinger and R. P. Soni, Formulas and Theorem for the Special Functions of Mathematical Physics, Springer-Verlag, New York, 1966.

16. M. Abramowitz and I. A. Stegun, Editors, Handbook of Mathematical Functions, National Bureau of Standards, AMS-55, 1964.

17. G. N. Watson, Theory of Bessel Functions, Cambridge University Press, 1966, p. 503.

18. O. Einarsson, "The Step Voltage Current Response of an Infinite Conducting Cylinder," Trans. Roy. Inst. Techn., Stockholm, Sweden, No. 191, pp. 1-25, 1962.

19. C. E. Baum, "On the Singularity Expansion Method for the Solution of Electromagnetic Interaction Problems," Interaction Note 88, December 1971.

20. L. Marin and R. W. Latham, "Analytical Properties of the Field Scattered by a Perfectly Conducting, Finite Body," Interaction Note 92, January 1972.

21. L. Marin, "Application of the Singularity Expansion Method to Scattering From Imperfectly Conducting Bodies and Perfectly Conducting Bodies Within a Parallel Plate Region," Interaction Note 116, June 1972.